ABSTRACT

Title of Document: DEVELOPMENT OF A DYNAMIC TEST FACILITY FOR ENVIRONMENTAL CONTROL SYSTEMS

Amr El-Sayed Alaa El-Din Gado, Ph.D., 2006

Directed By: Professor Reinhard Radermacher, Mechanical Engineering Department

Passenger cars and light trucks consume 80% of the total oil imported by U.S.A. Mobile air conditioners (MACs) increase vehicle fuel consumption and exhaust gas emissions. They operate most of the time in a transient state. It is currently impossible to test the performance of an air conditioner during transient operation without it being associated with its intended conditioned space, the car cabin.

In this research work a new smart test facility is designed, built, and verified. This facility makes it possible to test the MAC independent of the vehicle, but yet under realistic dynamic conditions.

The facility depends on simulation software that measures the conditions of the air supplied by the MAC and subsequently adjusts the conditions of the air returning to the MAC depending on the results of a thermal numerical model of the car cabin that takes into consideration sensible and latent loads, as well as passengers' control

settings. It was successful in controlling the temperature and relative humidity within ±0.9°C and ±5% of their respective intended values.

The test facility is used to investigate the dynamic performance of a typical R134a MAC system. The tests include pull-down, drive cycle, and cyclic on/off tests. The analysis focuses on the latent capacity and moisture removal due to the difficulty in measuring these variables during field tests. The results show that the most energy efficient method to pull-down the air temperature inside a hot-soaked cabin is to start with fresh air as long as the temperature in the cabin exceeds that of the ambient and then switch to recirculated air. The effect of re-evaporation is illustrated by showing the off-cycle latent capacity. Cyclic tests show that the net moisture removal rate has a minimum at around a 2 minute duty cycles. This implies a means of controlling the coil latent heat factor by varying duty cycle.

The automotive air conditioning system is numerically modeled and used in cooperation with the cabin model to conduct numerical tests. The numerical simulation results are compared to the experimental results and the error is less than 1.5 K of cabin air temperature.

DEVELOPMENT OF A DYNAMIC TEST FACILITY FOR ENVIRONMENTAL CONTROL SYSTEMS

By

Amr El-Sayed Alaa El-Din Gado

Dissertation submitted to the Faculty of the Graduate School of the
University of Maryland, College Park, in partial fulfillment
of the requirements for the degree of
Doctor of Philosophy
2006

Advisory Committee:
Professor Reinhard Radermacher, Chair
Dr. David Didion, NIST Fellow
Associate Professor Keith Herold
Associate Professor Kenneth Kiger
Assistant Professor Bao Yang
Professor M. Sherif Aggour

Dedication

Lovingly dedicated to my parents and my brother Taher Gado.

Acknowledgements

First and foremost, my deepest gratitude and my love go to my family who has devotionally supported me throughout the years. My mother, father, and brother, I can never repay your debt.

My sincere appreciation goes to my advisor, Prof. Reinhard Radermacher, for his guidance and for providing me with the opportunity to work at the prestigious Center for Environmental Energy Engineering in the University of Maryland, College Park.

A warm thank you also goes to my immediate supervisor, Dr. Yunho Hwang, for his help, and to all my colleagues in the CEEE for having made my time there enjoyable and unforgettable.

Special thanks are also extended to Bill Butler, Emerson Climate Technologies, for his help in reviewing the English language of this dissertation.

Table of Contents

Dedication ii
Acknowledgements iii
Table of Contents iv
List of Tables vi
List of Figures vii
Nomenclature ix
Chapter 1: Introduction 1
1.1 Overview 1
1.2 Literature Review 3
1.3 Automotive Air Conditioning 9
1.4 The Importance of Mobile Air Conditioners and Their Economic and Environmental Impact: 10
1.5 The Challenges in Dynamic Testing 12
1.6 Objective, Focus, Selected Approach, Expected Benefits, and Plan of Research 14
Chapter 2: The Cabin Model 21
2.1 Introduction 21
2.2 Review of Previous Cabin Models 22
2.3 The Cabin Model 24
2.3.1 The Physical Model 24
2.3.2 Model Assumptions 24
2.3.3 The Numerical Model 25
2.3.4 Inputs and Outputs 27
2.4 Solution of Cabin Model 27
2.5 Verification of The Model 28
2.6 Sensitivity Analysis 29
2.7 Using The Cabin Model 30
Chapter 3: Construction of The Dynamic Test Facility 35
3.1 Introduction 35
3.2 The Original Steady-state Test Facility 35
3.3 The Dynamic Control Software 36
3.3.1 Control Based on Outputs of Cabin Model 37
3.3.2 Control Based on Time-sequence 38
3.4 Verification of Control Accuracy 40
3.5 Lessons Learnt from Control of Test Facility 42
3.6 Advantages and Limitations of The Dynamic Test Facility 42
3.6.1 Advantages 42
3.6.2 Limitations 43
Chapter 4: The Experimental Test System 54
4.1 Introduction 54
4.2 The Experimental Setup 54
4.3 Instrumentation, Measurements, and Data Acquisition 55

4.3.1 Refrigerant-side Measurements 55
4.3.2. Air-side Measurements 56
4.3.3 System-level Measurements 57
4.3.4 Data Acquisition 57
4.4 Assessment of The Experimental System 57
4.5 Dynamic Temperature Measurement Error 59
Chapter 5: Experimental Results 68
5.1 Introduction 68
5.2 Pull-down Tests 68
5.3 Drive Cycle Tests 70
5.4 Drive Cycle Tests with Thermostats 73
5.5 Cycling Tests 74
5.6 Conclusions 82
5.6.1 Conclusions from Pull-down and Drive-cycle Tests 82
5.6.2 Conclusions from the Off-cycle Attributes (Cooling and Humidification) 83
5.6.3 Conclusions from the Cyclic Tests 83
Chapter 6: Dynamic Modeling 101
6.1 Introduction 101
6.2 Literature Survey about Previous Models 101
6.3 TRANSREF (TRANSient simulation of REFrigeration systems) Program 105
6.4 Dynamic Modeling of Automotive Systems 107
6.4.1 Automotive Cabin 107
6.4.2 Automotive Evaporator and Latent Capacity 108
6.4.3 Automotive Orifice 111
6.4.4 Other Automotive Components 112
6.5 Modeling Results and comparison with Experimental Results 113
6.6 Conclusions 114
Chapter 7: New Contributions, Future Work and Epilogue 123
7.1 New Contributions 123
7.2 Future Work 123
7.3 End Notes 124
7.4 Long-term Vision 124
References 125

List of Tables

Table 1.1 1997 Cars Census (Bahatti, 1999) 16
Table 2.1 Input Values for Verification of the Cabin Model..... 31
Table 3.1 Four Cases of Temperature Control..... 44
Table 3.2 Values of the Control Factors 44
Table 4.1 Specifications of System Components 62
Table 4.2 Location of Refrigerant Thermocouples and Pressure Transducers 62
Table 5.1 Test Matrix of Pull-down Tests 85
Table 5.2 Test Matrix of Drive Cycle Tests 85
Table 5.3 Duty Cycles and Number of Cycles of Cyclic Tests 86
Table 6.1 Four of The More Popular Vapor Compression Models 115
Table 6.2 Comparison Between The Accuracy of Three Modeling Programs..... 115
Table 6.3 TRANSREF Inputs of Evaporator Component 115
Table 6.4 TRANSREF Inputs of Condenser Component..... 116
Table 6.5 TRANSREF Inputs of Compressor Component..... 116
Table 6.6 TRANSREF Inputs of Orifice Component..... 117

List of Figures

Figure 1.1 Schematic of The Basic Vapor Compression System 16
Figure 1.2 Energy Flow in Start-up Case vs. Steady State Case 16
Figure 1.3 Typical Automotive Air Conditioning System 17
Figure 1.4 US06 Standard Drive Cycle 17
Figure 1.5 Capacity, Power Consumption and Coefficient of Performance During Start-up of an Automotive System (Laboratory Data)..... 18
Figure 1.6 Breakdown of U.S.A. Oil Consumption for the Transportation Sector in 2000..... 18
Figure 1.7 Typical Laboratory Test Facility for Steady State Testing 19
Figure 1.8 Wind Tunnel of Behr GmbH (www.behrgroup.com) 19
Figure 1.9 Wind Tunnel of General Motors Corp. (Hill et al., 2004)..... 20
Figure 1.10 Results of Literature Survey on Dynamic Automotive Testing 20
Figure 2.1 Physical Model of Passengers' Compartment and Thermal Loads..... 31
Figure 2.2 Cabin Model Verification Results 32
Figure 2.3 Results of Time sensitivity Analysis..... 32
Figure 2.4 Results of h_c-sensitivity Analysis 33
Figure 2.5 Screen Shot of the Software for Data Acquisition and Control 34
Figure 3.1 Refrigeration Circuit of Environmental Chamber or Loop 44
Figure 3.2 Example of a Time Sequence 45
Figure 3.3 Example Text File of the Time Sequence 45
Figure 3.4 Screenshot of The Cycle operator of The Dynamic Control Software 46
Figure 3.5 Schematic of The Two Control Layers 46
Figure 3.6 Temperature Control in Outdoor Simulator 47
Figure 3.7 Relative Humidity Control in Outdoor Simulator 47
Figure 3.8 Pull Down during Loaded Test in the Indoor Side..... 48
Figure 3.9 New European Drive Cycle..... 48
Figure 3.10 Absolute Error During Running NEDC 49
Figure 3.11 Refrigerant Temperatures During NEDC..... 49
Figure 3.12 Refrigerant Pressures During NEDC..... 50
Figure 3.13 Air Temperatures During NEDC..... 50
Figure 3.14 Effective Cabin Interior Temperature During Load Model Test..... 51
Figure 3.15 Load During Load Model Test 51
Figure 3.16 Drive Cycle for Load Model Test 52
Figure 3.17 Air Temperatures for Load Model Test..... 52
Figure 3.18 Capacities and COP During Load Model Test 53
Figure 4.1 Installation and Configuration of The Test System..... 63
Figure 4.2 Picture of The Automotive Condenser 63
Figure 4.3 Picture of the Automotive Evaporator..... 64
Figure 4.4 Picture of The Automotive Compressor, Torque Meter, Electric Motor and RPM Sensor 64
Figure 4.5 Calibration Curve of The Refrigerant Flow Meter..... 65
Figure 4.6 An Exposed Junction Thermocouple Immersed in Refrigerant 65
Figure 4.7 Refrigerant Temperature at Evaporator Outlet..... 66

Figure 4.8 Coefficient of Convection Heat Transfer from Thermocouple Bulb 66
Figure 4.9 Dynamic Temperature Measurement Error 67
Figure 5.1 Pull-down at Ambient = 30°C & 50% RH for Tests with Hot-soak 86
Figure 5.2 Pull-down at Ambient = 41°C & 32% RH for Tests without Hot-soak 87
Figure 5.3 Energy Consumption and COP of Pull-down Tests with Hot-soak 87
Figure 5.4 Energy Consumption and COP of Pull-down Tests without Hot-soak 88
Figure 5.5 Cabin Temperatures During NEDC 88
Figure 5.6 Cabin Relative Humidity During NEDC 89
Figure 5.7 Degrees of Superheating and Subcooling During NEDC 89
Figure 5.8 Refrigerant Temperatures During NEDC 90
Figure 5.9 Refrigerant Pressures During NEDC 90
Figure 5.10 Compressor Power during NEDC 91
Figure 5.11 Capacity During NEDC 91
Figure 5.12 Refrigerant Capacity and Power During NEDC 92
Figure 5.13 System Performance During NEDC 92
Figure 5.14 Cabin Temperatures During NEDC with Thermostat 93
Figure 5.15 Cabin Humidity During NEDC with Thermostat 93
Figure 5.16 Capacity and COP During NEDC with Thermostat 94
Figure 5.17 Moisture Removal During Cyclic Tests 94
Figure 5.18 Moisture Removal During Cyclic Tests – Short Cycles 95
Figure 5.19 Moisture Removal Rate During Cyclic Tests 95
Figure 5.20 Moisture Removal Rate During Cyclic Tests – Short Cycles 96
Figure 5.21 Coil Surface Temperature During Cyclic Tests 96
Figure 5.22 Drain Pan at the Beginning of an Off-cycle 97
Figure 5.23 Drain Pan 90 Minutes into an Off-cycle 97
Figure 5.24 Capacity and Power as Ratio of Steady State Capacity and Power 98
Figure 5.25 Capacity and Power as Ratio of Steady State Capacity and Power – Short Cycles 98
Figure 5.26 Coil Sensible and Latent Heat Factors 99
Figure 5.27 Coil Sensible and Latent Heat Factors – Short Cycles 99
Figure 5.28 Coefficient of Performance as a Function of Duty Cycle 100
Figure 5.29 COP as a Function of Duty Cycle – Short Cycles 100
Figure 6.1 Flowchart of Capacity Calculation in Evaporator Component 118
Figure 6.2 Sensitivity Analysis for Number of Evaporator Segments 119
Figure 6.3 Numerical vs. Experimental Refrigerant Temperatures 119
Figure 6.4 Numerical vs. Experimental Refrigerant Pressures 120
Figure 6.5 Numerical vs. Experimental Refrigerant Flow Rate 120
Figure 6.6 Numerical vs. Experimental Cabin Air Temperature 121
Figure 6.7 Numerical vs. Experimental Power Consumption 121
Figure 6.8 Numerical vs. Experimental Cooling Capacity 122
Figure 6.9 Numerical vs. Experimental Latent Capacity 122

Nomenclature

ACRONYMS AND ABBRIVIATIONS:

A/C : Air Conditioner

A/I : Analog Input

AHU : Air Handling unit

ANSI : American National Standards Institute

A/O : Analog Output

ASHRAE : American Society of Heating, Refrigerating and Air-conditioning Engineers, Inc.

COP : Coefficient Of Performance

D/I : Digital Input

D/O : Digital Output

EPA : Environmental Protection Agency

LMTD : Logarithmic Mean Temperature Difference

MAC : Mobile Air Conditioner, A/C for a passenger car or light truck

NEDC : New European Drive Cycle

NTU : Number of Transfer Units

PID : Proportional plus Integral plus derivative

PAG : Polyalkylene Glycol

RPM : Revolution Per Minute

TXV : Thermostatic Expansion Valve

SYMBOLS:

A : Area, m^2

a : Anticipation factor, dimensionless

C_p : Specific heat at constant pressure, kJ/kg-K

C_v : Specific heat at constant volume, kJ/kg-K

C : Specific heat of solid, kJ/kg-K

Const.: Constant in equation 1.1

d : Diameter, m

e : Error, difference between set point and process value for a controlled parameter.

e' : Error of the next step, difference between set point of the next control step and process value of a controlled parameter, if known.

G : Specific gravity, dimensionless

h : Convective heat transfer coefficient, kW/m^2-K

h_{fg} : Latent heat, kJ/kg

i : Enthalpy, kJ/kg

k : Thermal conductivity, kW/m-K

L : Height of fin, m

M : Mass, kg

m : Mass flow rate, kg/s

P : Pressure, kPa

Q : Load or capacity, kW

RH : Relative humidity, %

S : Set point of any controlled parameter

T : Temperature, K

t : Time, s

U : Overall heat transfer coefficient, kW/m^2-K

U_m : Mass transfer coefficient, kg/m^2-s

V : Volume, m^3

W : Humidity Ratio (moisture content), kg/kg

GREEK SYMBOL：

δ : Thickness, m

ϕ : Fin efficiency, dimensionless

γ : Heat capacity ratio, C_p / C_v, dimensionless

η : Efficiency or effectiveness, dimensionless

μ : Viscosity, kg/m.s

ρ : Density, kg/m^3

τ : Time constant, s

SUBSCRIPT：

amb : Ambient air

av : Average

c : Core, or interior mass

con : Condensate

cond : Condenser

cr : Critical

d : Deposits

e : Evaporator

ext : Exterior surface

f : fin

ft : fin-and-tube

ht : Heat transfer (convection and conduction)

i : Interior surface

iv : Infiltration and/or ventilation air

lat : Latent

m : Mixture, or return air

o : Cabin, overall

p : Pipe

ps : Passengers, sensible

pl : Passengers, latent

r : Room, or inside of cabin

s : Supply air

s/h : Superheat

sen : Sensible

sol : Solar radiation

ss : Steady State

sys : Entire system

w : Wall condition

GREEK SUBSCRIPT :

∞ : free-stream condition

DIMENSIONLESS GROUPS:

Bi: Biot number

Le : Lewis number

Nu : Nusselt number

Pr : Prandtl number

Re : Reynolds number

Sc : Schmidt number

Chapter 1: Introduction

1.1 Overview

Humans occupy wide stretches of the land. In different geographic places, and throughout a year, it is not uncommon for some humans to spend their day-to-day lives in climates as hot as 45°C while others to have to cope with -35°C weather. To some extent, humans depend on air conditioning systems to make the conditions of the ambient air more suitable for their living. The main task of an air conditioner is to produce enough cooling or heating capacity to offset a space's sensible and latent thermal loads and therefore maintains the temperature and humidity of the conditioned space at an acceptable value.

In doing so, the air conditioning system operates under certain boundary conditions; such as the thermal loads to which the system is subjected on both its outdoor and indoor sides, and the user settings which include temperature setting, airflow rate setting, and, in the case of an automotive system, compressor rotational speed setting.

The focus of this research work is on vapor compression air conditioning systems. The basic vapor compression system is shown in Figure 1.1 and is composed of four components; a compressor, condenser (outdoor heat exchanger during the cooling mode), expansion device, and an evaporator (indoor heat exchanger in the cooling mode).

There are two types of loads which a heat pump is subjected to during steady state operation, space loads and outdoor air loads (ASHRAE, 2005 a). Space loads, such as heat transfer, solar radiation, and heat generated by the occupants and other heat sources, alter the condition of air inside the conditioned space. Outdoor-air loads, such as infiltration air heat or ventilation air heat, result from introducing fresh air to the conditioned space.

The boundary conditions imposed on a heat pump system are, therefore, continually varying by nature. They dictate the parameters of operation of the heat pump, such as the high-pressure level and its corresponding temperature, low-pressure level and corresponding temperature, refrigerant quality at exit of heat exchangers, and

refrigerant charge inside each of the cycle components. These parameters are unique for each set of boundary conditions imposed on the heat pump.

The outdoor unit of a heat pump is typically subjected to ambient atmospheric conditions, including solar radiation. The indoor unit is subjected to the conditions inside the place where it is in, which are close to atmospheric conditions if the heat pump system has been off for a long period of time. When the compressor is then turned on, the air surrounding the indoor unit is soon to be cooled down (or heated up in winter) while the outdoor unit remains subjected to ambient atmospheric conditions. The period from the start of the system (the cut-on) until the air in the conditioned space reaches its designed conditions, as well as any subsequent periods the system takes to readjust to steady state after a change in boundary conditions, is called a transient period.

A common method to handle the variation in boundary conditions is to use control devices, such as thermostatic expansion valves (TXV), electric expansion valves, or variable displacement compressors. Each time a control device reacts to a change in a boundary condition, the heat pump comes to a balance at a different set of operational parameters.

Another method to control the capacity of a heat pump is to cycle the compressor on and off depending on a signal from a thermostat placed inside the conditioned space to sense its temperature. When the compressor is turned off, there is nothing else in the system to maintain the high-pressure level in the condenser (or gas cooler) and the low-pressure level in the evaporator; therefore the refrigerant starts to migrate from the condenser to the evaporator passing through the expansion device. Some expansion devices allow fast migration, such as the capillary tube and the orifice, and some allow very little or minimum migration, such as the thermostatic expansion valves, especially those with no bleed port. Migration continues for some time until the pressures are equalized. Afterwards, migration will continue as a result of temperature difference as long as there is one.

Migrating refrigerant carries energy with it and travels from a hot heat exchanger to a colder heat exchanger (Mulroy and Didion, 1983). The temperature of the migrated refrigerant, as well as the temperature of the air surrounding the heat exchangers,

causes the evaporator to heat up to a temperature above its steady state operating temperature as well as causing the condenser to cool down. Furthermore, the migrated refrigerant carries lubrication oil with it and thus changes the distribution of the lubricant in the system from its steady state distribution. During the compressor off-period the air in the conditioned space is altered by the thermal loads while there is no capacity to offset them; therefore the temperature and the relative humidity of the space begin to change.

Figure 1.2 explains diagrammatically the flow of energy during system start-up versus the steady state. It is therefore concluded that during any transient period a heat pump is subjected to additional loads that materialize in redistribution of the refrigerant, as well as the lubricant oil circulating with it, among the different components of the system. This causes readjusting of the operating parameters, such as the temperature of the different parts of the system and the temperatures and pressures of the refrigerant to their new operating values, and reconditioning the thermal mass of the conditioned space to the steady state air temperature. These loads are, by nature, time-dependent. They are at their peak at the beginning of the transient period and decrease with time until they diminish. Therefore the case during the transient period is similar to the case of an undersized system working at a lower efficiency than the design one. The coefficient of performance (COP – defined as the ratio between the cooling capacity and the power consumption) of the system during the transient period suffers from a loss whose magnitude depends on the deviation of the real operating conditions from the design conditions. This loss is called the transient loss. However, what is referred to as loss might also be thought of as potential savings.

1.2 Literature Review

In 1992 Janssen et al. defined the cyclic losses as the difference between the energy consumption of a system with a continuously running compressor and a system with a cycling compressor, both having the same operating temperatures and the same cooling load. They attributed the looses to three different phenomena:

thermodynamic, where the thermal load of the heat exchangers of a cycling system is higher than in the continuously running system during the on-cycle which leads to lower evaporation temperature and higher condensation temperature, start/stop losses which happens in systems having a capillary tube, where the refrigerant flows from the condenser to the evaporator during the off-cycle and the refrigerant evaporates in the condenser and condenses in the evaporator, and compressor losses which happen specially in small hermetic compressors because the efficiency of such compressors is a function of their capacity. Janssen et al. investigated the effect of cycling with frequency from 2 cycles/hr to 8 cycles/hr (one cycle every 7.5 minutes) and found that as the frequency increases, the thermodynamic losses decrease (owing to the decreased fluctuations in the heat exchanger temperatures) and the start/stop losses increase but the positive effect of lower thermodynamic losses is more than counterbalanced by the negative effect of the start/stop losses such that there is a clear reduction of the COP with increasing cycling frequency. On the contrary, when they installed a shut off valve that closes the condenser during off-cycles, the COP increased with increasing cyclic frequency because the valve eliminates the start/stop losses. They anticipated that the system with a shut-off valve will theoretically approach the maximum efficiency at very high cycling frequency.

Tanaka et al. (1982) suggested some techniques to improve startup performance that include: designing the heat pump to be as light as possible, keeping the refrigerant charge as small as possible and preventing the liquid refrigerant from flowing into the evaporator after the heat pump stops. Wang and Wu (1990) installed a magnetic cut-off valve in the liquid line that was closed on compressor shut down to prevent refrigerant from migrating. As a result, energy losses were reduced resulting in a 4% reduction in motor power. However, Coulter and Bullard (1997) argued that refrigerant migration allows the system pressure to equalize, reducing the required starting torque of the compressor motor. They also argued that increasing the number of moving parts in the system by adding a shut-off valve increases chances of failure and reduces system reliability.

Mulroy and Didion (1983) conducted experiments on a nominal three tons of refrigeration split system operating in the cooling mode. The system was fitted with pneumatically actuated valves to divide it into 5 sections; outdoor coil, compressor and accumulator, vapor line, liquid line, and indoor coil. By shutting off the valves after short periods of operation, Mulroy and Didion were able to track the amount of refrigerant in each of the five sections. Their results shows that before starting up the system 11% of the refrigerant charge was in the condenser and 56% of the charge was in the evaporator, while at steady state operation, these values were 46% and 11%, respectively. The authors explained that the primary source of initial transient loss is that the unit is effectively undercharged by the amount of liquid refrigerant trapped in the accumulator. As the accumulator returns its retained liquid to the system, the condenser pressure increases causing the capillary flow rate to increase toward its steady state value. They were also able to show that the instantaneous capacity at start up as a ratio of steady state capacity can be represented by an exponential equation with two time constants on the form of Equation 1.1.

$$Q = Q_{ss}\left(1 - e^{-t/\tau_1}\right)\left(1 + const. \times e^{-t/\tau_2}\right) \qquad 1.1$$

The performance and behavior of the system during the transient period is dependant mainly on the performance of the compressor and expansion device and the configuration of the system such as the presence of equipment such as accumulator, receiver, suction line heat exchanger, or oil separator. These components affect the length of, and the power consumption during, the transient period. Mulroy (1986), while continuing experiments on the same system previously employed by Mulroy and Didion (1983), found that the removal of the accumulator and the installation of shut-off valve in liquid line improved the cyclic performance by about the same level. Increasing the charge increases the cyclic losses in cooling mode but decreases it in heating mode.

Kim and Bullard (2001) investigated the shut-down and start-up characteristics of a residential R410A split system with a capillary tube. Their results suggested that after

pressures stabilize during off-cycle, the refrigerant accumulated in the evaporator tend to be two phase and that accumulated in the condenser is superheated vapor. They went on to confirm previous results by Mulroy and Didion (1983) about describing the system performance (capacity and COP) during start-up using two exponential time constants. They gave detailed explanation for the behavior of system parameters after shut-down. They drew attention to that a reduced refrigerant charge implies reduced cyclic losses and therefore better system dynamic performance.

By mounting the different components of the system on balance scales, Belth et al. (1988) were able to calculate the change of refrigerant charge with time in each component while the system is running without the need to shut down the system. Their test setup, however, included zigzag tubes to reduce the stiffness of refrigerant lines, which caused an artificial increase in the total system refrigerant charge.

Hwang and Kim (1998) introduced experimental results showing the reaction of suction and discharge temperatures and pressure to a sudden increase in compressor speed. They concluded that refrigerant migration is the most important factor in an experimental result analysis.

The migrating refrigerant also carries some energy with it to the evaporator. Whether this energy will be transferred to the evaporator air, or remain in the refrigerant, depends on the temperature of the evaporator air and the evaporator. If the evaporator heats up to a temperature higher than the air temperature, it will heat the air, and then this energy will represent extra load on the system when it is switched on. The amount of energy that is carried with the migrating refrigerant to the evaporator air was estimated by Rubas and Bullard (1995) for a household refrigerator to be 4% of the steady state capacity in case of liquid migration, and 7% of the steady state capacity in case of vapor migration.

Ehrbar et al. (2003) investigated the capacity reduction in on/off operation of heat pumps in heating mode using computer simulation and experiments. The evaporator

was modeled as a 3-storage model: one for the refrigerant, one for the metal structure, and one for the heat source. The condenser was designed as a 4-storage model (in case of shut down as 3-storage model). The thermostatic expansion valve is modeled only as a node, without storage. Ehrbar et al. concluded that the start-up time constant increases with an increasing temperature difference between the heat source and the heat sink.

Mithraratne et al. (2002) turned their attention to hunting (the cyclic change in expansion valve position). They showed that for a fixed static superheat setting (SSS) the amplitude of hunting oscillations increases with decreasing heat load. When the heat load was fixed, the amplitude of hunting increased with decreasing SSS. Increasing the time constant of the thermostatic expansion valve bulb decreases the amplitude of hunting.

Judge and Radermacher (1995) experimentally compared the transient and steady state performance of HFC407C with HCFC22. Their results indicated that the cyclic losses of HFC407C in the cooling and heating modes are higher than those of HCFC22 by 23.3% and 11.3%, respectively.

Murphy & Goldschmidt (1985) focused their transient numerical analysis on the condenser and liquid line during start-up. They were able to achieve that by modeling the condenser, the compressor, and the capillary tube but using experimental data to substitute for evaporator performance. Two conclusions can be drawn from their research. First, an oversized condenser reduces the start-up pressure peak and hence the compressor power, but it also reduces the initial capillary tube flow rate and therefore, it does not contribute to the overall improvement of start-up performance. Second, the longer the liquid line the slower the system will be in reaching steady state because of the delay in flooding the capillary tube.

Ataer (2004) focused on the transient behavior of a finned-tube cross-flow heat exchanger. His analytical model can predict the reaction to a step change in the inlet temperature of the hot fluid.

The second law of thermodynamics, in particular the non-dimensional entropy generation, was used by Ratts and Brown (2000) to quantify the thermodynamic losses of the individual components of a cycling-clutch orifice-tube refrigeration system. Their experimental results show that compressor cycling and thermal dissipation in the condenser are the biggest sources of losses. Compressor cycling increases the average operating compression temperature ratio while decreases the average operating pressure ratio and therefore the isentropic efficiency of the compressor decreases with the increase in compressor cycling. They suggested that using a variable capacity compressor could improve compressor efficiency.

Murphy and Goldschmidt (1979) and Goldschmidt et al. (1980) concluded that the transient losses due to cycling differs for a heat pump in cooling and in heating modes and therefore the losses are not a function of only the thermal mass of the coils. They suggested that the losses depend on the thermostat setting and the dead-band.

Katipamula & O'Neal (1991) identified five variables that affect transient performance of heat pumps: percent on time, thermostat cycling rate, indoor temperature, outdoor temperature & indoor relative humidity. They concluded after a review of literature that losses due to transient effects can be as much as 20%. A combination of high cycling rate and low percent on-time caused maximum losses in capacity.

Tassou et al. (1983) compared between a system with variable speed compressor and a system with fixed speed compressor in on/off operation. The capacity modulated system, with a speed reduction limitation of half the compressor rated speed, can offer more than 10% improvement in seasonal energy utilization efficiency over the conventional system.

Vargas and Parise (1995) used a power law control action to provide the necessary compressor speed variations according to ambient conditions. They compared between this variable speed compressor and on/off control and concluded that variable speed control allows for less oscillations in room temperature and also saved 11% energy in 500 seconds.

Didion and Kelly (1979) proposed a new rating procedure for seasonal performance of heat pumps, which included part load cyclic tests and steady state tests. The new rating is based on Cooling Seasonal Performance Factor in cooling mode and Heating Seasonal Performance Factor in heating mode.

In 1993, O'Neal & Katipamula suggested the use of a non-dimensional time variable in modeling the on/off cycling performance. They argued that the non-dimensional time proposed captures the primary influences of cycling losses: system time constant, fraction on-time, and cycling rate.

1.3 Automotive Air Conditioning

Figure 1.3 shows an air conditioning system of a car (Althouse et al. 2000). Automotive air conditioners, also known as mobile air conditioners (MACs), are typically equipped with open-type compressors that are belt-driven from the engine of the vehicle and therefore run at a variable rotational speed. The rotational speed of the compressor varies between a low value in idling case and a high value in driving case. Figure 1.4 shows a U.S.A. standardized drive cycle used for testing the exhaust gas emissions of cars. The air face velocity on the outdoor coil, which is placed in the front of the vehicle, also changes, within limits, according to the vehicle traveling speed.

To deliver enough capacity at any rotational speed, MACs are usually fitted with charge management devices such as suction accumulators or receivers. These devices store an amount of refrigerant that becomes available to the system in cases of high

loads or high compressor rotational speeds. The side effects of these devices are additional thermal mass to be readjusted and an increased refrigerant charge that need to be redistributed in the system and therefore a longer transient period. Indeed the automotive air conditioners have more variables that change with time and operate for more time in a transient state that they represent a bigger challenge than any other application.

Figure 1.5 shows, from the moment of turn-on, the power consumption and the capacity as a ratio of the steady state capacity of an automotive system running at a constant rotational speed. The area above the capacity curve is what is called the transient losses. The ratio of the capacity over the power consumption is called the coefficient of performance (COP). Figure 1.5 also shows how the COP changes with time. The pull down test shown in this figure is done with recirculated air. It might take up to 30 minutes to reach steady state with fresh air return. By simple integration according to the formula in Equation 1.2, the transient loss in the first 15 minutes of operation can be calculated as 11% of the delivered capacity. If it is further assumed that the system would turn off for 5 minutes for every 15 minutes of operation, then the transient losses in an hour would be 33%. That is 33% more capacity could have been delivered if the operating parameters of the system would to stabilize as soon as the compressor runs.

$$Loss = \frac{\int (Q_{ss} - Q)\,dt}{\int Q\,dt} \qquad 1.2$$

1.4 The Importance of Mobile Air Conditioners and Their Economic and Environmental Impact:

Contrary to what many people believe, automotive air conditioners are not just devices for comfort. Automotive air conditioners are important for the following reasons:

- They maintain the driver's alertness by providing suitable weather conditions in the cabin.
- They provide demisting to maintain visibility, as mandated by the Federal Motor Vehicle Safety Standard number 103 (National Highway Traffic Safety Administration, 1999), which specifies that "each vehicle shall have a windshield defrosting and defogging system."
- They save energy, in comparison to opened windows at vehicle speed higher than 45 mi/hr (Meyer et al., 2003 and Hill et al., 2004) and depending on vehicle and air direction.

Table 1.1 is taken from Bahatti (1999) and it shows that in 1997, 84.5% of the cars in U.S.A. were air conditioned, while this ratio worldwide was only 46.8%. Martini et al. (2003) mentioned that in 1995 more than 90% of the new cars sold in U.S.A and Japan were equipped with an air conditioning system. However, the benefit of having an air conditioner in the automobile does not come without a cost. Eighty percent of the oil that U.S.A. imports is used just for driving cars and light trucks (Lovins et al., 2004). Figure 1.6 (Lovins et al., 2004) gives a more detailed break-down of U.S.A. oil consumption used in the transportation section.

The MAC requires a vehicle to burn more fuel, not only to operate it, but also due to the additional weight of its components. The extra fuel consumption means more exhaust gas emissions. There are also the refrigerant emissions resulting from normal operational leakage, leakage due to accidents, and leakage due to end-of-life disposal of the air conditioning system (Shwartz et al., 2002). This gives to the automotive air conditioner both an environmental significance as well as an economic one. Hwang (2004) reported that 8% of the automotive section global warming emissions are caused by the A/C. Martini et al. (2003) from Fiat reported that during an urban drive cycle the A/C system can increase fuel consumption by up to 70%. While Hendricks from the National Renewable Energy Laboratory (Hendricks, 2003) reported that during the SCO3 drive cycle – which is a U.S.A. standardized test for measuring exhaust gas emissions published by the EPA - the average impact of the A/C system over a range of light-duty vehicles was to increase 1) fuel consumption by 28%, 2)

carbon monoxide emissions by 71%, 3) nitrogen oxide emissions by 81%, and 4) non-methane hydrocarbons by 30%.

1.5 The Challenges in Dynamic Testing

Figure 1.7 shows a typical laboratory test facility for testing the performance of heat pumps. It is composed of an outdoor environmental chamber and an indoor environmental loop (or sometimes chamber). The outdoor chamber houses the outdoor unit of the heat pump. Automotive condensers are usually placed inside an open-ended duct with a fan to control the airflow rate across them. The indoor loop is a closed air loop that houses the evaporator and circulates a certain rate of airflow to facilitate accurate calculation of evaporator airside capacity. Both the chamber and the loop have air-handling units that condition the air temperature and relative humidity to desired values that depend on the requirements of the test being conducted and maintains these values constant. Such a facility is suitable only for conducting steady state tests.

Referring to Figure 1.2, it is clear that in the transient state the refrigerant-side capacity is not equal to the airside capacity. The difference between them is the thermal storage term $m_{sys} C_{sys} dT_{sys} / dt$ of the heat pump, which includes thermal mass of the refrigerant and the thermal mass of the materials (usually metals) of which the system is constructed. The thermal storage of the conditioned space itself, which is composed of a sensible term $m_r C_r dT_r / dt$ and a latent term $m_r dW_r / dt$, in turn reduces the cooling capacity that is applied to the load. Thermal storage terms are time dependent, i.e. the condition of air that returns to the evaporator changes with time depending on the heat capacity of the conditioned space.

Simply put, if the same heat pump is used to cool down two places that are different in heat capacity (e.g. size), the time that it takes to reach a specific temperature will be longer for the place with higher heat capacity. Therefore, testing an air conditioner during the transient period of operation is impossible without installing it in the space it is intended for. Except in the case of operation with 100% fresh air return where the

conditioned space in this case does not affect the conditions of the air at the inlet of the evaporator coil.

If the conditioned space was a refrigerator, it is relatively easy to place it inside an environmental chamber. But if the conditioned space was a car cabin, it becomes more challenging to place it inside a laboratory. To meet this need, big automotive companies construct wind tunnels large enough to house a car. Figure 1.8 (Behr, 2004) and Figure 1.9 (Hill et al., 2004) show examples of such wind tunnels. It is clear from the pictures how big and costly these wind tunnels can be. The financial capability of owning these wind tunnels is only within the reach of the few. To the best of the author's knowledge, there are no universities that have dynamic testing capability for automotive systems.

The question might be raised about how researchers conduct transient tests currently. Prototype tests are normally performed on roads or tracks or in wind tunnels. However, road and track tests do not yield repeatable data compared to the controlled environment conditions tests in wind tunnels (Ghani & Aroussi, 2001 and Ghani et al. 2000). Numerical modeling also is a popular tool in dynamic automotive A/C testing. Perez et al. (2003), El Bakkali et al. (2003), Kampf et al. (2003), Magnetto et al. (2003), Hager et al. (2003), and Schlenz et al. (2002) are just a few of the researchers who have resorted to this method. By referring to Figure 1.10, a survey of 60 literature articles published between 1999 and 2004 indicated that 18% of the research work was conducted numerically, 71% was conducted on real cars (on road, track, or in wind tunnel), and 3% used a scaled down physical model of the car. Researchers from Luxembourg (Idris & Cowell, 2003) conducted their field tests on a vehicle in North Sweden to investigate ice build-up in automotive heat pumps. Hrnjak (2002) and Hrnjak and Hill (2003) used a hot water heat exchanger placed in the same duct as the evaporator to impose some thermal storage effect in order to evaluate the thermal performance and efficiency of various automotive refrigerants and cycle options. This method, however, is not capable of providing a realistic load profile on the evaporator.

1.6 Objective, Focus, Selected Approach, Expected Benefits, and Plan of Research

It is the goal of this research to conduct transient tests on air conditioning systems in a laboratory environment under realistic dynamic conditions. This allows investigating the transient losses and thus improving the transient performance of air conditioning systems. It is the objective of this research to measure performance variables, such as latent and sensible load that are not available for measurement in an actual vehicle.

The focus will be on automotive climate control systems in the cooling mode. By conducting laboratory experiments on MACs, important performance indicators, such as the sensible capacity and latent capacity, will be readily measurable while otherwise difficult or impossible to measure in field tests. The moisture removal during cycling is of particular importance due to the difficulty of measuring it in field tests.

The selected approach is to substitute the car with computer software that adjusts the conditions inside the typical environmental test chamber and test loop to the air conditions that would occur inside a real vehicle. This way, the air-handling unit of the environmental loop would have replaced the cabin loads and the conditions of the return air to the evaporator coil would have been adjusted to the return air conditions from a real car cabin. And thus, the air conditioning system behaves just like if it was placed in a real vehicle.

It is expected that this approach will reduce both the development costs and the required time of evaluating the dynamic performance of MACs by combining simulation and experimentation. It has the potential of reproducing more realistic results than pure numerical simulations. Moreover, it will contribute to the overall quality of MAC research and development by putting affordable testing capabilities within the reach of more research institutions. This approach is most useful on the prototype-testing level, but also starting from the design stage until the final-product evaluation stage.

To achieve the proposed goal, the following research tasks are identified:

1. Simulate the car cabin thermal behavior in a numerical model.
2. Verify the cabin model.
3. Add control capabilities to the existing steady state test facility.
4. Verify the accuracy of the control.
5. Build and instrument a test system.
6. Run steady-state verification test for energy balance.
7. Run transient tests.
8. Evaluate test data.
9. Update simulation model and compare to experimental results.

In the remaining part of this dissertation, chapter two will include the numerical cabin thermal model and its verification, chapter three will describe the changes introduced to the test facility and the accuracy of the control, chapter four will give the specifications of the test system, chapter five will present and discuss the test results, and chapter six will introduce a simulation effort made on the whole-system level, whose results to be compared with the experimental results.

Table 1.1 1997 Cars Census (Bahatti, 1999)

	U.S.A. Fleet	World Fleet
Number of Vehicles	198×10^6	647×10^6
Number of Vehicles with A/C	168×10^6	303×10^6
Ratio of A/C Vehicles / Total	84.5%	46.8%

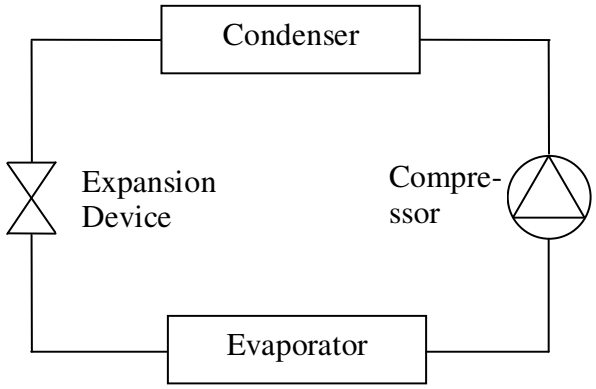

Figure 1.1 Schematic of The Basic Vapor Compression System

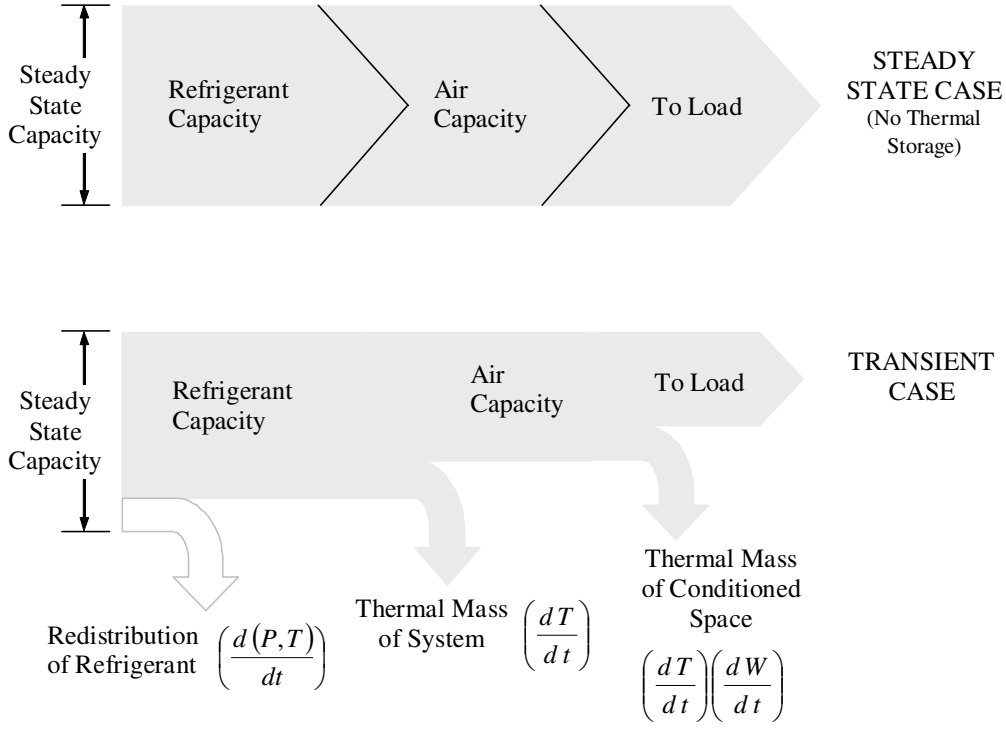

Figure 1.2 Energy Flow in Start-up Case vs. Steady State Case

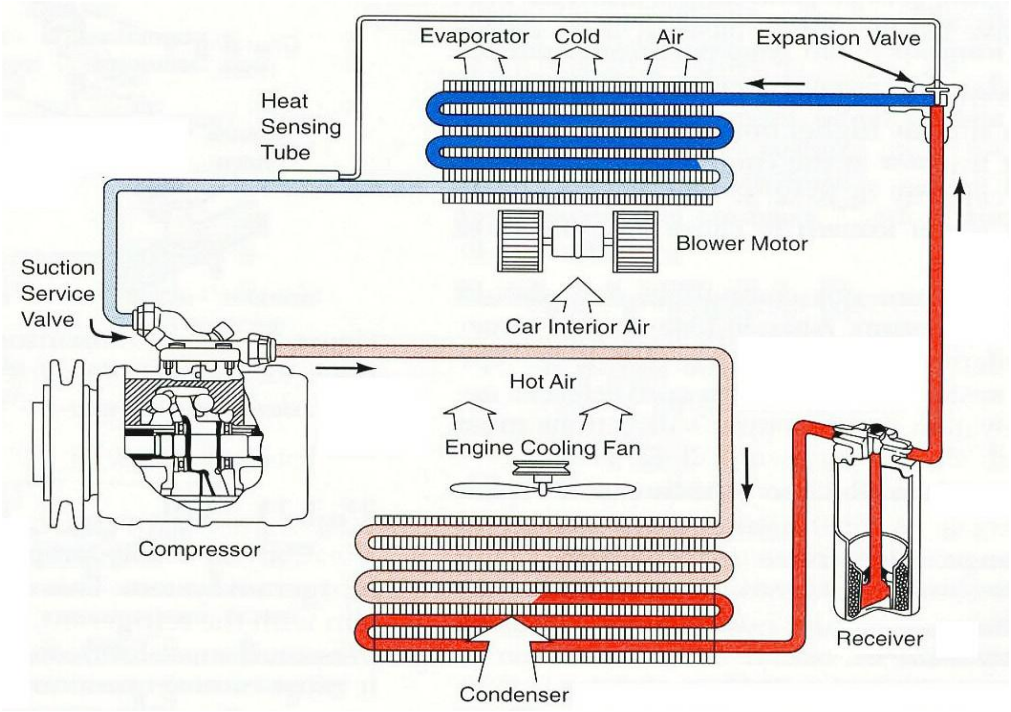

Figure 1.3 Typical Automotive Air Conditioning System

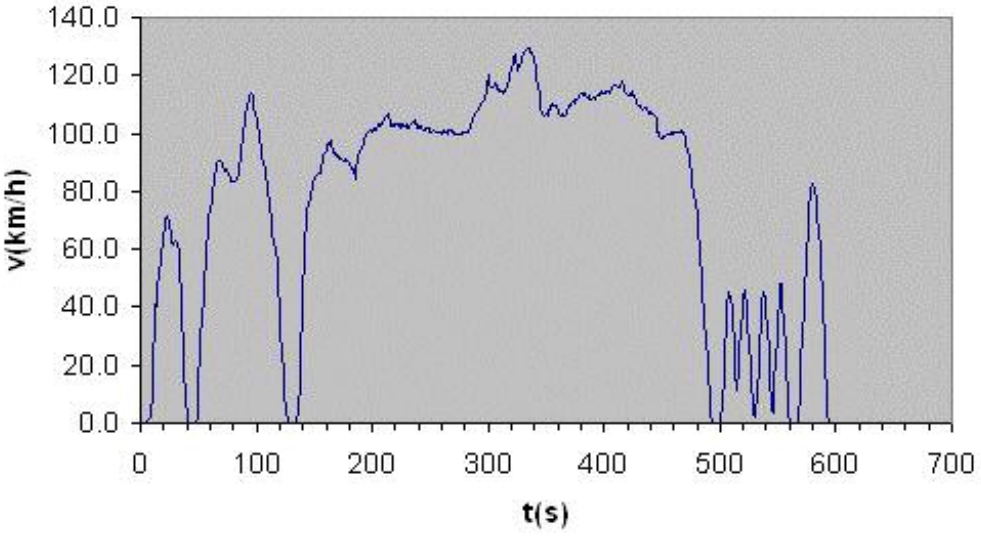

Figure 1.4 US06 Standard Drive Cycle

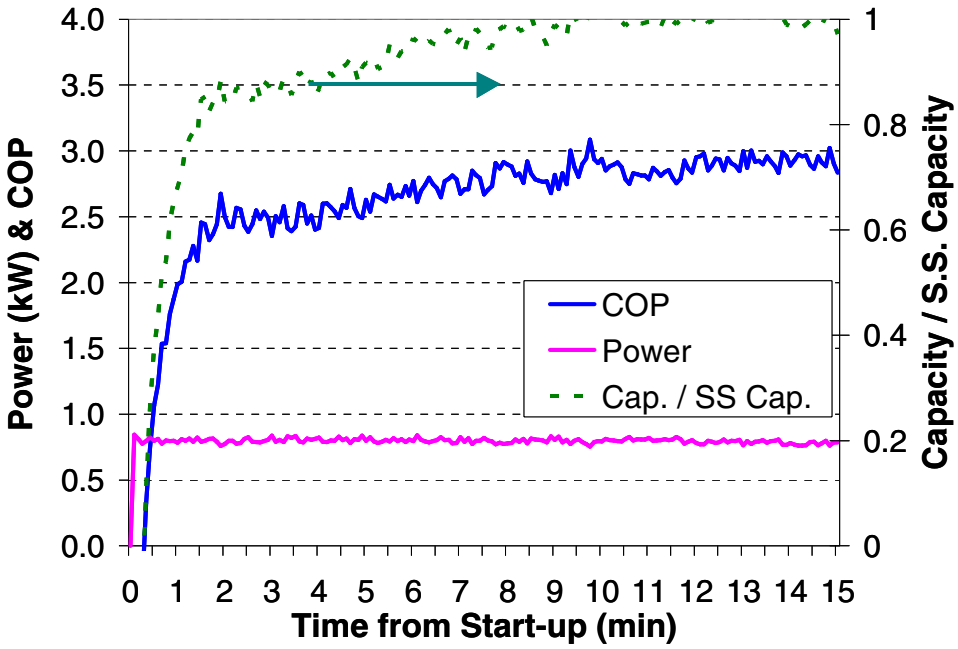

Figure 1.5 Capacity, Power Consumption and Coefficient of Performance During Start-up of an Automotive System (Laboratory Data)

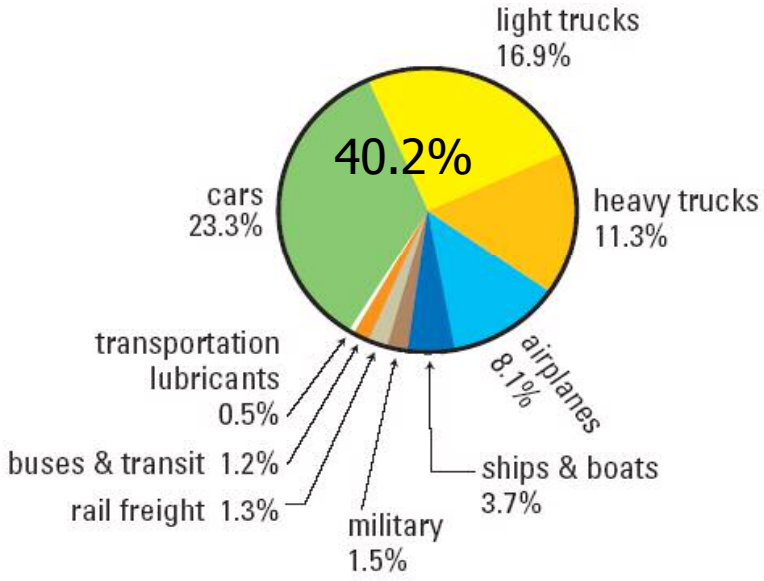

Figure 1.6 Breakdown of U.S.A. Oil Consumption for the Transportation Sector in 2000

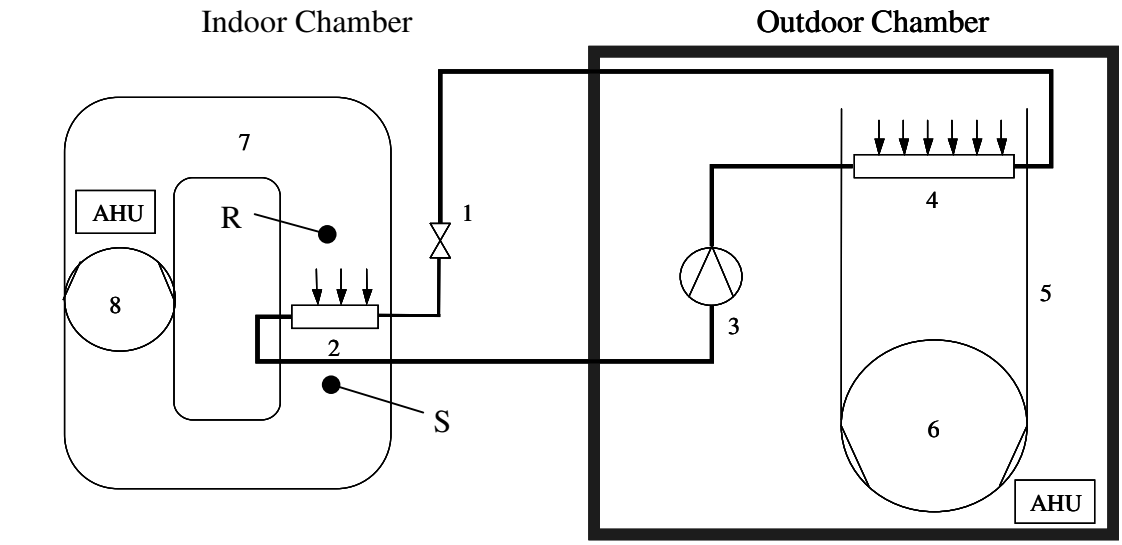

1: Expansion device, 2: Evaporator, 3: Compressor, 4: Condenser, 5: Condenser air duct, 6: Condenser fan;
7: Evaporator air duct; 8: Evaporator fan, R: Return air section, S: Supply air section.

Figure 1.7 Typical Laboratory Test Facility for Steady State Testing

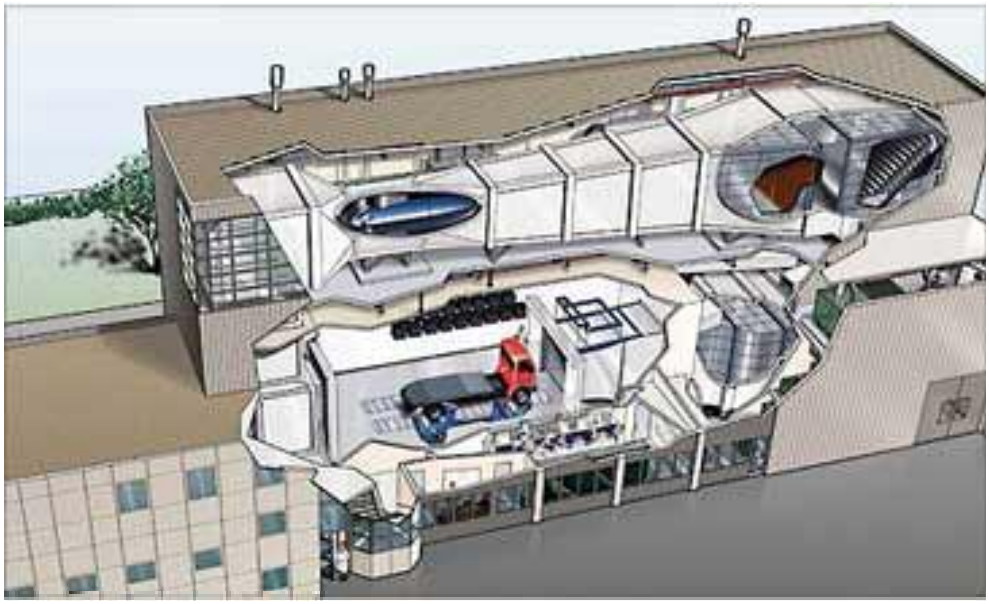

Figure 1.8 Wind Tunnel of Behr GmbH (www.behrgroup.com)

Fan Power = 315 kW, Heat Exchanger Face Area = 33 sq. m)

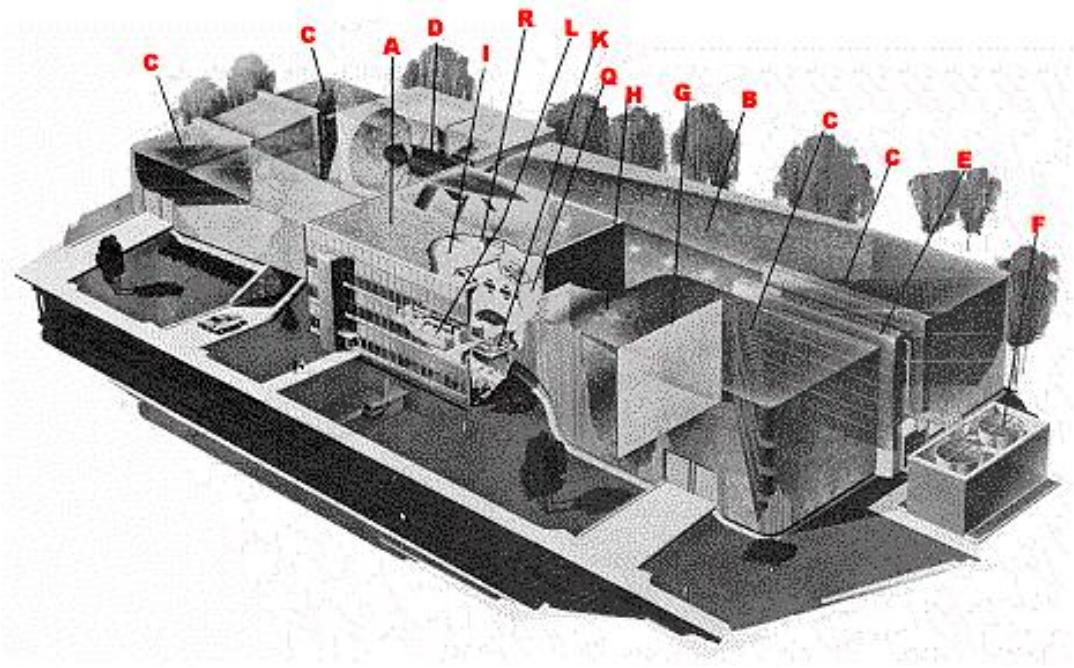

Figure 1.9 Wind Tunnel of General Motors Corp. (Hill et al., 2004)

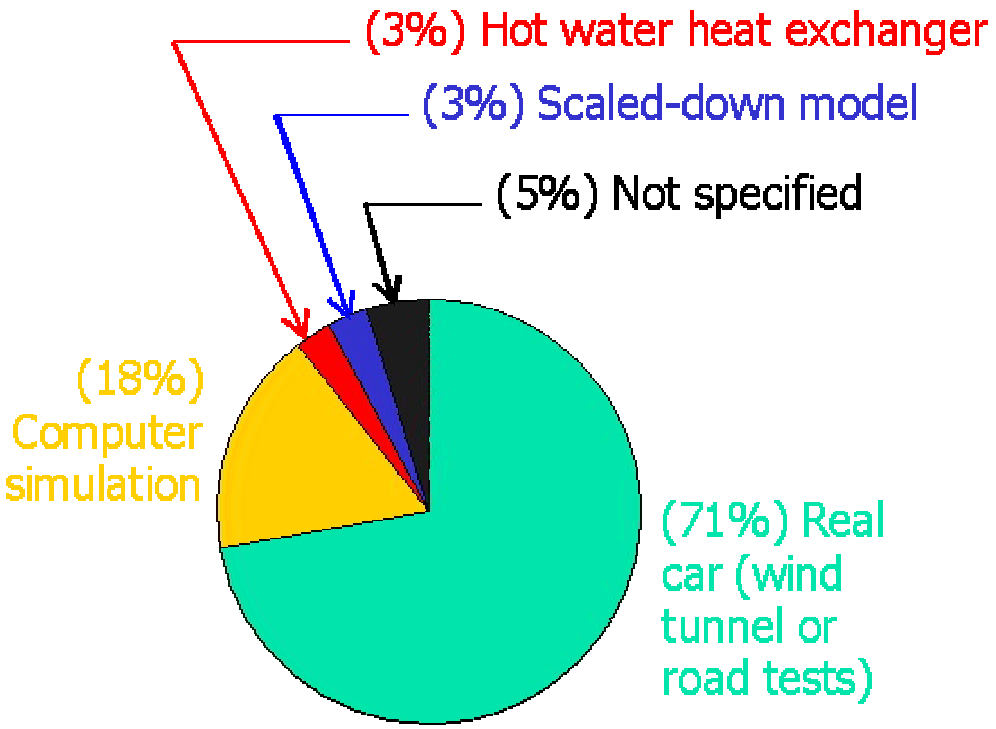

Figure 1.10 Results of Literature Survey on Dynamic Automotive Testing

Chapter 2: The Cabin Model

2.1 Introduction

The cabin model is a transient simulation of the thermal behavior of the passengers' compartment of an automobile. Its main purpose is to communicate in real time with the controller of an air-handling unit of the psychrometric loop housing the evaporator of an automotive climate control system under test. The test facility and the test system will be described in details in Chapters 3 and 4, respectively.

Its inputs are: a brief description of the physical and thermal characteristics of the cabin, thermal loads on the cabin (e.g. number of passengers, condition of ambient air, and solar incidence), passengers' control settings (e.g. fan speed and temperature setting) and the mode of air supply to the cabin (e.g. recirculated air or fresh air or mixture between them). The model uses these inputs to calculate the condition of the air that returns to the evaporator of the climate control system and to control thermostat actions. The condition of the air in the psychrometric loop is then adjusted to the calculated return air condition so that the dynamic behavior of the climate control unit can be tested and evaluated as if it is installed in a real vehicle. That is to say the cabin model simulates real-world boundary conditions around the climate control unit being tested and eliminates the necessity of testing a complete vehicle.

The functions of the thermal simulation software can be listed as follows:

1. To measure the conditions; i.e. temperature and relative humidity of the air downstream of the evaporator coil; i.e. the supply-air conditions. The supply-air is at the section designated "S" on Figure 1.7.
2. To calculate, using a numerical simulation model, the effect of a specific pre-chosen real car cabin on the supply-air and therefore determine the conditions of the return-air; i.e. the conditions of the air leaving the cabin going back to the evaporator coil.
3. To control the air-handling unit of the indoor loop such that the air temperature and relative humidity are adjusted according to the return-air

conditions calculated using the simulation model. The return-air is at the section designated “R” on Figure 1.7.

It is further required to be able to run climatic profiles (such as a variation of temperature and relative humidity with respect to time) and standardized drive cycles on the air conditioning system under test. And therefore the software would have the additional function of controlling the rest of the boundary conditions, such as the air conditions in the outdoor environmental chamber and the rotational speed of the compressor and the rotational speed of the fan moving the condenser air.

To fulfill its purpose, the model must have the following features:

- It has to be quick enough to be used in real-time calculations. The simulation time should be less than the actual time step.
- It has to be easily integrated with data acquisition and control software.
- It should be accurate. It should take into consideration the latent as well as the sensible loads, viz. heat transfer, solar, persons, thermal storage, and the infiltration or ventilation loads.

2.2 Review of Previous Cabin Models

Ding and Zito (2001) presented a first order differential equation that relates the cabin heat transfer coefficient, panel discharge temperature and volumetric air flow to average cabin air temperature. They suggested a method to experimentally determine overall heat transfer coefficient of the cabin but their model neglected thermal storage and latent loads as well as infiltration and passengers’ loads. Other researchers; Choquart et al. (2003), Huang and Han (2002), Han et al. (2001), and Aroussi and Aghil (2001); used CFD models to predict the cabin air conditions and obtained good agreement between their results and experimental results. CFD models require detailed dimensions of the cabin and the locations of the air vents and can produce detailed results of the spatial variation of the velocity and temperature fields inside

the cabin and therefore are more suitable for assessing the thermal comfort of passengers or evaluating defrost conditions.

Huang (1998) developed a mathematical model that predicts the lumped temperature and humidity variations inside the cabin under design and operating conditions. The model is composed of four coupled nonlinear ordinary differential equations; namely, dry-air mass balance, moisture mass balance, cabin-air energy balance, and interior-mass energy balance. However, the model uses a constant built-in ventilation rate and does not allow the change of supply airflow rate. Moreover, this model requires detailed information about the construction of the cabin, its color, characteristics of the glass, location of car, ground solar reflection coefficient, as well as height and weight of passengers. Khamsi and Petitjean (2000) modeled both the cabin and the A/C system components. Their model is based on a modular concept in which the elementary models of each component are coupled with the models of the other components. Very little is described in their work about the equations they used to model the cabin and the method of solution. Similar deficiencies exist in the works by Thelon and Zoz (2003) and Kohler et al. (1996). Kataoka (2001) used Navier-Stockes equation and the energy equation to predict the air velocity and temperature distribution in the cabin. He employed finite elements method based on the Cartesian coordinate system in spatial integration where a first order upwind scheme is applied to convection terms. For this, he divided the whole region into small cubic elements and therefore required very detailed geometric inputs. Roy et al. (2003) studied the thermal heat transfer in a car cabin and its effect on the equivalent temperature of the cabin and concluded that the radiative heat transfer is the most significant source responsible for energy consumption and passengers' discomfort. Their study employed in-house software. Several other commercial packages are available, such as KULI (Magna – Steyr, 2001) and MACSim (ARMINES, 2002), but these packages include closed-source software that can't be adapted to the present purpose.

From the foregoing literature review it is apparent that there is no model that can readily serve the present purpose and that a new model has to be developed.

2.3 The Cabin Model

2.3.1 The Physical Model

The physical model of a cabin is shown in Figure 2.1. Ambient air at condition T_{amb} and RH_{amb} surrounds the cabin. The seats, dashboard, and other objects installed inside the cabin are collectively referred to as the "interior mass" and referred to by using the suffix "c". After passing through the evaporator coil, the air is supplied to the cabin at condition T_s and RH_s, where it is heated to the cabin condition T_r and RH_r due to various thermal loads, namely, heat transfer with ambient air, solar radiation, and load due to passengers and ventilation or infiltration air. Other transient-period loads include thermal storage in interior mass and cabin air as well as convection from the interior mass. The condition of the air upstream of the evaporator coil is T_m and RH_m which is either the same as ambient air in 100% fresh air mode, or the same as the cabin air in 100% recirculated air mode (with or without infiltration), or it is a mixture between cabin air and ambient air.

2.3.2 Model Assumptions

The following are the basic assumptions of the cabin model:

- Solar load is constant. This is true for relatively short test periods.
- Radiation from cabin components to air is neglected due to the small difference in temperature.
- Latent and sensible load due to each passenger is constant.
- Heat transfer from engine compartment, trunk, and floor are neglected. This is due to the thermal insulation between these spaces and the cabin, as well as the lack of forced convection between them.
- Thermal storage in cabin walls is neglected for simplicity.
- Coefficient of heat transfer does not change with vehicle speed. Meyer (2002) reported that in the range between 32 km/h to 128 km/h the heat transfer coefficient is essentially constant. This is because the most significant component of the overall hat transfer is the internal convection.

- Heat transfer along air ducts is neglected.
- Properties of air and of interior mass are spatially uniform (lumped capacitance method). This is supported by the fact that the air is supplied to the cabin through several vents at different locations. Several researchers; Ding and Zito (2001), Huang (1998), Rugh et al. (2001), and Kojima et al. (1999), have used this assumption with acceptable results.

2.3.3 The Numerical Model

For simplicity, the cabin sensible and latent loads are treated separately, i.e., there is one set of equations that has temperature as the main variable and another set with humidity as the main variable. However, the air properties are calculated at the corresponding temperature and humidity in each time step. This method has provided acceptable results as will be shown later in the verification section. The sensible part of the cabin model is given by Equations 2.1, 2.2, and 2.3 which represent the energy balance of cabin air sensible heat, energy balance of interior mass, and adiabatic mixing of dry air, respectively.

$$M_r C_{pr} \frac{dT_r}{dt} + M_c C_c \frac{dT_c}{dt} = -m_e C_{pe}\left(T_m - T_s\right) + Q_{sol} + Q_{ps} + U_o A_o \left(T_{amb} - T_r\right) + m_{iv} C_{p,amb}\left(T_{amb} - T_r\right) \quad 2.1$$

$$M_c C_c \frac{dT_c}{dt} = -h_c A_c \left(T_c - T_r\right) \quad 2.2$$

$$m_{iv} C_{p,amb} T_{amb} + \left(m_e - m_{iv}\right) C_{pr} T_r = m_e C_{pm} T_m \quad 2.3$$

The two storage terms on the left hand side of Equation 2.1 are the thermal storage in the cabin air and in the interior mass, respectively. It is assumed that the constituents of the internal mass have the same specific heat and temperature. The only load that is constantly cooling down the air is the sensible capacity of the evaporator, which shows as the first term on the right hand side of Equation 2.1. The second term on the

right hand side of Equation 2.1 represents the portion of the solar radiation that is transmitted to inside the cabin through the glass and the metal of the cabin body. The third term is the sensible load due to passengers. The fourth term on the right hand side is the heat transfer (combined convection and conduction) with ambient air. For simplicity, this term assumes a single average value of the overall heat transfer coefficient for all the glass areas and the sheet metal areas of the cabin regardless of their orientation. The heat transfer with ambient air can be a heating load if the cabin air is colder than the ambient air or can be a cooling load if the cabin air has been hot-soaked by solar radiation to a temperature higher than the ambient temperature. The last term to the right hand side of Equation 2.1 represents the load on the cabin air as a result of introducing infiltration or ventilation air at the ambient condition to the evaporator coil. The second, third, and fourth terms on the right hand side of Equation 2.1 are what are usually referred to as the room sensible load in air conditioning load calculations, while the fifth term is what is usually referred to as the outside sensible load. At steady state, the evaporator sensible capacity must be equal to the room and the outside sensible loads. Equation 2.2 simply states that the change in the internal energy of the interior mass must come through convection at its boundary. Equation 2.3 is the adiabatic mixing of dry air at the mixing point just before the evaporator coil.

Similarly, two equations are solved for humidity, namely, cabin air latent energy balance, and moisture mass balance at the mixing point before the coil. These equations are provided as Equations 2.4 and 2.5, respectively, which represent the latent part of the cabin model.

$$M_r\, h_{fg}\, \frac{dW_r}{dt} = -\,m_e\, h_{fg}\, (W_m - W_s) + m_{iv}\, h_{fg}\, (W_{amb} - W_r) + Q_{pl} \qquad 2.4$$

$$(m_e - m_{iv}) W_r + m_{iv}\, W_{amb} = m_e\, W_m \qquad 2.5$$

The term to the left hand side of Equation 2.4 is the change in the latent energy of the cabin air over time, which is caused either by the dehumidification of moisture on the evaporator coil (first term on the right hand side) or by the introduction of infiltration

or ventilation air (second term on the right hand side) or passengers' latent load. Equation 2.5 is a mass balance on the water vapor; it resembles Equation 2.3 with the substitution of the humidity ratio W instead of enthalpy of dry air (C . T).

2.3.4 Inputs and Outputs

The following variables are measured and fed to the model as inputs:

- Supply air temperature T_s
- Evaporator airflow rate m_e
- Supply air humidity ratio W_s.

The model calculates and produces as output the following variables:

- Cabin air temperature T_r
- Interior mass temperature T_c
- Mixture air temperature T_m
- Cabin air humidity ratio W_r
- Mixture air humidity ratio W_m.

All the other parameters are considered constant and are entered by the user. The most significant output is the return air conditions. These conditions are used to control the air-handling unit of the psychrometric loop to simulate real-world conditions.

2.4 Solution of Cabin Model

The solution is obtained numerically for the two sets of equations by marching in time and substituting Δt for dt and $(T_i - T_p)$ for dT, where the subscript i refers to the present iteration and p refers to the previous one (Euler method). The numerical method was chosen for simplicity of integration with the simulation software.

Equations 2.1, 2.2, and 2.3 are solved for the cabin air temperature T_r, interior mass temperature T_c, and temperature of return air to evaporator coil T_m. The three sensible model equations are rearranged in the following linear form:

$$x_{11} T_{ri} + x_{12} T_{ci} + x_{13} T_{mi} = x_{14} \quad 2.6$$

$$x_{21} T_{ri} + x_{22} T_{ci} + x_{23} T_{mi} = x_{24} \quad 2.7$$

$$x_{31} T_{ri} + x_{32} T_{ci} + x_{33} T_{mi} = x_{34} \quad 2.8$$

The resulting three equations can be simply solved by one of many available numerical methods; the method that was used in this work is the Gauss-Jordon method. The same procedure is followed with Equations 2.4 and 2.5 and the equations are solved for the cabin air humidity ratio W_r, and the humidity ratio of return air to the evaporator coil W_m. During the calculation, air properties at each time step are calculated at the corresponding values of temperature and humidity ratio using XProps software, (Thermal Analysis Partners, 2005). For simplicity, C_{pe} is taken to be average between C_{ps} and C_{pm}.

2.5 Verification of The Model

There are plenty of experimental data available in the open literature about the pull-down or cyclic performance of automotive climate control systems, but none of them lists the complete properties needed to fully describe the cabin physical model and conditions at which the test was done. The most comprehensive set of values can be found in Huang (1998), which was used to verify the present model. Table 2.1 shows the values of the inputs that were used for verification.

Since Huang (1998) did not list all the values needed, some values had to be taken from other sources of literature. The overall (total) heat transfer coefficient was taken from Meyer (2002), where it was reported that its value stays almost the same at 4 W/m^2K over the range from 32 km/h to 128 km/h vehicle speed. Huang (1998) also did not give the value of the coefficient of convective heat transfer between interior mass and cabin air, and it is quite difficult to get an accurate estimate of it because of the complexity of flow pattern inside the cabin. Several values were tried until the value of 100 W/m^2K gave the best match between the model results and the

experimental results. This has made the comparison between the experimental results from Huang (1998) and the model results more like a calibration than verification. But for the purpose of applying a realistic dynamic load on the climate control system, calibration meets the requirements. The value of the coefficient of convective heat transfer between interior mass and cabin air is higher than what is expected, however, the reason can be attributed to the negligence of the heat transfer from the floor and other compartments adjacent to the cabin.

Figure 2.2 shows a comparison between the cabin air temperature from the model results and the experimental results taken from Huang (1998). The deviations of results from the experimental values have an average of 0.7°C, a maximum of 1.8°C and a standard deviation of 0.6°C.

2.6 Sensitivity Analysis

The time step used to solve the model equations to generate the solution given in Figure 2.2 is 1 second. Several other time steps were tried but it was concluded that the solution is not sensitive to the time step in the range between 0.1 second to 10 seconds. Figure 2.3 shows the results of the sensitivity study; the lines fall on one another such that they are practically indistinguishable.

To check the effect of a change in the value of the coefficient of convective heat transfer between interior mass and cabin air, h_c, another sensitivity analysis was performed. Various values of h_c between 70 W/m^{2}K and 130 W/m^{2}K were tested. If the resulting curves were to be plotted, they would not be easily distinguishable from each other. Instead, the deviation between the results and the experimental values from (Huang 1998) is given in Figure 2.4, which shows that the average deviation increases to only 0.95°C when h_c = 70 W/m^{2}K, but the maximum deviation would have increased to 2.5°C instead of 1.8°C. The highest value of the maximum deviation curve happens during the initial pull-down at around 5 minutes into the test, at which point the model gives a lower value for the cabin temperature than the experimental measurement.

2.7 Using The Cabin Model

The entire numerical model and solution scheme were programmed in LabVIEW ® software, (National Instruments, 2005), which is used for both data acquisition and control. This gave a very satisfactory degree of integration between the measurement of the model inputs, the solution of the model equations, and the availability of the model outputs for control purposes. A screen shot of the program is shown in Figure 2.5. With a 2 seconds time step, the program takes only 28 seconds to simulate a 120 minute profile in Figure 2.2.

By specifying the ambient conditions of the test (parameters 1 and 2 in Table 2.1, also shown in Figure 2.5) and the physical model of the cabin (parameters 4 to 10 in Table 2.1) to the program and running it with setting the airflow rate to zero, the program can calculate the degree of soak to which the temperature of the cabin air will raise if the car was left under the specified solar load and ambient conditions for a an extended period. Afterwards, to start testing the climate control system, the user enters the degree of soak and specifies the number of passengers and their settings (parameters 11 to 13 in Table 2.1) and runs the program simultaneously with the climate control system that is installed inside of the psychrometric loop and chamber. The program continuously measures the values of the air temperature and relative humidity downstream of the evaporator coil, as well as the air flow rate (parameters 13, 14 and 15 in Table 2.1) and calculates what the return air temperature and relative humidity should be. Accordingly, the program dynamically adjusts the air conditions upstream of the evaporator coil through a PID control circuit, as will be discussed in detail in Chapter 3.

Table 2.1 Input Values for Verification of the Cabin Model

No.	Parameter	Value	Source
1	Ambient temperature and relative humidity	43.3°C and 65%	Huang (1998)
2	Solar load	950 W	Huang (1998)
3	Degree of soaking	16.7°C	Huang (1998)
4	Surface area of cabin	30 m^2	Huang (1998)
5	Overall heat transfer coefficient of cabin wall	4 W/m^2-K	Meyer (2002)
6	Internal volume of cabin	8 m^3	Huang (1998)
7	Interior mass of cabin	200 kg	Huang (1998)
8	Specific heat of interior mass	400 J/kg-K	Huang (1998)
9	Surface area of interior mass	3 m^2	Typical value
10	Convective heat transfer coefficient between interior mass and cabin air	100 W/m^2-K	Estimated
11	Number of passengers	0	Huang (1998)
12	Amount of fresh air	0	Huang (1998)
13	Blower setting	120 g/s	Typical value
14	Supply air temperature	Profile	Huang (1998)
15	Supply air relative humidity	Profile	Typical profile

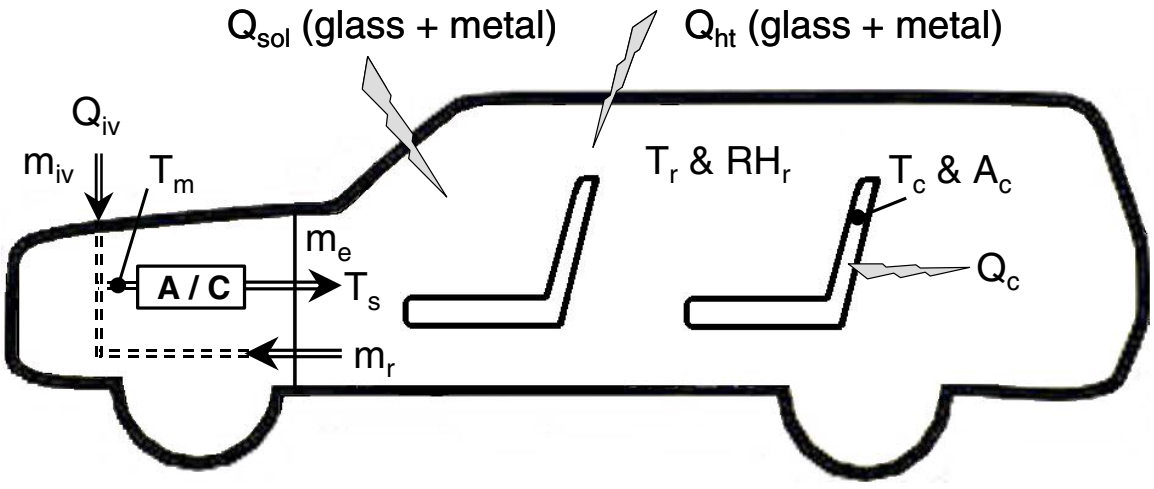

Figure 2.1 Physical Model of Passengers' Compartment and Thermal Loads

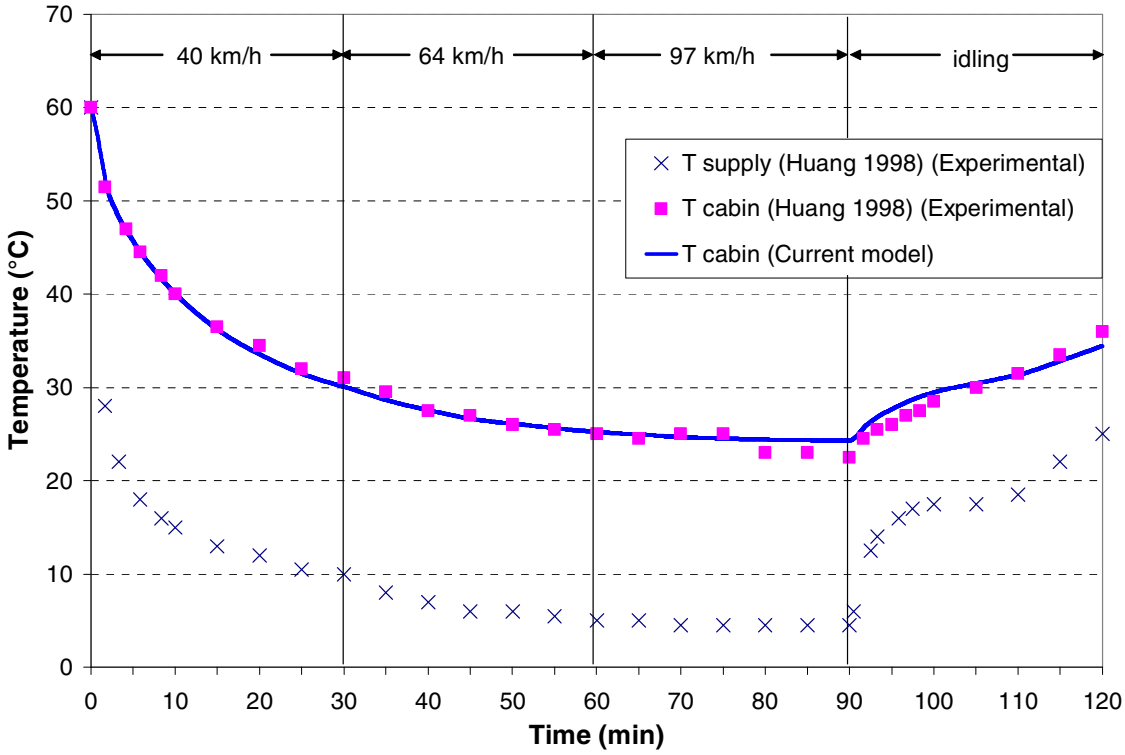

Figure 2.2 Cabin Model Verification Results

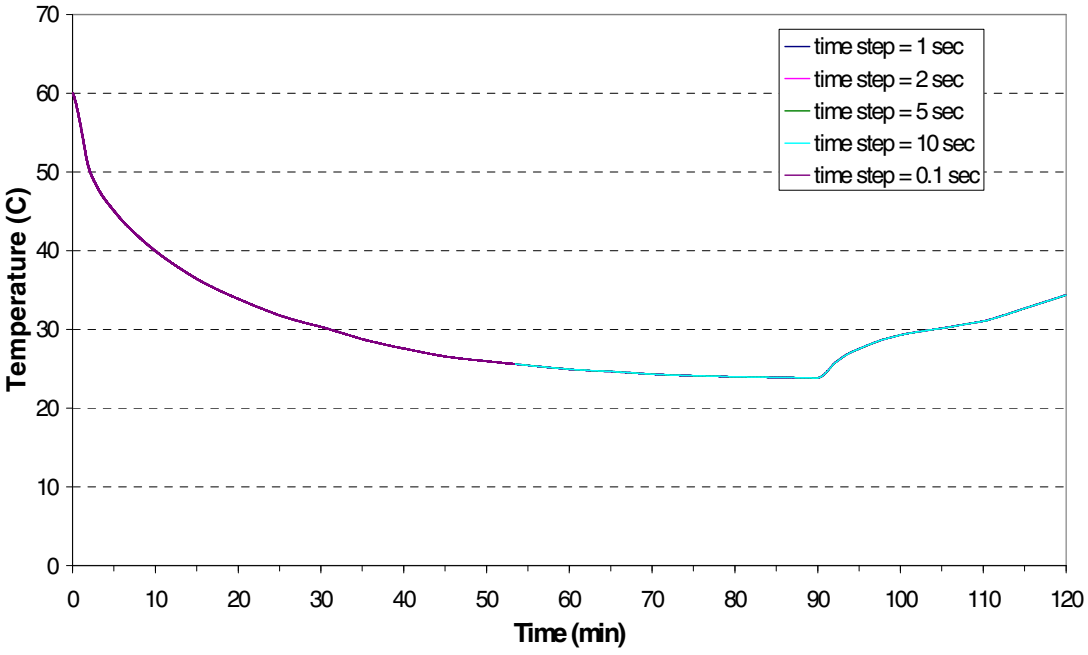

Figure 2.3 Results of Time-sensitivity Analysis

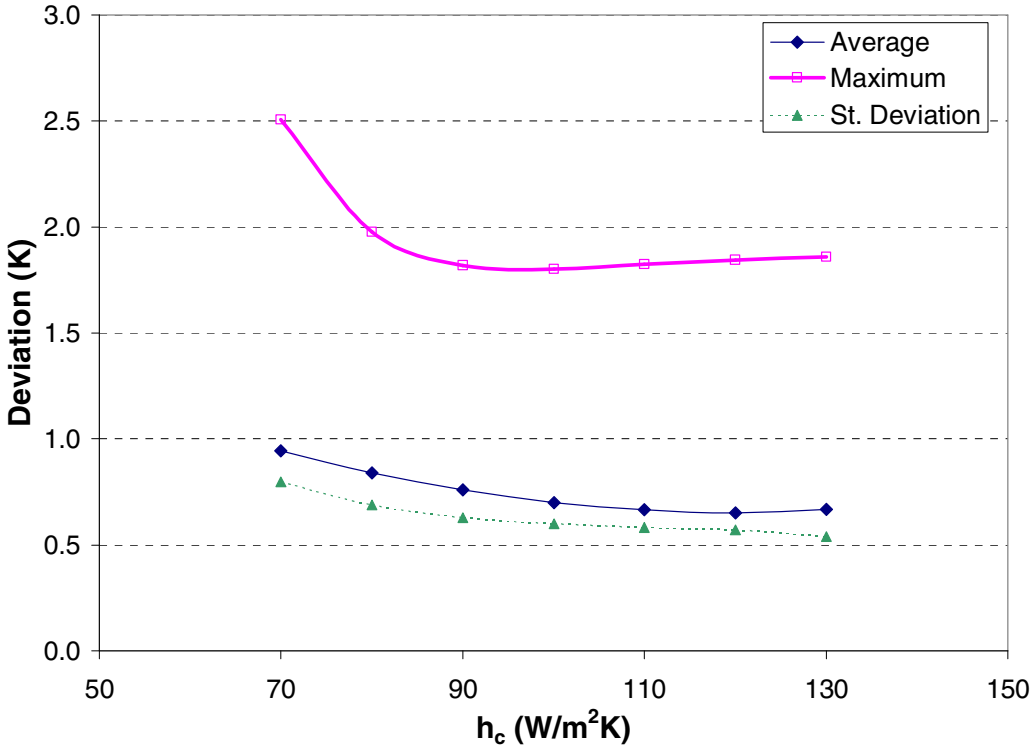

Figure 2.4 Results of h_c-sensitivity Analysis

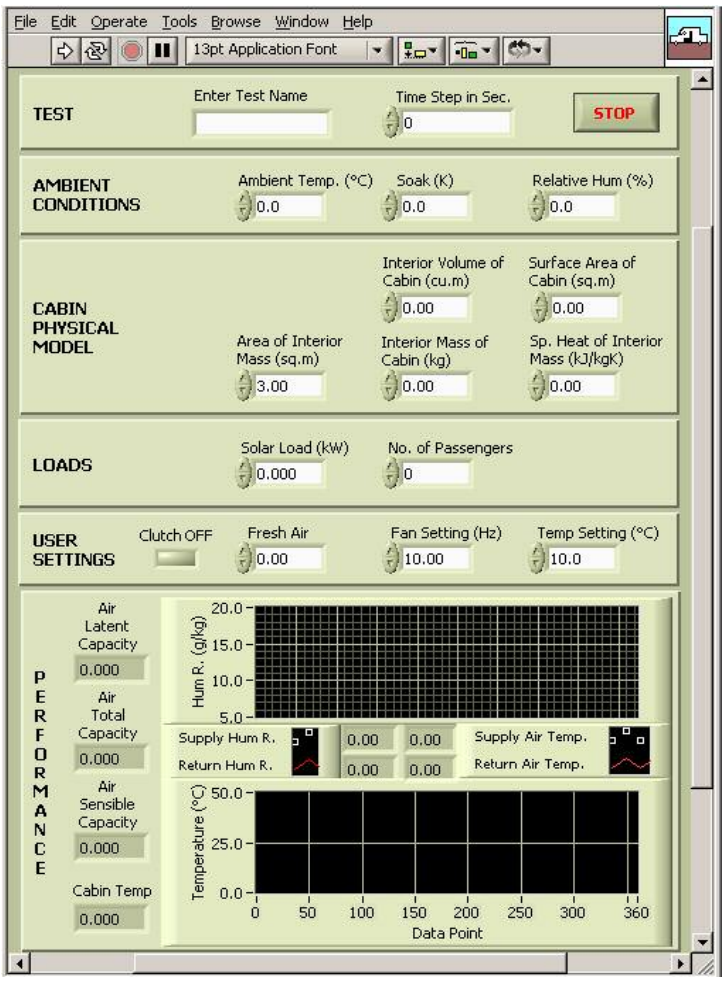

Figure 2.5 Screen Shot of the Software for Data Acquisition and Control

Chapter 3: Construction of The Dynamic Test Facility

3.1 Introduction

To be able to fully apply the dynamic boundary conditions on an automotive air conditioning system, some modifications must be made to upgrade the current steady state test facility so that it becomes able to simulate:

- Variations in air conditions
    - On the outdoor side (ambient conditions, viz. temperature and relative humidity).
    - On the indoor side (temperature and relative humidity according to the outputs of the cabin model).
- Drive cycles
    - Variations in compressor RPM due to drive patterns.
    - Variations in condenser air velocity due to drive patterns.
- User-specified settings
    - Evaporator fan speed.
    - Return air mode (fresh or recirculated or mixture).
    - Temperature setting.

These modifications, which are mainly control challenges, will complete the construction of the dynamic test facility.

3.2 The Original Steady-state Test Facility

This section describes the test facility before the beginning of the research work at hand.

The original steady state test facility is shown in Figure 1.6 and was explained briefly in Section 1.5 of Chapter One. Both the outdoor simulator and the indoor simulator have air handlers to control the properties of air inside them. Both air handlers have a DX (refrigerant) coil, electric heater, humidifier, and means for dehumidification.

Each AHU has one PID controller that controls temperature and another for humidity. The refrigeration circuit of the air handler is shown in Figure 3.1 and has a hot-gas bypass. The temperature controller actuates the hot-gas bypass valve, liquid-line valve, and the electric heater. If the controller determines there is a need for cooling it opens the liquid-line solenoid valve and closes the hot-gas bypass valve. If the controller determines there is a need for heating it turns on the electric heater. Table 3.1 describes the four different control scenarios that can happen. The humidity control is simpler; whenever there is a need for humidification the humidifier is on, and whenever there is a need for dehumidification the dehumidifier is on. Experience with the current system configuration has established that tight temperature and humidity control can be achieved in the steady state case.

The indoor loop fan, condenser duct fan and compressor motor are powered by means of a variable frequency inverters. The temperature and humidity PID controllers and frequency invertors all accept remote set points in the form of an analog signal (e.g. 0 to 5 VDC or 4 to 20 mA) that the controller uses to scale the value of temperature, relative humidity, or frequency, between specified upper and lower limits.

3.3 The Dynamic Control Software

The control requirements for this research project are threefold:

- To adjust the set points dynamically based on the output of the cabin model. This is applicable for the temperature and relative humidity in the indoor psychrometric loop.
- To adjust the set points dynamically based on a pre-determined time-sequence. This is applicable for the compressor and condenser fan rotational speed in case of running a drive cycle, or the temperature and relative humidity in the outdoor chamber in case of simulating changes in weather conditions.
- To adjust the RPM of the indoor loop fan, using its frequency inverter, based on the fan setting selection in the cabin model program.

Adjusting the rotational speed of the indoor loop fan according to the fan setting in the cabin model is not a dynamic situation and might take place just a few times during a test, or even not at all. Controlling the indoor airflow rate is achieved simply when the cabin model sends an analog input signal to the remote set point pin of the frequency inverter causing it to adjust to the required new set point.

3.3.1 Control Based on Outputs of Cabin Model

The cabin model program sends remote set points to the temperature and humidity controllers to control the indoor loop temperature and relative humidity based on the outputs of the model. In this case, however, a feed-forward communication is not sufficient to insure a close match between the required value of the controlled parameter and the actual value. For this reason, the cabin model program was equipped with PID control capability. Each time step, the program measures the process value of the controlled parameter (e.g. temperature or relative humidity) upstream of the evaporator coil and calculates the error, *e*, which is the difference between the measured value and the desired value. This error is used in a typical PID function of the sort shown in Equation 3.1 to calculate the set point S_{adj}, where *S* denotes the controlled parameter, either temperature or relative humidity.

$$S_{adj} = S + f_{PID}(e) = S + P.e + \frac{1}{I}\int e.dt + D\frac{de}{dt} \qquad 3.1$$

where,

S_{adj} is the adjusted set point,

f_{PID} is a proportional plus integral plus derivative function,

e is the error,

P is the proportional constant,

I is the integral constant, and

D is the derivative constant.

Therefore, the value of the set point that the PID controller or the relative S_{adj} is sent to is not exactly the same value which is the output of the cabin model, but

The benefits of this approach will be discussed later. Nevertheless, the *P*, *I*, and *D* factors need to be tuned to their best values. The values that resulted in the least error were empirically determined and are listed in Table 3.2.

3.3.2 Control Based on Time-sequence

When it is required to run a time-sequence of compressor RPM and condenser fan RPM that represents a drive cycle, or a time-sequence of outdoor temperature and relative humidity that represents changes in weather conditions, the full time-sequence is known beforehand. The dynamic control software is equipped with means for the user to enter the sequence and run it. An example time-sequence is shown in Figure 3.2 where the variable on the Y-axis could be temperature, relative humidity, or RPM. The coordinates of the break points can be represented in a simple text file such as the one shown if Figure 3.3, where the first row of data represents time and the second represents the controlled variable. The software reads the data points and interpolates between them to calculate the values between the breakpoints. The interpolation scheme was written in LabVIEW especially for this research work.

At each time step, the software measures the value of the controlled parameter and compares it with the desired value based on the interpolation. The difference between the two values is the error, *e*, which the software uses to calculate the adjusted set point that is sent to the corresponding controller.

In this case, the next set point (controlled parameter value) is already known in each time step, therefore the dynamic control software takes advantage of this feature while sending the set points to the controllers by further adjusting the set points according to Equation 3.2.

$$S_{adj} = S + f_{PID}\{(1-a)\,e + a\,e'\} \qquad 3.2$$

where,

f_{PID} is a proportional plus integral plus derivative function,

a is anticipation factor, a constant specified by user, varies between *0* and *1*.

e is the error, i.e., the difference between S and the measured process value,

e' is the difference between *S* of the next step (if known) and the process value.

The function f_{PID} is a PID equation similar to the one previously given in Equation 3.1.

Weighing the error according to a factor, *a*, called the anticipation factor, has proven to be very useful in mitigating over- and under-shootings around sharp changes in the profile of the controlled parameter. The value of the *a* factor has to be tuned similar to the values of P, I, and D. The value for the *a* factor is determined empirically and is given in Table 3.2.

To further clarify what the anticipation factor does, suppose the set point of a controlled parameter, e.g. humidity, is to be kept constant at 0.5 then suddenly changes to 0.8. If the anticipation factor was not used, then the instantaneous value of the error at the point the change occurs would be 0.3 RH. However, with the use of the anticipation factor, the process value would start increasing at the time step before the change happens to reach a value higher than 0.5 by the time it should be 0.8.

Figure 3.4 is a screen capture of the user interface of the time sequence operator portion of the dynamic control software. The software continuously graphs two values of the controlled parameter; the desired and the measured. In Figure 3.4 the two lines are on top of each other as such they can not be distinguished.

To reiterate, there are two layers of control implemented on the dynamic simulator; viz. software control and hardware control. This concept is best illustrated in Figure 3.5. The hardware control refers to the physical controllers that were part of the original steady state test facility, while the software control refers to the control capability built into the software written for this research work. This approach has the following benefits:

1. The process value of the temperature, relative humidity, or RPM follows the set (desired) point more closely.
2. The dynamic test facility software is independent of the hardware.
    a. Any faults in the measuring sensors that the temperature and humidity controllers use does not affect the accuracy of the control.

b. The tuning of the temperature and humidity controllers is not of high importance as long as the control software PID parameters are well tuned.

3.4 Verification of Control Accuracy

Tests were conducted with the purpose of verifying the control accuracy of the dynamic test facility and the interaction between the software and the system under test. Four categories of tests where conducted. In the first category, the unloaded tests, the temperature and relative humidity were controlled according to a pre-set time sequence to verify the accuracy of the dynamic simulator control while there is no system running in the chamber. The time sequences were arbitrarily designed to impose harsh changes of the controlled parameter. Figures 3.6 and 3.7 show the results of this category of tests. Each figure shows the profile of set points, how closely the process value followed the set point, and the difference between the set points and the process values, which is the error. It is clear from the figures that the absolute error in controlling temperature was within ± 0.5°C (1°F) and the absolute error in controlling relative humidity was within ± 2%.

The second category of tests was the loaded tests category in which there was a test system running and representing a load on the simulator while the dynamic simulator imposed a pre-specified temperature pull down profile on the indoor side. The details of the test system are the subject of Chapter 4. In this category of tests the air temperature and relative humidity inside the indoor loop were not used by the dynamic control software to impose the pull down, rather the pull down profile shown in Figure 3.8 was pre-specified and imposed on the loop. The conditions of the test shown in Figure 3.8 were: 35°C dry bulb ambient (outdoor) air and no soaking. The compressor was running at 2100 RPM and the clutch was engaged just at the start of the test. In this test category the accuracy of the control was within ± 0.8°C but only at the beginning of the test and when there was a sudden change in direction.

In the third category, the New European Drive Cycle (NEDC) (Wertenbach, 2003) was imposed on the system, which was turned on at the beginning of the cycle. The

NEDC is shown in Figure 3.9 and the RPM error encountered is shown in Figure 3.10. Figures 3.11 to 3.13 show an example test where the conditions were 100 % fresh air return at 30°C, 60% relative humidity and no soak. In this test the dynamic control software did not have to control the temperature and relative humidity because the test conditions specify 100% fresh air return; rather the software controlled the compressor RPM and condenser fan RPM. Figures 3.11, 3.12, and 3.13 show how the refrigerant temperatures, refrigerant pressures, and air temperatures vary as a result of the cycle, respectively. It is not the purpose at this point to analyze the behavior of the different system parameters during the cycle, but rather to verify the reaction of the system to the imposed cycle.

In the fourth category of tests, the load model tests, the dynamic test facility imposed a load on the system. The cabin model developed in Chapter 2 was not used, rather a simple load equation such as Equation 3.3 was used.

$$Load = Const.(T_{amb} - T_s) + Const.(T_r - T_s) + SolarConst. \quad 3.3$$

where,

T_{amb} is the ambient temperature

T_r is effective temperature inside the cabin, given by a pre-specified profile shown in Figure 3.14

T_s is evaporator outlet temperature, measured by the dynamic control software

The load is presented in Figure 3.15 versus time. After the heat pump has pulled down the evaporator outlet air to 15°C at a constant idling speed of 650 RPM, a simple drive cycle was started as shown in Figure 3.16. Figures 3.17 and 3.18 show results of a test where the conditions were 35°C dry ambient air and 5°C soak. Figure 3.17 shows how the air temperatures vary as a result of the cycle. Figure 3.18 shows the airside sensible and latent capacities as well as the refrigerant side capacity and the airside COP.

3.5 Lessons Learnt from Control of Test Facility

Having accurate control over the test facility starts with having proper vapor compression cycle configuration. The condensing units of the test facility, both indoor and outdoor sides, have a hot-gas bypass lines that allows for accurate temperature control. The condensing unit must have enough capacity to cause the desired rate of cooling or heating or humidification or dehumidification. Figures 3.6 and 3.7 show that the test facility was able to cause quick changes in temperature and relative humidity. The measuring instruments also need to be fast and accurate enough. Other than the cycle hardware, a well-tuned software control is also an important step in having an overall accurate control. All the PID parameters of the control as well as the period of the control cycle have to be well-tuned.

3.6 Advantages and Limitations of The Dynamic Test Facility

After examining the results of the verification of the dynamic test facility, it was concluded that the two layers of control and the introduction of the anticipation factor have led to satisfactory results in terms of the control being robust and accurate in following both pre-specified time sequences and the outputs of the cabin model. Also the communication between the control software and the system under test was verified and the ability to sense the performance of the system as a result of a dynamic change was verified. The advantages and disadvantages of the new test facility and dynamic testing method as compared to the conventional methods, such as road tests and wind tunnels, can be summarized as follows:

3.6.1 Advantages

- Fair comparison between different systems under the same realistic conditions by avoiding differences in field installations. By testing the vapor compression system independently of the car, more repeatable results could be achieved.
- Easy to build and operate and less costly compared to a wind tunnel.

- Much smaller in size than a wind tunnel and can fit any size of system unlike a wind tunnel.
- Tests become easier and more systematic because airside instrumentation is integrated into the facility and do not have to be installed in the vehicle then removed at the end of the test.
- Can accommodate future changes easier than a full-scale wind tunnel.

3.6.2 Limitations

- Doesn't give spatial distributions, which makes it not fit for comfort studies.
- Cannot simulate everything, e.g. rain or snow. For this purpose, additional devices, such as spray heads, have to be installed.

Table 3.1 Four Cases of Temperature Control

	Liquid-line valve	Hot-gas bypass valve	Electric heater
Need for cooling, not heating	open	closed	off
Need for heating, not cooling	closed	open	on
Need for cooling and heating	open	closed	on
No need for cooling or heating	closed	open	off

Table 3.2 Values of the Control Factors

	P	I	D	*a*
Temperature	4	22	0	0.2
Humidity	0.5	2	0	0.2
RPM	1	0	0	0.2

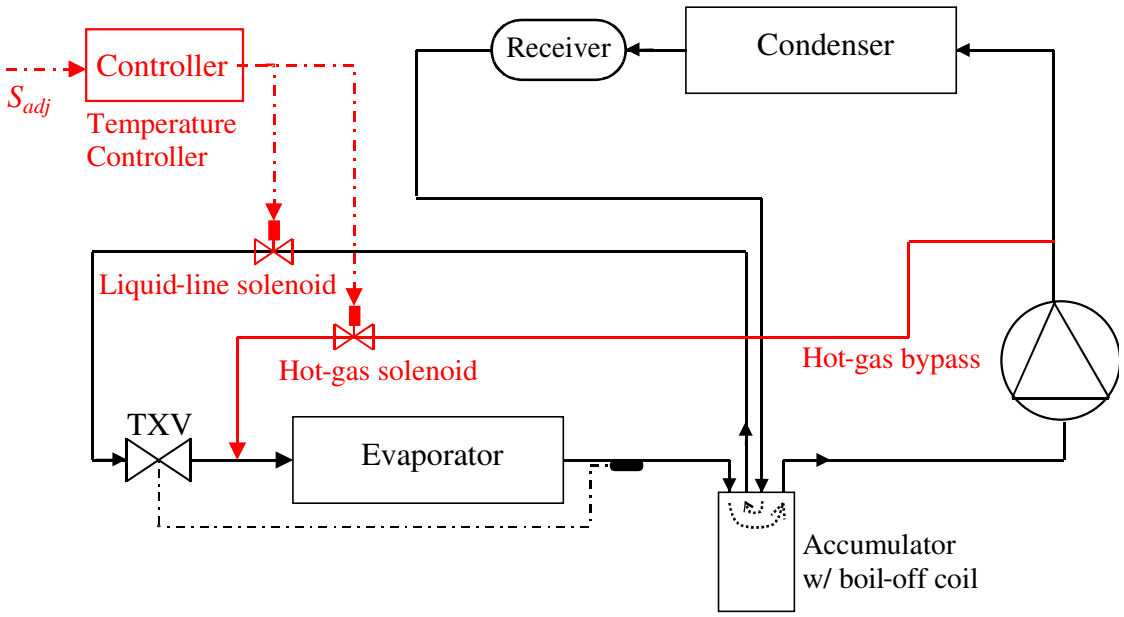

Figure 3.1 Refrigeration Circuit of Environmental Chamber or Loop

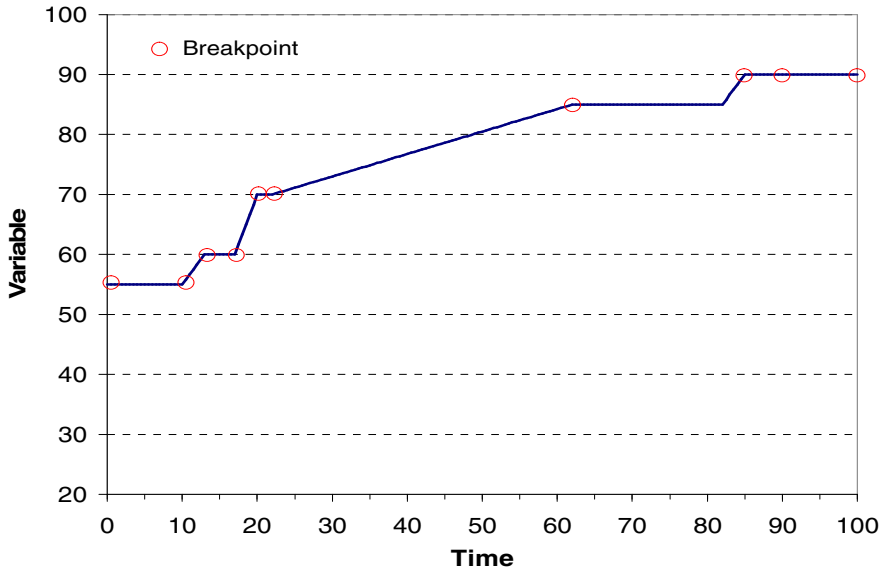

Figure 3.2 Example of a Time Sequence

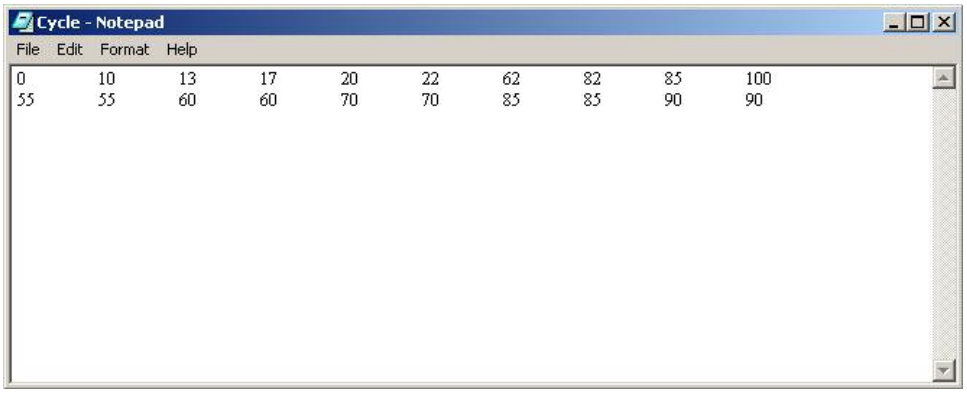

Figure 3.3 Example Text File of the Time Sequence

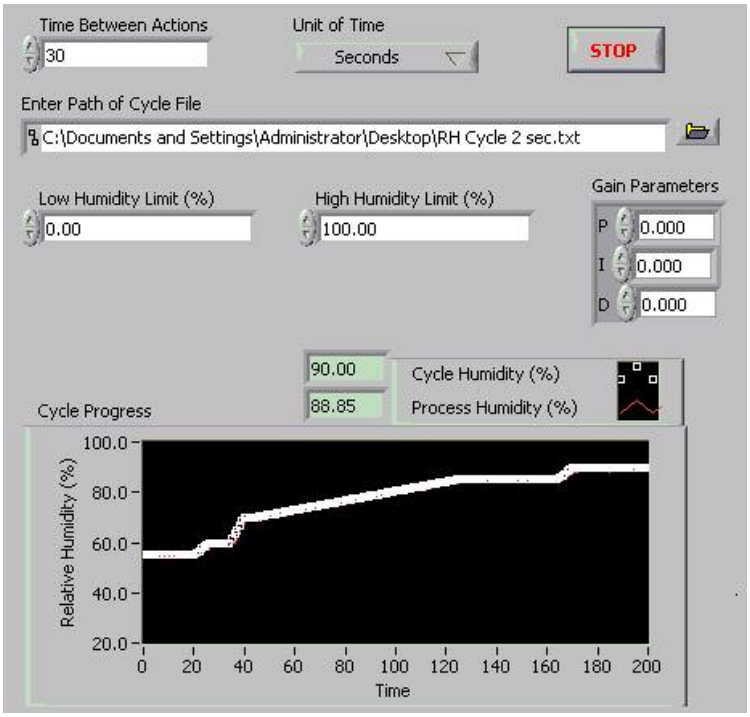

Figure 3.4 Screenshot of The Cycle operator of The Dynamic Control Software

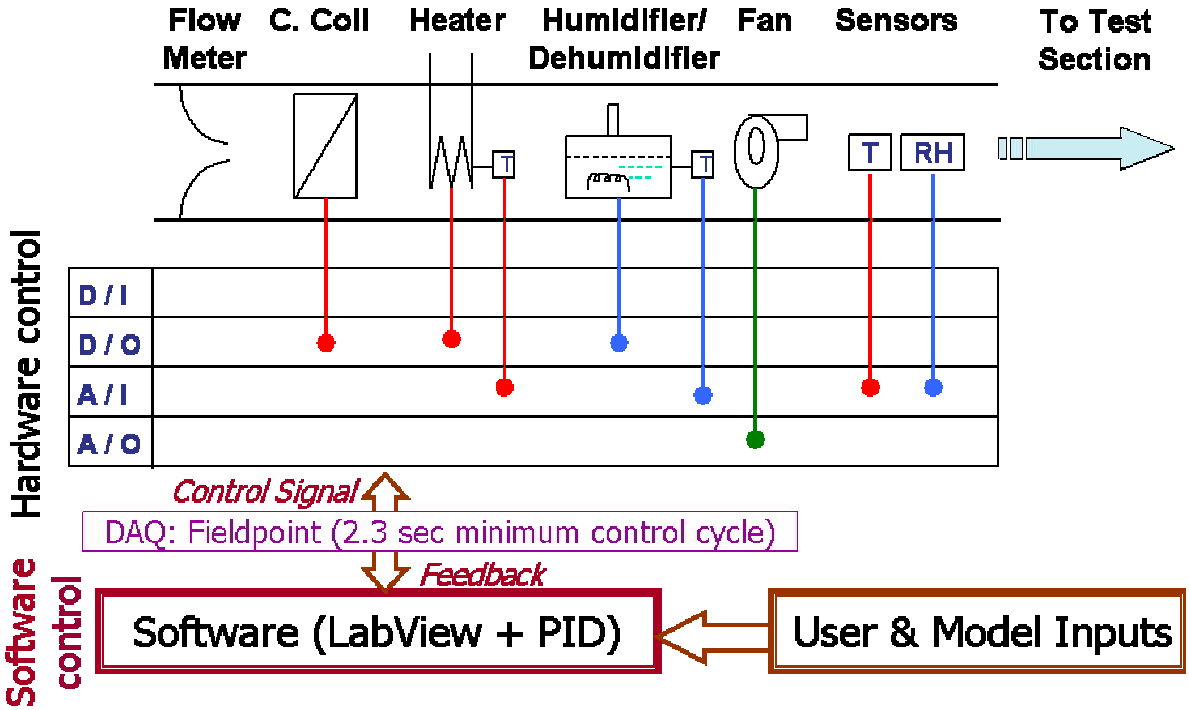

Figure 3.5 Schematic of The Two Control Layers

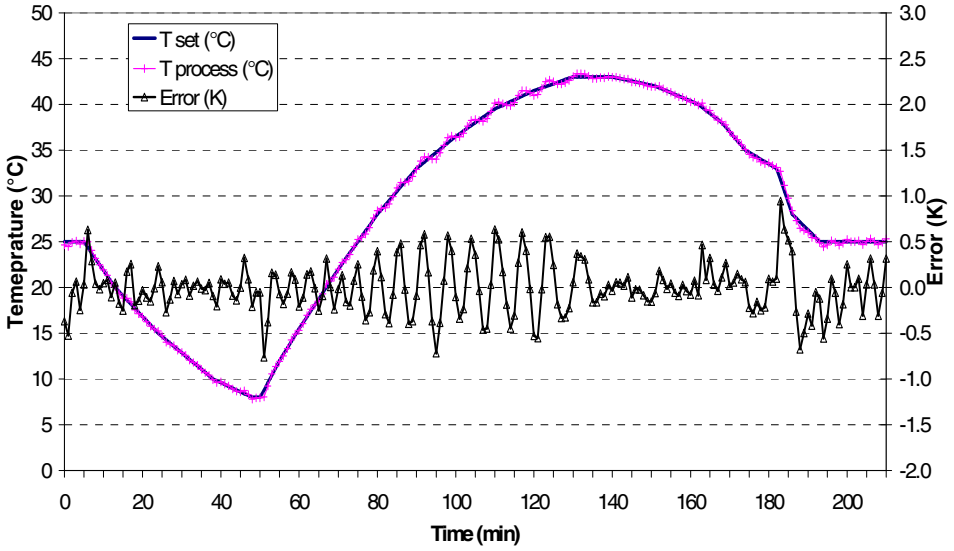

Figure 3.6 Temperature Control in Outdoor Simulator

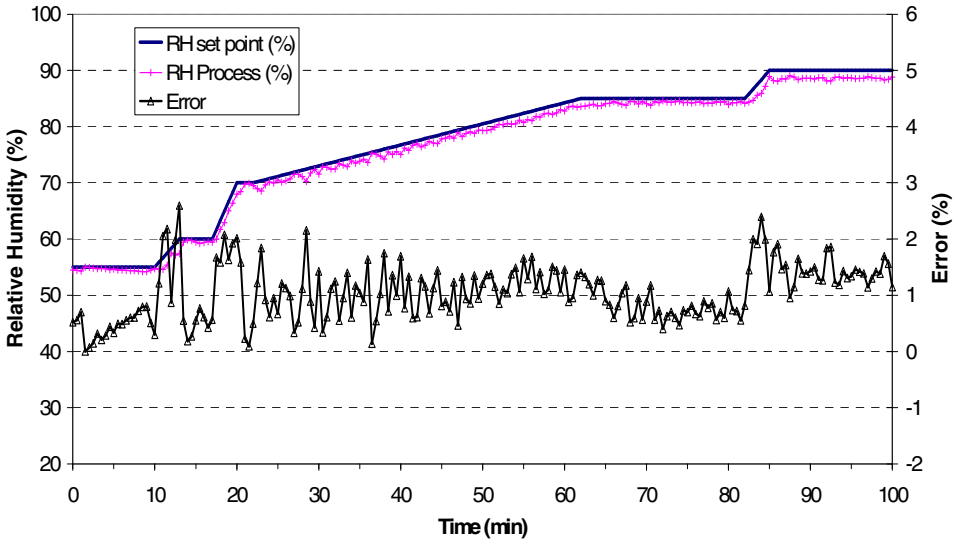

Figure 3.7 Relative Humidity Control in Outdoor Simulator

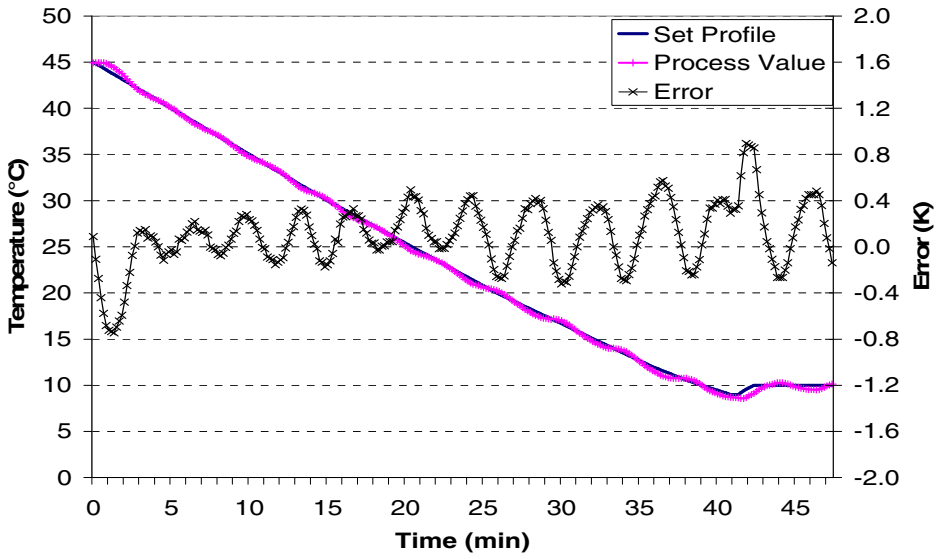

Figure 3.8 Pull Down during Loaded Test in the Indoor Side

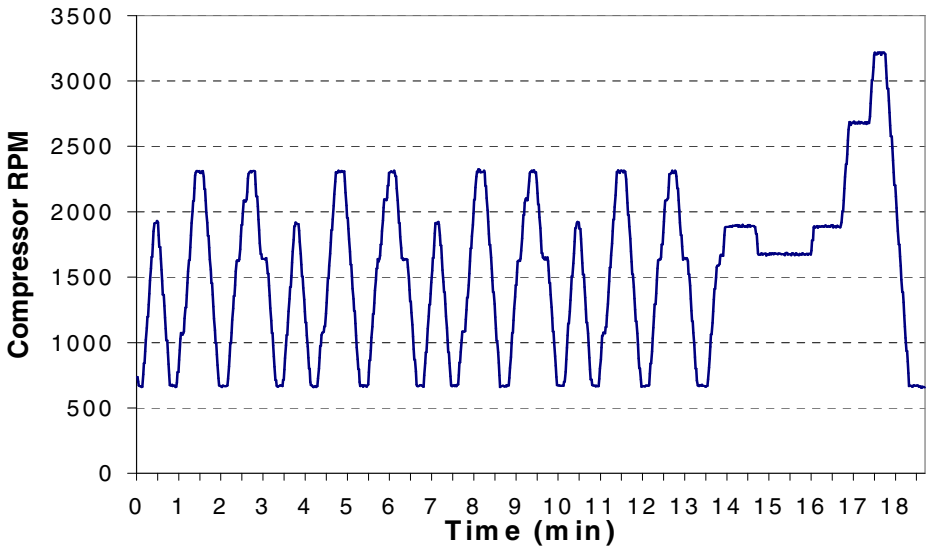

Figure 3.9 New European Drive Cycle

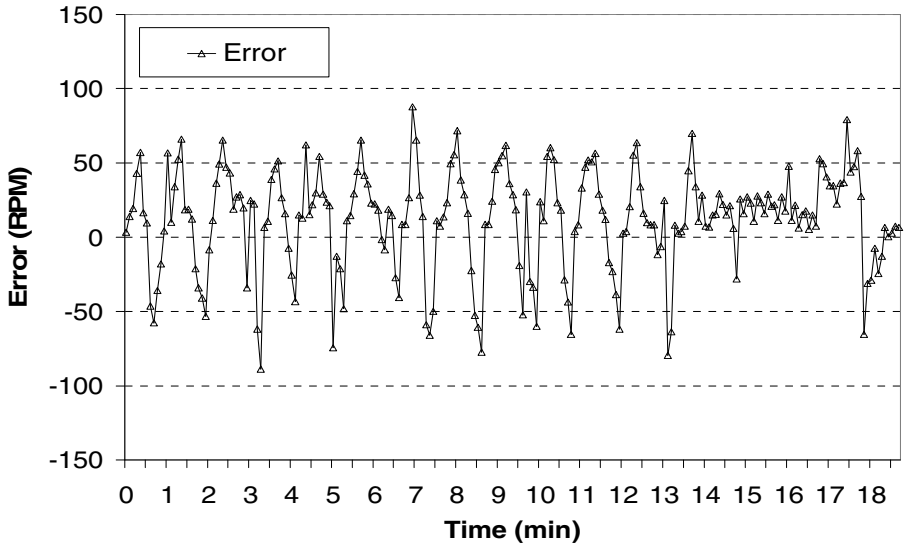

Figure 3.10 Absolute Error During Running NEDC

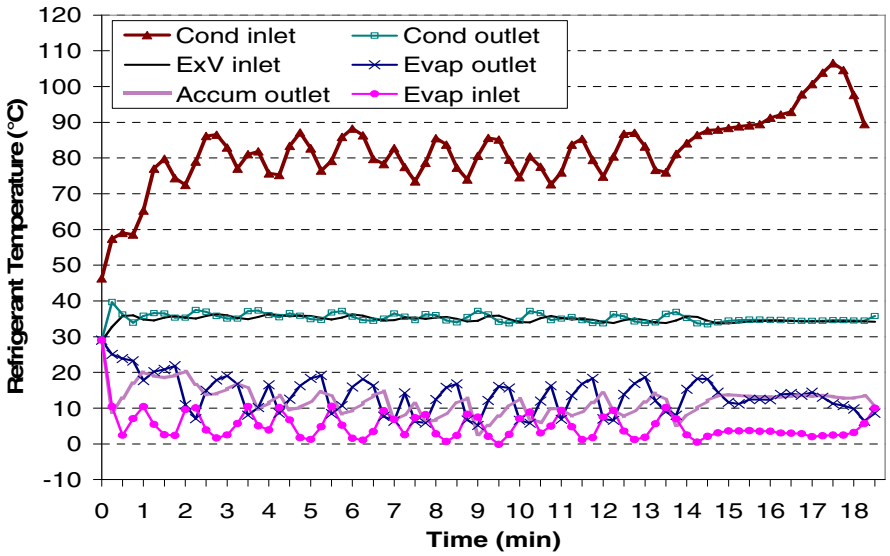

Figure 3.11 Refrigerant Temperatures During NEDC

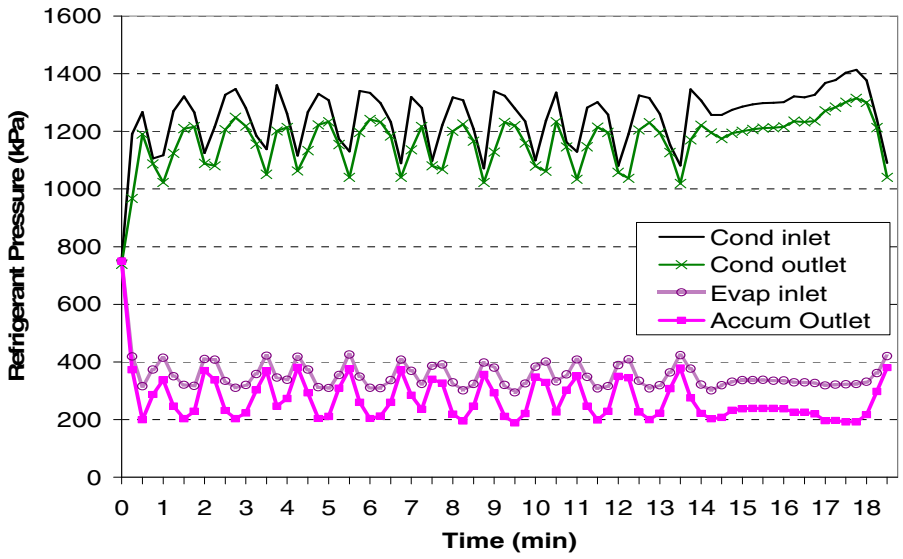

Figure 3.12 Refrigerant Pressures During NEDC

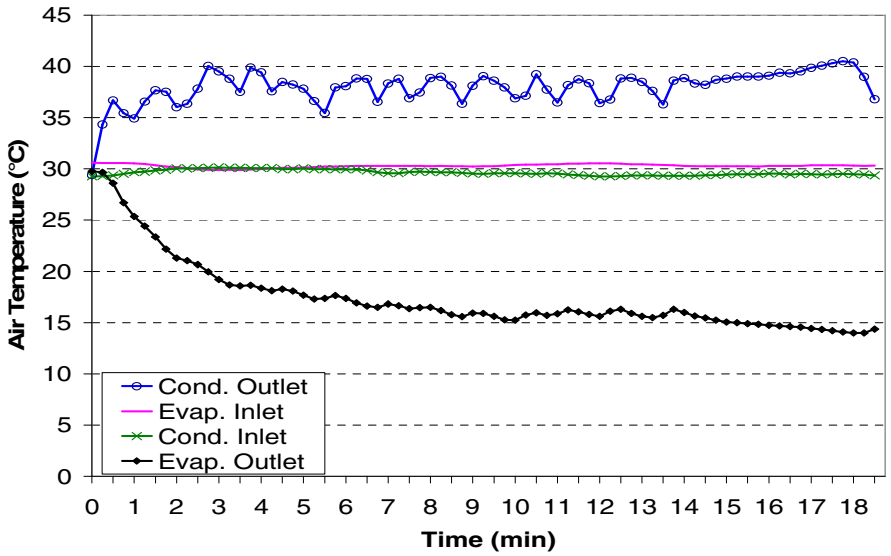

Figure 3.13 Air Temperatures During NEDC

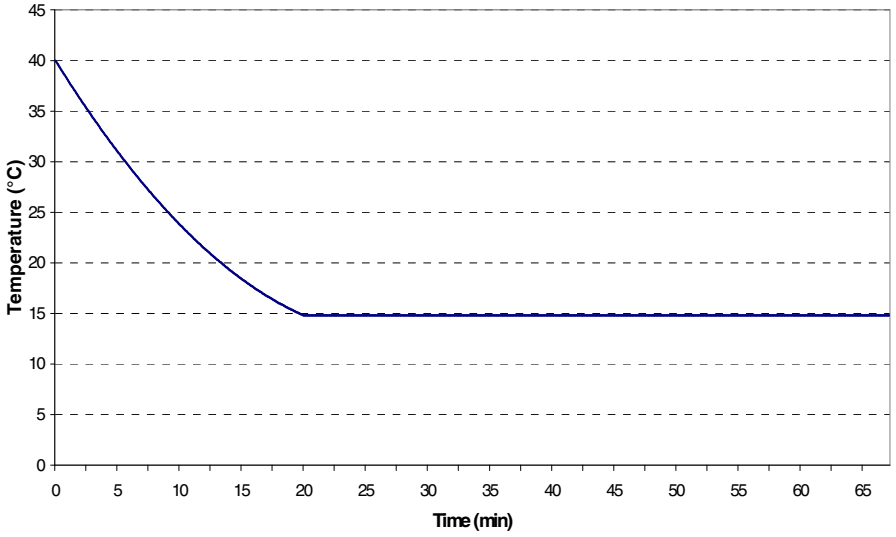

Figure 3.14 Effective Cabin Interior Temperature During Load Model Test

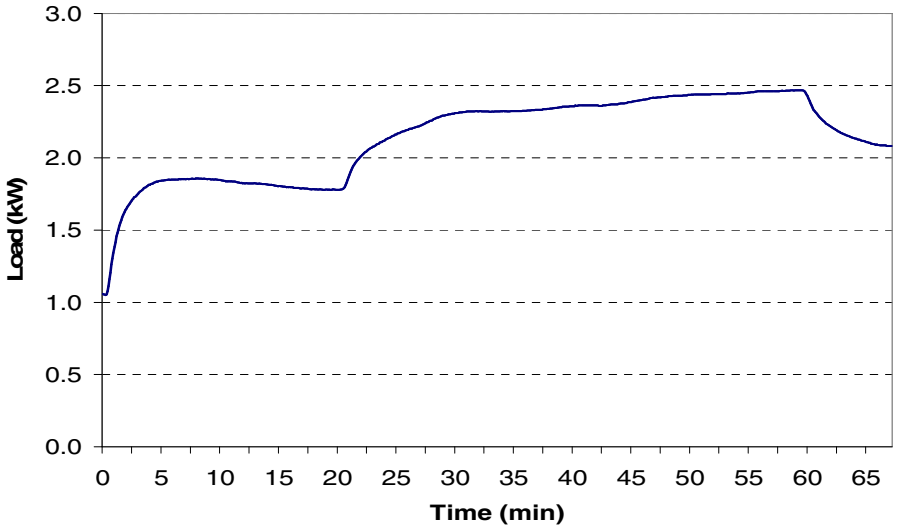

Figure 3.15 Load During Load Model Test

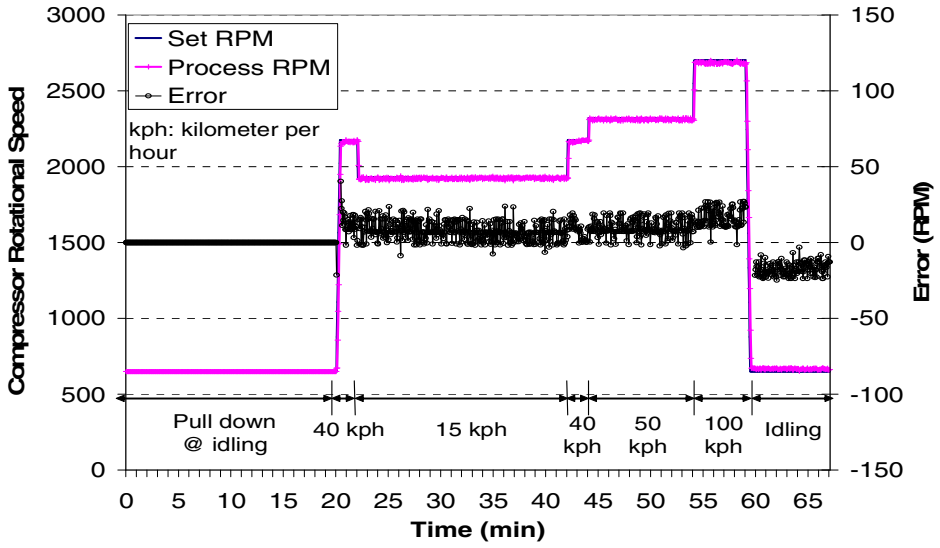

Figure 3.16 Drive Cycle for Load Model Test

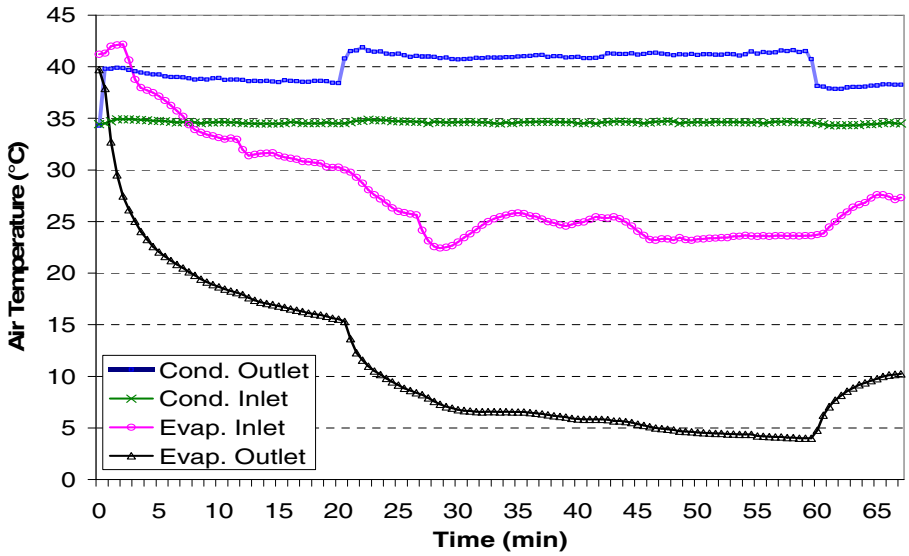

Figure 3.17 Air Temperatures for Load Model Test

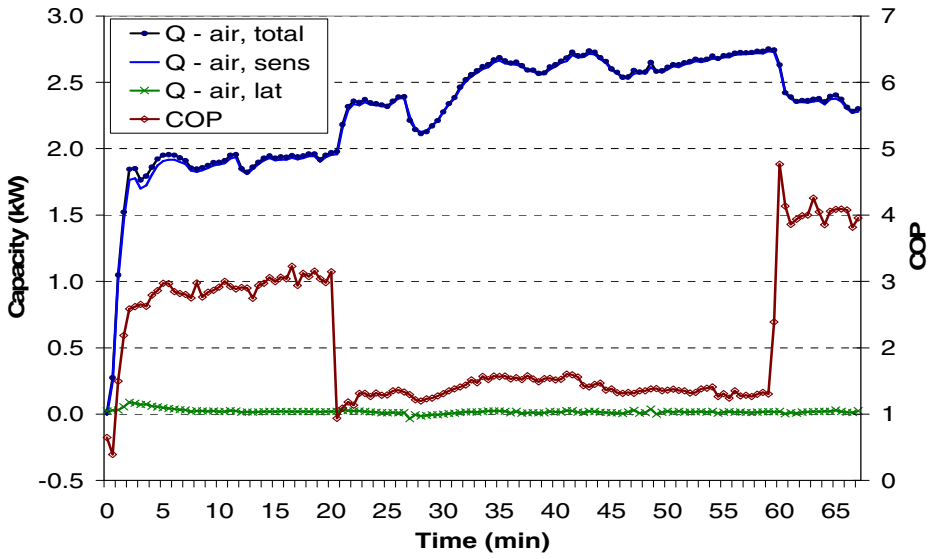

Figure 3.18 Capacities and COP During Load Model Test

Chapter 4: The Experimental Test System

4.1 Introduction

Automotive air conditioning systems have two typical configurations; either with a short tube orifice or with a thermostatic expansion valve (TXV). In the case of a short tube orifice, an accumulator is always used to prevent any liquid refrigerant supply to the compressor and to store excessive refrigerant in partial-load operating conditions. A TXV controls the refrigerant mass flow rate to ensure a certain degree of superheat at the evaporator outlet, in which case there is no need for a suction accumulator. However, there is a need for a liquid-line receiver to store the extra refrigerant at the time of off-design operation. The TXV system has, in general, a better COP over the wide range of operating conditions in automotive air-conditioning (Preissner 2001).

4.2 The Experimental Setup

A Typical R134a automotive air conditioning system was constructed by me especially for the purpose of this research work. It has a serpentine evaporator, fin-and-tube condenser, open-drive compressor, manual metering valve and a suction accumulator. The metering valve replaces the short tube orifice for the purpose of adjusting the refrigerant mass flow rate during the initial shakedown tests, but once a suitable opening was achieved, it was left at this opening throughout the rest of the tests and therefore it is, in effect, a short tube orifice. Some attributes of the system components are listed in Table 4.1, which includes more details than needed for conducting experimental tests. However, these details are relevant in Chapter 6 when discussing the numerical simulation portion of this research work.

Figure 4.1 shows details of the test system. The evaporator was installed inside the indoor simulator. The expansion valve was installed in close proximity to the evaporator but outside of the indoor simulator to be easily accessible during the tests. The compressor and accumulator were installed inside the outdoor simulator. The

condenser was installed inside an open-ended air duct inside the outdoor simulator. Care was taken to make the refrigerant connecting lines as short as possible and to raise the compressor to almost the same level as the condenser in order to resemble the actual installation in a real car.

Both the indoor simulator loop and the condenser duct have variable speed fans. The indoor loop is insulated with a 1-inch thick thermal insulation to reduce convective heat transfer errors in the air/refrigerant energy balance. Figures 4.2 and 4.3 are pictures of the condenser and the evaporator, respectively.

The open-drive compressor is driven by means of a 10 HP electric motor, which is operated by a variable frequency inverter. Care has been taken while tightening the belts between the motor and the compressor such that, after several hours of operation, the belts were usually only warm to the touch, indicating both good alignment and tightness. Just as in a real-car installation, the compressor is connected to the other components of the system with flexible hoses to damp the vibrations. The compressor uses 240 cm^3 of Polyalkylene Glycol (PAG) lubricating oil. This type of oil has high affinity for moisture. Care has been taken to expose the oil to atmospheric air as little as possible and to evacuate the system properly before charging the refrigerant. Figure 4.4 is a picture of the compressor and drive assembly.

4.3 Instrumentation, Measurements, and Data Acquisition

4.3.1 Refrigerant-side Measurements

On the refrigerant-side, the system is equipped with sensors to measure:

- Temperatures
- Pressure
- Mass flow rate

One coriolis mass flow meter is placed in the liquid line to measure the mass flow rate of refrigerant. Its relative accuracy varies from 0.26% at 40 g/s to 0.67% at 8.8

g/s. Several thermocouples and pressure transducers were placed in various locations, as listed in Table 4.2, to measure the temperature and pressure of the refrigerant. The accuracy of the pressure transducers is 0.55 PSI and their time constant is 5 ms.

Special care has been taken when selecting thermocouples because of the challenges in dynamic temperature measurements. During transient operation, the refrigerant temperature cannot be measured from the outer surface of the pipes because of the thermal storage of the pipe metal. Also in dynamic situations the measurements need to be quick, which poses a challenge when measuring temperatures because measuring temperature is usually slower than other measurements due to the relative slow rate of heat transfer. All the thermocouples used are in-stream thermocouples. To insure the quickest possible measurements, thermocouples were selected to have exposed junctions and to be of 1.6 mm (1/16 inch) in diameter, which is the thinnest practical diameter that could be found commercially. The dynamic temperature error will be analyzed more closely in Section 4.5.

In addition to these measuring instruments the system is also equipped with thermocouples along the circuits of both heat exchangers, thermocouples on both the compressor and the accumulator shells, and both in-stream and surface thermocouples along the vapor line.

4.3.2. Air-side Measurements

On the air-side, the facility is equipped with sensors to measure:

- Dry bulb temperatures
- Relative humidity
- Differential pressure and flow rate

Grids of nine equally spaced thermocouples are used to measure the average air dry bulb temperatures upstream and downstream of the evaporator and upstream of the condenser. A grid of six thermocouples is placed right after the nozzle in the condenser duct to measure the average air dry bulb temperature at the condenser outlet. To calculate the latent capacity of the system, it is necessary to measure one more property of the evaporator air. This is done by placing a dew point sensor before

and after the evaporator. These dew point sensors measure also the relative humidity of the air. The fastest feasible dew point meter commercially available is used. Nevertheless, this meter has a time constant of 15 seconds. The slowness of this sensor will be taken into consideration while analyzing the experimental results in Chapter 5.

The flow rates of evaporator air and of condenser air are measured by means of nozzles. The volumetric airflow rate is calibrated as a function of the pressure drop across the nozzle by using electric heaters. The air temperature is taken into account when calculating the mass flow rate.

4.3.3 System-level Measurements

A torque meter is mounted between the compressor and the electric motor. Also the rotational speed of the compressor is measured by means of an RPM sensor. From the torque and the rotational speed, the power consumption of the compressor can be calculated. The torque meter and RPM sensor are shown in Figure 4.4.

4.3.4 Data Acquisition

Data acquisition hardware from National Instruments was chosen. Its frequency varies according to the nature of the signals being measured, whether it is voltage or current and whether they need post processing such as thermocouple voltages. The slowest scan rate was that of the thermocouples, which was once every 2.3 seconds. It was hence decided that 2.5 second is the minimum data acquisition cycle to be used.

4.4 Assessment of The Experimental System

In steady state operation, the capacity as calculated from the airside is the same as calculated from the refrigerant side. This presents a useful criterion to check the accuracy of the instrumentation and data acquisition. Standard test procedures such as ANSI/ASHRAE 116-1995 (ANSI/ASHRAE, 1995) specify that the two values of the

capacity must agree within 6% of each other. On the contrary, during transient operation, the airside capacity and the refrigerant-side capacity are not equal. The difference between them was demonstrated earlier in Figure 1.1 and is the result of the energy storage in the system. This discrepancy poses another challenge for dynamic testing. The best method to overcome this challenge is by conducting all feasible calibrations and checks to verify that the calculated capacity is accurate. The following calibrations and checks were conducted:

- All airside and refrigerant-side thermocouples were calibrated as connected to the data acquisition system using an Omega CL24 (Omega, 2003) thermocouple calibrator whose accuracy is 0.3K.
- All pressure transducers were calibrated, also as connected to the data acquisition system, using nitrogen gas and an Eaton pressure calibrator.
- Refrigerant mass flow sensor was calibrated by passing a metered amount of water (at constant pressure) and gauging the time. The calibration curve is given in Figure 4.5.
- The air flow rates in the evaporator duct and in the condenser duct were calibrated using electric heaters by measuring the power consumption of the heaters and the air temperatures before and after them.
- The evaporator air relative humidity as calculated using the dry bulb and dew point measured values agrees, within 0.4%, with the relative humidity measured by the dew point meter.
- With the evaporator fan on to circulate the air in the indoor air loop and with the system off, the air temperatures and the in-stream refrigerant temperatures agree within less than 0.5K.
- With the evaporator fan on to circulate the air in the indoor air loop and with the system off, the measured refrigerant temperature at evaporator inlet and outlet agree, within less than 0.5K, with the saturation temperature as calculated from the measured pressure.
- The heat loss from the evaporator loop to the surrounding ambient air was calibrated, at different temperatures, using an electric heater powered through a variable voltage power supply and measuring the air temperature inside the

loop and outside of it. The result was Equation 4.1, which was integrated with the capacity as calculated from the air side (the air-side capacity).

$$Q_{loss}\left(kW\right)=0.00984\times\left(T_{amb}-T_{loop}\right) \quad 4.1$$

where T_{loop} is the average temperature inside the evaporator loop

- During steady state operation of the system, the latent capacity as calculated using the dew point values measured by the dew point meters, agree within 2% with the latent capacity calculated by collecting the evaporator condensate.
- During steady state operation of the system, the error in heat balance between the refrigerant-side capacity and the air-side capacity is less than 4%. This heat balance check was repeated several times throughout the whole battery of tests and most of the time the error was less than 3%.
- Finally, the steady state performance of the system under several operating conditions was documented. This proved very useful later on when it was noticed that the operating pressures of the system drifted. After investigation, it was determined that moisture had contaminated the lubricating oil of the compressor. The oil was changed (following standard procedure) and subsequently a filter dryer was added to the system. The system was restored to its original performance and the doubtful test results discarded.

4.5 Dynamic Temperature Measurement Error

As mentioned earlier, the dynamic nature of the experiments represents a challenge in terms of quickness of temperature measurements. Figure 4.6 shows a thermocouple immersed in a flow of refrigerant. The advantage of using a small bulb thermocouple for measuring the temperature as compared to a big bulb thermocouple or a thermistor is that the small dimension of the bulb and its high thermal conductivity (copper-constantan) will effectively result in a very small Biot Number (Bi) that indicates a negligible internal resistance to the flow of heat. Therefore the average temperature of the thermocouple bulb is not lagging its surface temperature in time. However, due to the difference in specific heat between the thermocouple bulb and

the refrigerant, they take different periods of time to reach the same temperature. Therefore, in a transient case, if the thermocouple senses a certain temperature *T*, then the temperature of the refrigerant is not equal to *T*. The magnitude of the difference between the temperature of the refrigerant and the temperature that the thermocouple senses is the focus of this section.

The time constant of the refrigerant thermocouples is given by the manufacturer (Omega, 2003) to be 4.3 seconds in air at 19.8 m/s velocity and at atmospheric temperature and pressure. According to (Moffat, 1962) the dynamic error in temperature measurement can be described according to Equation 4.2:

$$Dynamic\,error = \frac{\rho\, c\, d}{4\, h}\left(\frac{dT}{dt}\right) \qquad 4.2$$

where ρ is the density of thermocouple bulb,

c is specific heat of thermocouple bulb,

d is diameter of thermocouple bulb, and

h is coefficient of convection between the bulb and the refrigerant.

The values of ρ, *c*, and *d* remain unchanged if the thermocouple is immersed in air or in refrigerant, but the value of *h* changes. By approximating the shape of the bulb to a sphere, the value of the average Nusselt number can be calculated from the relationship given in Equation 4.3 (Bejan, 2003), which is valid for a sphere under the following conditions:

Medium: liquid or gas

$3.5 > Re > 76{,}000$

$0.71 < Pr$

$1.0 < \mu / \mu_w < 3.2$

$$Nu_{av} = 2 + \left(0.4\,\mathrm{Re}^{1/2} + 0.06\,\mathrm{Re}^{2/3}\right)\mathrm{Pr}^{0.4}\left(\frac{\mu}{\mu_w}\right)^{1/4} \qquad 4.3$$

where, *Nu* and *Re* are based on the diameter of the sphere

μ_w is calculated at the bulb wall temperature

It is initially assumed that μ/μ_w is equal to unity because the difference in temperature between the free stream and the bulb is expected to be small. It is further expected that the dynamic temperature error at the evaporator outlet is bigger than at the evaporator inlet because:

- The heat transfer between gaseous refrigerant and thermocouple is poor compared to that of two-phase flow to thermocouple at the evaporator inlet.
- The rate of change of temperature at evaporator outlet is bigger than at the evaporator inlet.

The change of temperature with respect to time at the evaporator outlet during a typical pull down test is shown in Figure 4.7, which is taken from experimental results. Reynolds and Prandtl numbers can be calculated at temperature values in the figure and using the pipe diameter and flow rate at the evaporator outlet. The results are:

Maximum Re (evaporator outlet) = 67,000

Minimum Pr (evaporator outlet) = 0.75

which are within the validity limits of Equation 4.3.

Hence, the Nusselt number can be calculated, and consequently h. The resultant h is given in Figure 4.8.

The remaining values of the type T (Copper – Constantan) thermocouple that are needed for Equation 4.2 are:

$\rho = 8899$ kg/m^3

$c = 394$ J/kg.K

$d = 0.6096$ mm

By using these values with the temperature values from Figure 4.7 again in Equation 4.2, the dynamic temperature error at evaporator outlet can be calculated. The results are shown in Figure 4.9. It is clear from the figure that the dynamic temperature measurement error at evaporator outlet is negligible with respect to the accuracy of the thermocouples. This can be attributed to the small size of the thermocouple bulbs that were selected and also to the relatively slow rate of change of temperature. It is clear also from Figure 4.9 that the error at evaporator inlet is smaller than that at evaporator outlet.

Table 4.1 Specifications of System Components

Component	Specification
Refrigerant	R-134a
Compressor	Type: reciprocating piston. No. of cylinders: 7 Swept volume: 155 cm^3 Mass: 4.5 kg without clutch Surface area: 608 cm^2 Oil type: PAG Oil quantity: 240 cm^3
Condenser	Type: fin-and-tube Dimensions: 44.5 cm high x 57.8 cm wide x 2.24 cm deep Fin density: 20 fins per inch Fin thickness: 0.1 mm Internal volume : 600 cm^3 Total outer surface area: 8.41 m^2 Material: all aluminum
Evaporator	Type: Serpentine Dimensions: 27 cm high x 25.5 cm wide x 7.8 cm deep Fin density: 12 fins per inch Fin thickness: 0.16 mm Internal volume: 600 cm^3 Total outer surface area: 3.0 m^2 Material: all aluminum

Table 4.2 Location of Refrigerant Thermocouples and Pressure Transducers

Location	Thermocouple	Pressure Transducer
Compressor suction	√	√
Compressor discharge (before condenser)	√	√
Condenser outlet	√	√
Before expansion valve	√	√
After exp. valve (before evaporator)	√	√
After evaporator	√	√
Before accumulator	√	√
After accumulator	√	

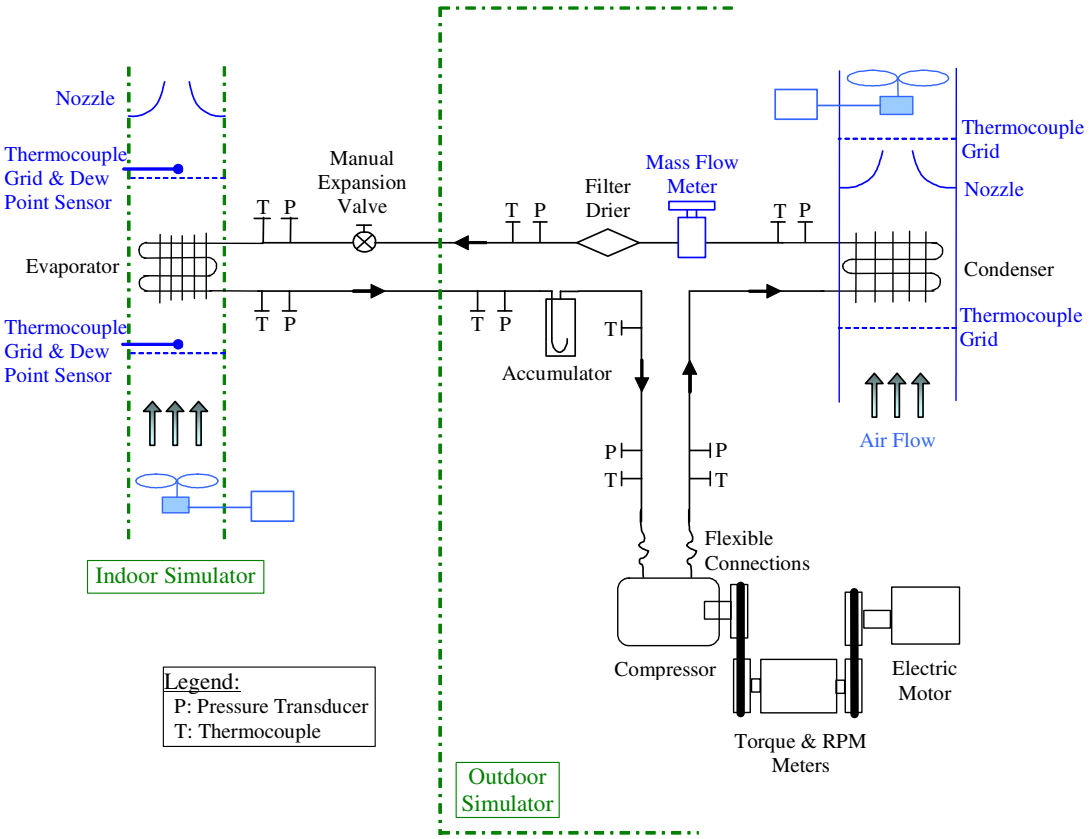

Figure 4.1 Installation and Configuration of The Test System

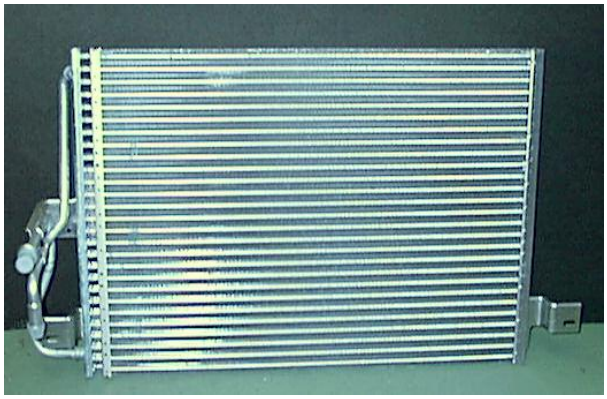

Figure 4.2 Picture of The Automotive Condenser

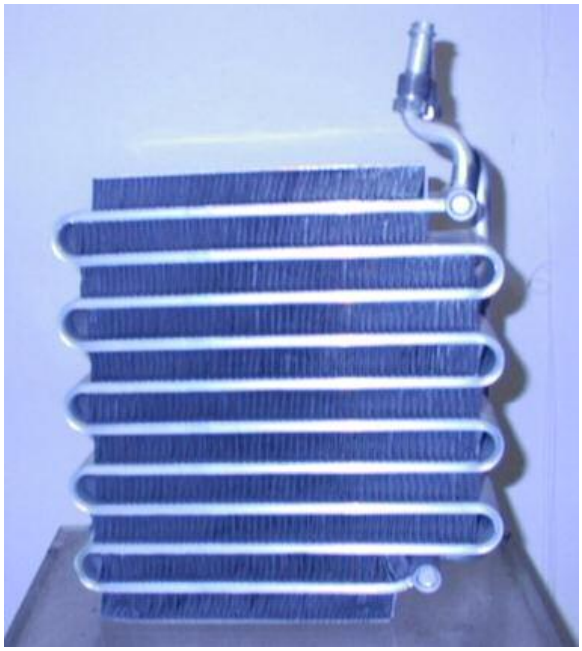

Figure 4.3 Picture of the Automotive Evaporator

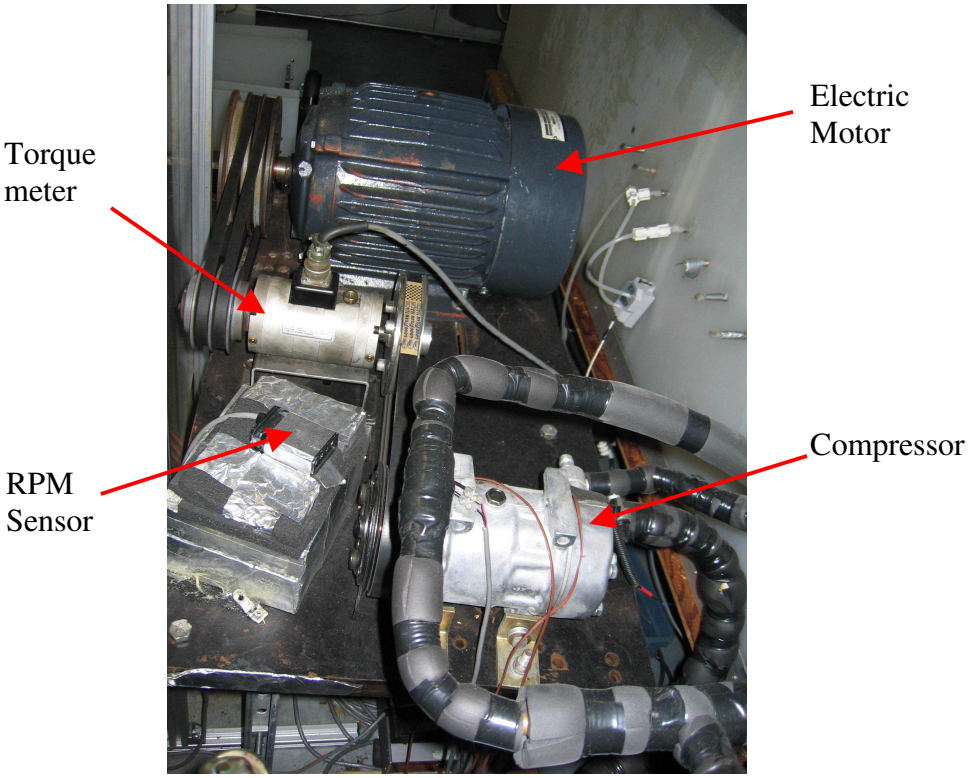

Figure 4.4 Picture of The Automotive Compressor, Torque Meter, Electric Motor and RPM Sensor

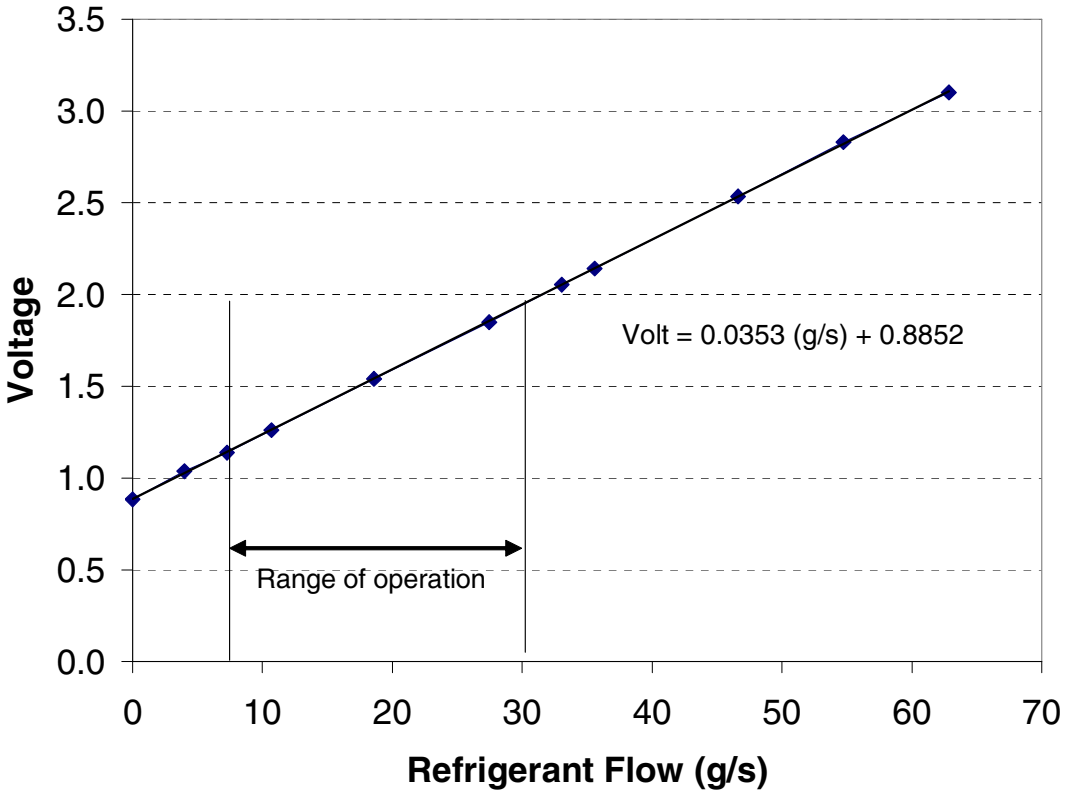

Figure 4.5 Calibration Curve of The Refrigerant Flow Meter

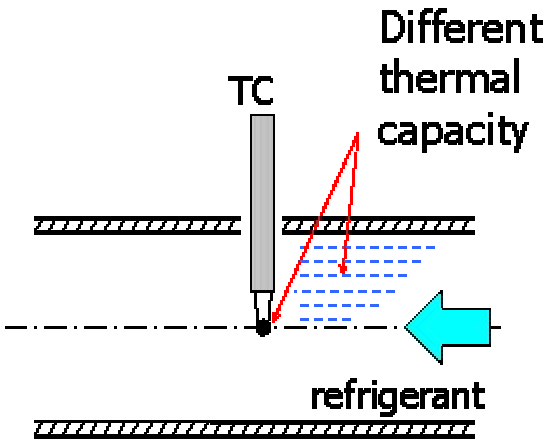

Figure 4.6 An Exposed Junction Thermocouple Immersed in Refrigerant

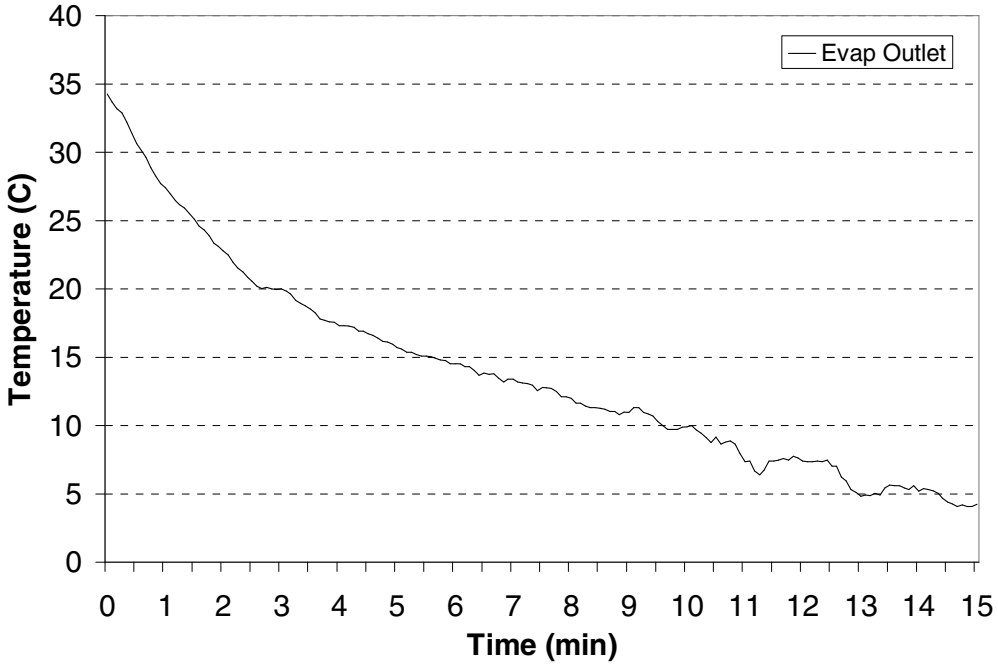

Figure 4.7 Refrigerant Temperature at Evaporator Outlet

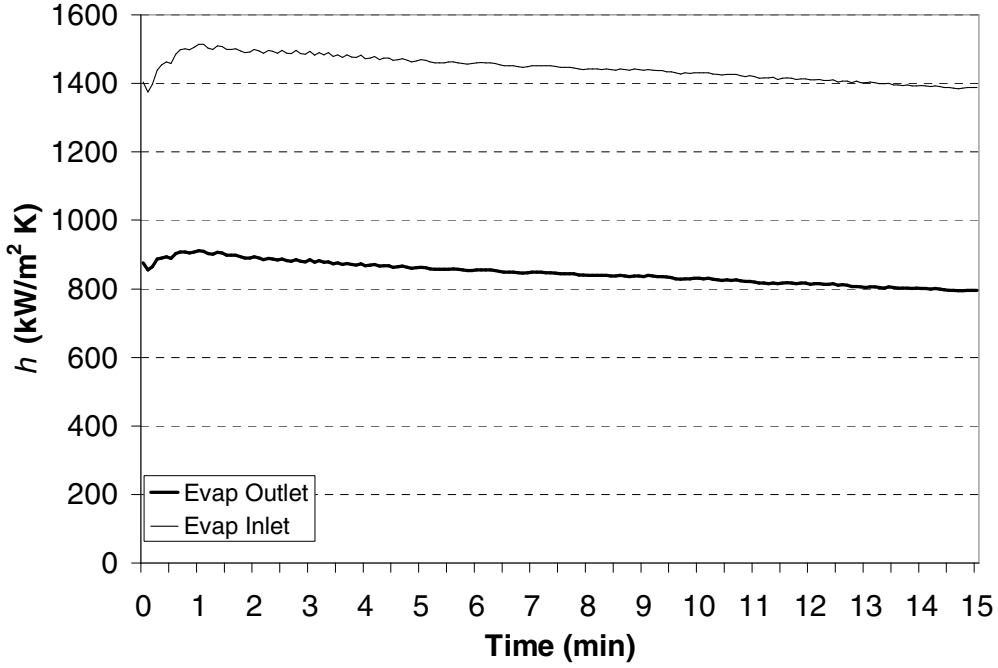

Figure 4.8 Coefficient of Convection Heat Transfer from Thermocouple Bulb

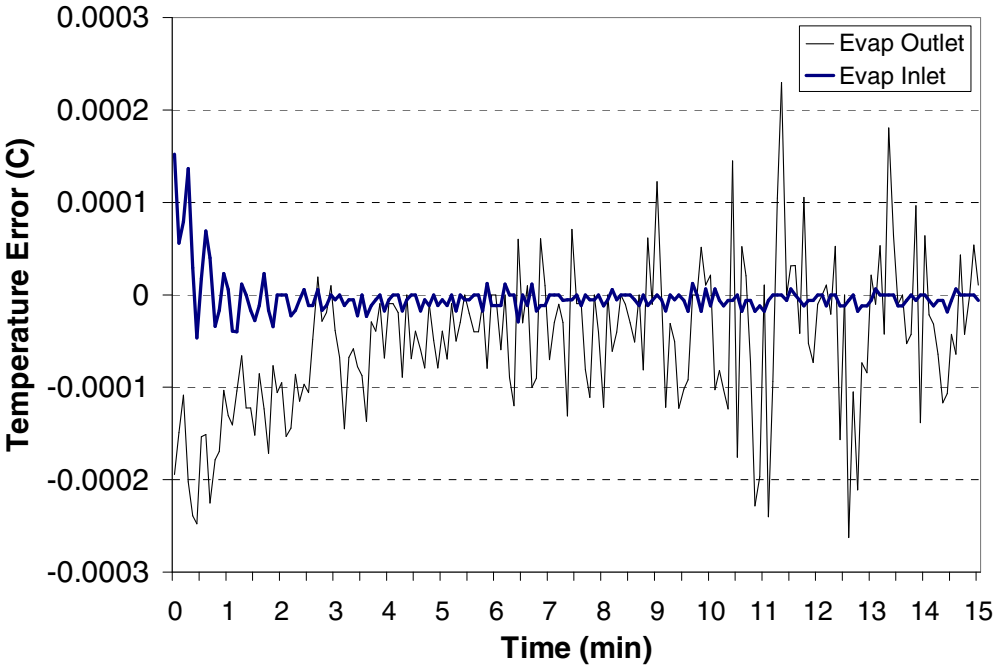

Figure 4.9 Dynamic Temperature Measurement Error

Chapter 5: Experimental Results

5.1 Introduction

In this chapter, the dynamic performance of the automotive test system will be investigated. Several types of tests will be conducted; drive cycles, pull-down tests and cycling tests. The analysis of results will focus on capacity and moisture removal. Methods to improve the performance of automotive air conditioners will be highlighted.

5.2 Pull-down Tests

The first category of tests focuses on the time period and the energy consumption needed for the automotive system to decrease the temperature inside the cabin to 24°C. The test matrix shown in Table 5.1 was designed for this purpose. All the tests start at cabin temperature 41°C, either because the ambient is at 41°C and the cabin temperature is equal to the ambient air temperature, or because the ambient air temperature is equal to 30°C but the cabin has been hot-soaked to 41°C (soaking is when the cabin air temperature is higher than fresh air temperature due to solar radiation). The relative humidity associated with the hot soak case, 32%, is a result of sensible heating from 30°C and 50% RH to 41°C. Tests 1 to 8 in the test matrix include pull-down in both the idling and the driving conditions, with fresh air and with recirculated air, and with or without hot-soak. To avoid complicating the test matrix, all the tests are conducted at the same evaporator and condenser air speeds. Test number 9 starts with fresh air until the temperature inside the cabin is equal to the ambient temperature, then switches to recirculated air. Test number 10 was added to investigate the effect of the elevated condenser temperature due to radiation and recirculation near the ground, as reported in (Inui & Tomamtsu, 2004 and Sumantran et al., 1999). All the tests end when the temperature inside the cabin (that is the temperature of the air returning to the evaporator) is equal to 24°C.

The results of the first category of tests are shown in Figure 5.1, which gives the pull-down period of the tests with hot-soak (tests number 1, 3, 5, 7, 9 & 10 in test matrix), and Figure 5.2, which gives the pull-down period of the tests without hot-soak (tests number 2, 4, 6 & 8 in test matrix). The cabin air temperature recorded during the tests is plotted against time in those figures. Both figures show that the cabin air temperature does not drop to 24°C in case of fresh air; which indicates that the air conditioner is undersized for the cabin size used in the tests, however, the final temperature in case of driving condition is lower than idling condition. The final temperature is also lower in case the ambient temperature is 30°C than in the 41°C ambient case. In the four tests with recirculated air (idling and driving with recirculated air in Figure 5.1, and idling and driving with recirculated air in Figure 5.2) the cabin temperature drops to 24°C. As expected, the driving case is faster than the idling case in pulling down the cabin air temperature. The cabin air temperature reaches 24°C after approximately 29 minutes in the idling case, regardless of the temperature of the ambient air, and after 17 minutes in the driving case, also regardless of the temperature of the ambient air.

When the temperature of the air on the condenser was raised 5 K higher than the ambient air temperature, the pull down period was approximately 3.5 minutes longer than the case without the temperature rise. At driving conditions and recirculated air, the pull down period was much shorter as given by the thick solid line in Figure 5.1. However, when the cabin is soaked under the sun, the initial temperature that exists inside the cabin is higher than the ambient temperature at the beginning of the pull-down period, and therefore it is beneficial to start the system on the fresh air mode rather than the recirculated air mode. When the cabin temperature reaches the ambient temperature, the mode should be switched to recirculated air. This scenario is demonstrated by the thin solid line in Figure 5.1 and the result is that it is about 2 minutes faster to pull down with this scenario. The coincidence of the first part of the line representing this scenario and the line representing the pull-down with fresh air scenario speaks well for the repeatability of test results.

Not only it is faster, but it is also more energy efficient to pull down with this scenario, as can be seen in Figure 5.3, which gives the energy consumption and the

COP of the tests with hot-soak. The energy consumption is given in kJ until the cabin temperature drops to 24°C. The COP was calculated by dividing the total capacity delivered during the test by the total compressor power consumption during the test. The fresh-then-recirculated air scenario has 12.3% less energy consumption and 21.6% higher COP than just recirculated air. Figure 5.3 also gives the energy consumption during the two cases of idling. When the condenser air is 5°C hotter than the ambient the energy consumption is 30.7% higher and the COP is 18.1% lower. If the driving and the idling cases are compared, it can be calculated that the driving case consumes 64% more energy and has 52.5% less COP than the idling case.

Figure 5.4 shows the energy consumption and the COP for the tests without hot-soak. It should be noticed by comparing Figure 5.4 and Figure 5.3 that in the case without hot-soak, the energy consumption is slightly higher, and the COP is slightly lower than the case with hot-soak. This can be attributed to the lower initial relative humidity in the case with hot-soak and also the lower condensing temperature in the case with hot-soak.

5.3 Drive Cycle Tests

A drive cycle is a relationship between vehicle speed and time. Standardized drive cycles represent typical highway and city driving patterns and are used to measure the fuel consumption and exhaust gas emissions of different cars (EPA, 2005). The relationship between the rotational speed of the air conditioning compressor and time during the New European Drive Cycle (NEDC) is shown in Figure 3.9. The NEDC takes a little less than 19 minutes to run and the RPM changes from 650 to almost 3250. The first 13 minutes of the cycle represent city driving while the remainder represents highway driving.

The New European Drive Cycle was imposed on the system according to the test conditions shown in Table 5.2. The system was started at the beginning of the test.

Figure 5.5 shows how the temperature of the cabin supply air changes with time as well as the change in the temperature of the internal mass. Figure 5.5 also shows the air temperature inside the cabin, as calculated by the cabin model, and as measured inside the indoor simulator loop. The difference between the calculated cabin air temperature and the measured cabin air temperature, which is less than 0.7°C as shown on the right-hand Y-axis of the figure, is an indicator for how accurate the temperature control of the dynamic simulator during the test is. Figure 5.6 shows the supply air and cabin air relative humidity as well as air mass flow rate. It is clear that the supply air RH fluctuates as a result of the fluctuations in compressor RPM. The compressor rotational speed fluctuations affect the evaporation temperature, as will be shown later, which in turn affects the condensation ability (latent capacity) of the evaporator and, therefore, the supply air RH fluctuates. However, after the supply air is mixed with the cabin air and is affected by the latent load (which is the passengers in this case), the cabin air relative humidity does not fluctuate as much due to the big volume of air inside the cabin. There are two lines in Figure 5.6 that represent cabin air RH; the calculated one and the measured one. It is clear that the difference between them is less than 4% RH. It can be also seen in Figure 5.6 that the air mass flow rate increases from 176 g/s to 185 g/s due to the increase of air density, which is caused by the drop in temperature.

Figures 5.7 to 5.13 illustrate the different air conditioning system parameters and performance, which are all affected by the fluctuations of compressor speed based on the drive cycle. To help understanding the trends shown in the figures, the refrigerant mass flow rate, which is an indicator of compressor RPM, is given in all the figures and plotted on the right-hand Y-axis. Figure 5.7 shows that the refrigerant mass flow rate fluctuates from 15 g/s to 28 g/s. Whenever the compressor RPM is high, the refrigerant flow rate is high, and vice-versa.

Figure 5.7 also shows the degree of superheating at evaporator outlet and the degree of subcooling at condenser outlet during the NEDC. It can be seen that whenever the RPM, and therefore the refrigerant mass flow rate, increases the degrees of superheating and subcooling increase due to the increase of heat transfer coefficient

which is caused by the increase in refrigerant velocity. This will be reflected on the capacity, as will be seen later.

Whenever the degree of superheat decreases, the evaporator inlet and outlet temperature curves, shown in Figure 5.8, cross each other. When the RPM, and therefore the refrigerant flow rate, increases, the evaporator outlet temperature increases due to the increased degree of superheating. The increase in evaporator outlet temperature causes an increase of condenser inlet temperature. The condenser outlet temperature is not affected much by the mass flow rate because the condenser outlet is always in the liquid state. It can be seen from Figure 5.7 that the subcooling was never lost during the test. The increased RPM and refrigerant flow rate causes a big pressure drop across the expansion orifice, which explains the drop in evaporator inlet temperature shown in Figure 5.8. The accumulator outlet temperature follows the evaporator outlet temperature with a time lag and a drop of amplitude that are proportional to the thermal mass of the accumulator body and the heat transfer from its surface.

Figure 5.9 shows the inlet and outlet pressures of both the evaporator and condenser. Whenever the compressor RPM decreases, and therefore refrigerant flow rate, the pressure drop of both heat exchangers decreases and the pressure ratio decreases. The decrease in pressure ratio and refrigerant mass flow rate causes a drop of compressor power as shown in Figure 5.10. It can be seen in the figure that the compressor power fluctuates between 0.5 kW and 2.0 kW.

The refrigerant-side capacity and the airside sensible and latent and total capacities are shown in Figure 5.11. It can be seen that whenever the RPM increases, and therefore the refrigerant flow rate, the capacities increase. The locations where the refrigerant-side capacity curve is discontinuous are when the superheat at evaporator outlet was lost and therefore the capacity could not be calculated. The refrigerant-side capacity is obviously more than the airside capacity as expected in a transient case, but the difference between them is decreasing. Whenever the RPM, and therefore refrigerant flow rate, increases the latent and sensible capacities increase because of the decrease in evaporation temperature. However, the latent capacity is more affected by the evaporation temperature. This is believed to be due to the condition of

the air upstream of the evaporator. If the inlet air was colder and dryer the fluctuations in the sensible capacity would have been bigger. Generally, the hotter the air upstream of the evaporator the more the change in sensible heat as a ratio of change in total heat will be. This is because of the slope of the saturated air line.

It is interesting to note the phase shift between the refrigerant mass flow rates, the capacities, and the compressor power consumption, which is the main focus of Figure 5.12. In the figure, it is clear that the airside capacity lags the refrigerant mass flow rate while the compressor power is in phase with the flow rate. This is because the transfer of heat from the air to the evaporator coil and then to the refrigerant is a relatively slower process than the redistribution of the refrigerant inside the system. It is difficult to notice in the figure if the refrigerant-side capacity is in phase with or slightly lagging the refrigerant flow rate. In order to investigate this, a faster and more accurate data acquisition system must be used.

Also of note in Figure 5.12 is that the fluctuations in power consumption are more than the fluctuations in capacity, and therefore the instantaneous COP decreases with the increase of compressor RPM as shown in Figure 5.13. However, the instantaneous COP is not meaningful in such a transient situation. For this reason, the air side capacity and the compressor power consumption were both integrated over time for the duration of the test. Their quotient, called the overall COP, is a better indicator for the system's performance. This value during this test was 1.72 as noted on Figure 5.13.

5.4 Drive Cycle Tests with Thermostats

In this test, the NEDC was imposed on the system under the same conditions listed in Table 5.2. The thermostat function was activated and set to 24°C ± 1°C. Because the cabin reaches 24°C near the end of the 18 minutes that are the cycle length, the cycle was repeated two times.

Figure 5.14 shows the different cabin temperatures. The supply air temperature is given by the dashed line and the internal mass temperature is given by the crossed line, which is decreasing slower than the air temperature. The cabin air temperature is

again given by two lines, one for the calculated values and another for the measured values. The cabin air temperature decreases to 23°C then starts fluctuating around 24°C. The difference between the calculated cabin air temperature and the measured cabin air temperature is shown on the right-hand Y-axis of the figure.

Figure 5.15 shows the supply air and cabin air relative humidity. As the system starts the RH downstream of the coil increases. When the system stops the coil loses its moisture capturing capabilities, therefore the RH of the supply air increases due to liquid carry over, and subsequently the RH inside the cabin increases also. Due to the thermostat action, the cabin air relative humidity fluctuates between 15% and 35%. The increase in cabin RH, from an energy point of view, is a load on the A/C system when it starts again, but from the point of view of comfort, it helps the passengers feel comfortable as long as it is within acceptable limits.

Figure 5.16 shows the capacities and the COP during the test. The line with the crosses is the latent capacity and it can be seen that it has a negative value during the compressor off periods; this is because of the re-evaporation. The line with the circles is the sensible capacity and it can be seen that during the off periods it does not drop to zero instantaneously. In total, the airside capacity has a small positive value during the compressor off periods. Figure 5.16 also shows the refrigerant-side capacity and the instantaneous COP calculated using the airside capacity.

5.5 Cycling Tests

The on-off operation is very common in vapor compression cycles, and therefore it is of particular importance to understand. A few observations can be drawn from previous tests, which are:

- During off-cycle there is capacity delivered (mainly sensible) but no power consumption.
- During off-cycle the condensate on the evaporator coil re-evaporates into the air. This represents a net loss of latent capacity.
- At the beginning of the on-cycle the power consumption builds-up faster than the capacity.

During short off-cycles the evaporator stays relatively cold and therefore it can deliver some capacity, but as off-cycles become longer, the evaporator heats up and may even reach a temperature that is higher than the air temperature for a period of time. At the beginning of an on-cycle the power consumption builds-up faster than the capacity and therefore the COP is low, but as an on-cycle becomes longer, the portion of it with low COP becomes less significant and does not affect the overall COP as much. It can be concluded that there will be differences in overall performance and energy utilization between a short-cycling system and a long-cycling system. The effect of cycling on the system is the focus of the present category of tests. Special attention will be given to the latent capacity.

In the cyclic tests category, the compressor is continuously cycled on and off within cycle length (duty cycle) that varies from 10 seconds to 4 hours. In each cycle, the compressor is on for 50% of the time and off for 50% of the time. The test conditions were:

- Indoor air: 25°C & 50% RH.
- Outdoor air: 35°C.
- Evaporator face velocity: 2.3 m/s.
- Condenser face velocity: 2.5 m/s.
- Compressor rotational speed: 2500 RPM.
- Return air mode: fresh air.

The different cycle duties that were run are listed in Table 5.3. At each duty cycle, the system was cycled several times to make sure it has reached cyclic steady state. Different system parameters such as temperature, pressure and mass flow rate were plotted against time and checked for cyclic steady state status. Only the cycles that exhibited cyclic steady state status were considered in the analysis. Table 5.3 lists the total number of cycles at each duty cycle and the number of cyclic steady state cycles that were used in the analysis. Cycle duties were chosen to concentrate on short cycle periods where there are sharp changes in performance parameters, then they become more widely spaced as cycle duties become longer. Tests at cycle duties of 2 and 4 hours do not reflect any practical situations, however they were conducted to confirm

the general trend of results and provide a means of checking this trend by checking the asymptotic values that the results approach.

Each test starts with the compressor energized continuously for an hour to ensure steady state has been reached. Then another hour follows where the condensate is collected. During this hour two checks are made; the latent capacity as calculated from the condensate is compared with the latent capacity as calculated from the humidity sensors, and the total airside capacity is compared with the refrigerant-side capacity. The results of these two checks were always an error less than 2% for latent capacity and an error of less than 4% for total capacity. Following this steady state period the compressor starts cycling. Several duty cycles might be grouped in one test. At the end of the test another steady state period follows for the reason of performing the two aforementioned checks and also to make sure that system operating parameters, such as temperatures, pressures and mass flow rate, have returned to the same values at which they started. During long duty cycle tests, such as the 2-hour and the 4-hour tests, the same two steady state checks were performed on the last period of the on-cycle as well. All these checks were performed because, as noted in Chapter 4, during cycling there is no method to check the accuracy of the results.

Figure 5.17 shows, on the X-axis, the cycle period (duty) starting from 10 seconds (5 seconds on and 5 seconds off) to 4 hours (2 hours on and 2 hours off). The Y-axis shows, in kilograms of water, the amount of moisture removed from the air, either during the on-cycle, or the off-cycle, or the complete cycle (both the on- and the off-portions). During the on-cycle, some moisture is removed from the air, the amount of which increases, almost linearly, as the length of the on-cycle increases. During the off-cycle, the condensate hanging to the evaporator coil re-evaporation and this is shown on the figure with negative value. The amount of re-evaporation levels-off as the coil has a fixed moisture holding capability. Therefore the net moisture removal increases with cycle period. It can be seen that the moisture-holding capability of this specific coil is about 0.2 kilograms

Figure 5.18 is the same as Figure 5.17 but zooms on the cycles up till 18 minutes only. The same 3 curves, condensation during on-cycle, re-evaporation during off-cycle, and net moisture removal can be seen again on Figure 5.18. It can be seen on the figure that 9 minutes of compressor-off time are not enough to re-evaporate all the condensate on the coil. Also it can be noticed that the net moisture removal on this figure becomes 2 orders of magnitude smaller than that at longer tests.

If the focus was shifted to tests shorter than 2 minute, enlarged in the insert, a reversal in trend can be seen; there is moisture removal during the off-cycle and re-evaporation during the on-cycle. This is physically meaningless, but it happens because the test period becomes comparable to the time constant of the humidity sensor (15 seconds). The slowness of the humidity sensors becomes a problem for tests shorter than 2 minutes.

The moisture removal rate, in grams of water per second, is shown in Figure 5.19 and Figure 5.20. The time used as bases to calculate the rate is the period of the complete cycle. That is why the moisture removal rate during the on-cycle at the longest test is exactly half of that at steady state, which is plotted at cycle period equals zero. It can be seen that the moisture removal during steady state is about 0.38 g/s and as the cycle increases in length, the coil can ultimately remove half of this amount during the on-cycle, but the moisture holding capacity decreases this value due to re-evaporation.

It is also interesting to notice that the moisture removal rate reaches the values that it levels-off at early, at about the 14-minute test. But then, because the moisture holding capacity is constant and the tests are getting longer, the re-evaporation decreases while the condensation doesn't. That is why the net moisture removal rate takes the shape in Figure 5.19, which is the shape of a check mark with a horizontal portion at the end.

It is also interesting to notice in Figure 5.20 that the net moisture removal during very short cycles (10 and 20 seconds) is comparable to that at long cycles (10 minutes and longer).

Figure 5.20 exhibits the same reversal in sign of the condensation and re-evaporation seen in Figure 5.18. However, the value of the net moisture removal is trustworthy and is not affected by the delay in humidity measurements because the time constant of the humidity sensor provides only a time shift but not an error in the values, and also the compressor is not cycled once, but several times. The net moisture removal is a minimum at 2-minute cycles, it is almost zero.

The question might arise as to why the moisture removal rate during very short tests is higher than that at relatively longer tests? This can be explained based on the coil surface temperature chart shown in Figure 5.21. The coil surface temperature at 4 different locations; viz. near evaporator inlet upstream of air, downstream of air, near evaporator outlet upstream of air and downstream of air, are plotted in Figure 5.21. The X-axis is represents the time during the tests, not the cycle period. There are six of 18-minute tests followed by six of 14-minute tests followed by eight of 10-minute tests and so on until eighty four of 10-secnd tests. There are also 4 straight broken lines that represent the time-weighed (over the whole cycle) averages at the four places for each test. Also in Figure 5.21 is a line that represents the dew point temperature of the evaporator upstream air.
The lines in Figure 5.21 overlap and can't be distinguished from one another, but the important thing to note is the range in which the surface temperature fluctuates and its average value and to compare those with the dew point temperature of the upstream air. It can be seen that during the relatively long tests the coil surface temperature fluctuate between a value higher than the dew point when the compressor is off and a value below the dew point when the compressor is on. While the cycles get shorter there is not enough time for the surface temperature to increase more than the dew point and stays lower even during the off-cycle. Therefore there is more moisture removal.

To check the possibility of un-drained condensate staying in the drain pan below the evaporator and then re-evaporating, the test portion of the indoor air loop was fitted with a clear side wall to allow for visualization. Figure 5.22 is a photo taken at the

beginning of an off-cycle where there were a few condensate pools that are not drained. After 90 minutes of off-cycle, another photo, Figure 5.23, was taken. Comparing the two photos show that some condensate was re-evaporated from the drain pan. However, empirically, only 2 or 3 grams were evaporated in 90 minutes and therefore the rate of evaporation is very small. From another point of view, the total extended surface area of the coil is 3.0 square meters while the surface area of the condensate pools is about 70 square centimeters, 400 times less than that of the coil. Therefore, it was concluded that the re-evaporation from the drain pan is negligible.

If focus is now shifted to the capacity and power consumption, Figure 5.24 gives these values as a percentage of their respective steady state values. The bottom line in the figure is the capacity delivered during the on-cycle only and this can't be higher than half of the steady state capacity because the on-cycle is only half the time of the total cycle. This value was calculated by integrating the capacity delivered during the on-cycle of all the cyclic steady state tests over time and dividing by the total time of the tests. It can be seen that it eventually increases to 0.5 but during the short tests it is lower than 0.5. This loss of capacity comes from two sources; the sensible capacity is lost because at the beginning of the on cycle the coil is not as cold as it should be, and the latent capacity, which is low at short cycle periods as was seen previously.

If the capacity delivered during the off-cycle was added to the on-cycle capacity the middle line in Figure 5.24 can be plotted. On a per-second basis, the off-cycle capacity is negligible during long tests but appreciable during short tests and therefore the middle line is higher than the lower line in short tests and approaches the lower line in long tests. It can be seen that the capacity recovers 48% of its steady state value at 18-minute cycle duty.

The power starts from a high value but quickly decreases as the portion of the test in which the power consumption is higher than the steady state value becomes less significant. It can be also noticed that the power levels off faster than the capacity.

Figure 5.25 is the same as Figure 5.24 but focuses on the short duty cycles. The capacity including the off-cycle is bigger than the capacity during the on-cycle only by the amount of air cooling and dehumidification that happens during the off-cycle as a result of the coil surface being colder than the air. This off-cycle capacity is negligible during the long cycles, but amounts for 58% of the total capacity at the 40-second cycle. There is no phenomenon whose effect is to decrease the power consumption than half that of the steady state case. It is also interesting to observe that the local minimum of the capacity has shifted from 40 seconds to 4 minutes just by considering the capacity during off-cycle. The conclusion here is that the cycle period affects the system capacity.

But what about the ratios of the sensible capacity and the latent capacity? It can be seen in Figure 5.26 that at steady state one quarter of the capacity is latent. But with cycling, this ratio drops quickly and then rises again. This trend, a check mark with a horizontal portion at the end is the same as the moisture removal rate, which makes sense because the latent capacity and moisture removal rate are strongly related. The latent capacity levels off at a value less than the steady state value because the curve considers the re-evaporation which is an un-regainable loss of latent capacity.
The fact behind sensible and latent capacities and cycling is that during on cycle there is latent capacity, during the off-cycle, there is loss in latent capacity. During the on-cycle there is sensible capacity and during off-cycle there is still some sensible capacity. Therefore, during on cycle the air is cooled and dehumidified, but during off-cycle the air is cooled and humidified. However, the total capacity is expected to have a positive value in all cases because the net moisture removal rate is positive in all cases as shown previously in Figure 5.19.

Figure 5.27 is the same as Figure 5.26 but details the short cycles. It can be seen that for cycle duties in the range of 10 seconds to 2 minutes, the coil latent heat factor varies from 0.17 to 0.01, a factor of 17 times. It can be hence concluded that it is possible to meet loads with different latent characteristics, loads that are high in latent demand or low in latent demand, by varying the cycle period. For example, a

programmable logic can be utilized such as to control the cycling of the compressor not only according to the thermostat, but also according to the load for the purpose of varying the latent and sensible ratios of the capacity.

But if this is to be done, it would be of interest to see how the coefficient of performance varies with the duty cycle, or in other words what is the cost of operating the system at different cycle duties? The COP is plotted in Figure 5.28 The whole-cycle COP was calculated by dividing the total capacity as a result of integration of the instantaneous capacity over time, including the off cycle and the re-evaporation, by the total power consumption also as a result of integrating the instantaneous power consumption over time. It was noted in Figure 5.24 that the power consumption levels off faster than the capacity and hence the dip in the COP curve. It is clear that the COP recovers 97% of its steady state value at 18-minute cycle duty.

The lower curve in the figure is just the division of the instantaneous capacity by the instantaneous power consumption.

The duty cycle at which the COP or capacity regain a specific portion of their steady-state values is expected to be dependent on the configuration of the system and the refrigerant charge. It might prove to be a useful indicator for cyclic performance.

Figure 5.29 is an enlargement of the short cycles portion of Figure 5.28. And the conclusion is that the system runs at different COP values when cycling at different cycle periods and therefore the programmable logic control need to take into consideration an optimization scheme. By cross-examining Figure 5.20, Figure 5.25, Figure 5.27, and Figure 5.29, it can be noticed that the net moisture removal rate, the total capacity, the coil latent heat factor, and the COP exhibit a local minima at 2 minutes, 4 minutes, 3 minutes, and 3 minutes, respectively.

To increase the validity of the results, some of the curves in the previous figures were fitted with error bars. These error bars represent 5% error, which is the same error during steady state. The reasoning behind this is to make the cyclic test results as accurate as the steady state tests.

5.6 Conclusions

In this chapter, several types of dynamic tests were conducted on the MAC using the dynamic test facility. The facility was successful in controlling the temperature within a range of ±0.9°C of the required temperature and the relative humidity within 5% of the required relative humidity. Moreover, the results showed that the dynamic test facility was capable of demonstrating the following transient phenomena:

- The effect of the thermal storage in the system mass was obvious in the difference between the refrigerant-side capacity and the airside capacity and also in the refrigerant temperature at accumulator outlet.
- The different time constants of the system were observed due to the different rates by which the power and the capacity build-up. The power builds up faster than the capacity and hence the COP decreases.

5.6.1 Conclusions from Pull-down and Drive-cycle Tests

- The best scenario to pull-down the cabin temperature was investigated. In case of a hot-soaked car cabin, and under the specific test conditions listed in section 5.2, starting the pull-down with fresh air then switching to recirculated air when the cabin temperature is equal to the outdoor ambient temperature saved 2 minutes in the time required to reach 24°C and cause a 12.3% reduction in energy consumption and 21.6% increase in COP. Also the case of fresh air represents a higher load than the case of idling at the specified ambient conditions.
- The effect of the thermostat action on the relative humidity inside the car cabin was observed. During the compressor-off period, the relative humidity inside the cabin increases.
- The effect of RPM fluctuations on the latent capacity and the sensible capacity was noted at the specified test conditions. The latent capacity was more affected than the sensible capacity because of the condition of the evaporator upstream air.

5.6.2 Conclusions from the Off-cycle Attributes (Cooling and Humidification)

- The off-cycle attributes were illustrated in the results. During the compressor off period (with the evaporator fan in operation) there is no power consumption, the sensible capacity decreases gradually, and the latent capacity reverses sign. Therefore the air is cooled and humidified. In general, the direction of the net flow of heat is from the air to the coil, and therefore the total air capacity at the specified test conditions has a small positive value.
- The effect of off-cycle attributes on the capacity and COP was shown. The capacity and the COP increase if the off-cycle cooling and humidification were considered.
- The effect of re-evaporation was illustrated by showing the off-cycle sensible capacity, latent capacity and total capacity. The coil moisture-holding capacity is 200 grams. Re-evaporation continued for slightly more than 9 minutes at the specified test conditions.
- The effect of the off-cycle capacity was shown to shift the location of minimum total capacity from 40 seconds (if off-cycle capacity was not considered) to 4 minutes at the specified test conditions.

5.6.3 Conclusions from the Cyclic Tests

- The effect of cycling on the capacity and COP was shown in the results. Both the capacity and COP decrease then increase again by increasing the cycle duty. At 18-minute cycle duty the COP recovers 97% of its steady state value while the capacity recovers 48% of its steady state value. This indicates the possibility of devising a new indicator for cyclic performance.
- The effect of cycling on the coil sensible and latent heat factors was shown in the results. The net moisture removal rate has a minimum at around 2 minute cycles at the specified test conditions. Its value at very short cycles is comparable to that at longer cycles. This was attributed to the evaporator coil surface temperature, which stayed relatively colder at short cycles. Whence the possibility of controlling the coil latent heat factor by varying duty cycle.

- The local minima of the net moisture removal rate, the total capacity, the coil latent heat factor, and the COP were found to be concentrated in the range of 2- to 4-minute cycles. This indicates that optimization is required in case of devising a control, based on cycling, to adjust COP or capacity or coil latent heat factor.
- The cycling losses are small in two cases: either the cycle is too long that the portion of the test where there is losses is negligible with respect to the total cycle length, or the magnitude of the losses is small because the off-cycle period is short. Moisture removal rate, total capacity, and COP at very short cycles have values comparable to steady state values. This indicates the possibility to enhance current cyclic efficiency by shortening cycling time.

Generally, the dynamic test facility is a cost-effective way to run transient tests in a laboratory. It eliminates the need for testing a full-scale car in a wind tunnel. The dynamic test facility has demonstrated potential for enhancing the transient behavior of automotive climate control systems in terms of pull-down speed, energy consumption, and capacity factors.

Table 5.1 Test Matrix of Pull-down Tests

S / N	Type	Amb. Temp (°C)	Amb. RH (%)	Degree of Soak (K)	Compressor RPM	Evap. air speed (m/s)	Cond. air speed (m/s)	Mode
1	Pull-down to 24 °C	30	50	11	800 (idling)	2.3	2.5	Recirculated air
2		41	32	0				
3		30	50	11				Fresh air
4		41	32	0				
5		30	50	11	2500 (driving)			Recirculated air
6		41	32	0				
7		30	50	11				Fresh air
8		41	32	0				
9		30	50	11	2500 (driving)			Fresh air until ambient temp. then recirculated air
10		30	50	11	800 (idling)			Recirculated air. Condenser air temp. = 35°C

Table 5.2 Test Matrix of Drive Cycle Tests

S / N	Type	Amb. Temp (°C)	Amb. RH (%)	Degree of Soak (K)	Comp. RPM	Evap. air speed (m/s)	Cond. air speed (m/s)	Mode
1	Pull down under New European Drive Cycle (NEDC)	30	50	5.6	--	2.3	2.5	Recirculated air

Table 5.3 Duty Cycles and Number of Cycles of Cyclic Tests

Cycle Length (Duty)	Total Number of Cycles	Number of Cycles Used in Analysis (Cyclic Steady State)	Total Period of test
4 hours	6	3	24 hours
2 hours	6	3	12 hours
18 minutes	6	3	108 minutes
14 minutes	6	3	84 minutes
10 minutes	8	5	80 minutes
6 minutes	12	9	72 minutes
4 minutes	14	8	56 minutes
2 minutes	20	9	40 minutes
1 minute	30	15	30 minutes
40 seconds	30	14	20 minutes
20 seconds	63	27	21 minutes
10 seconds	84	37	14 minutes

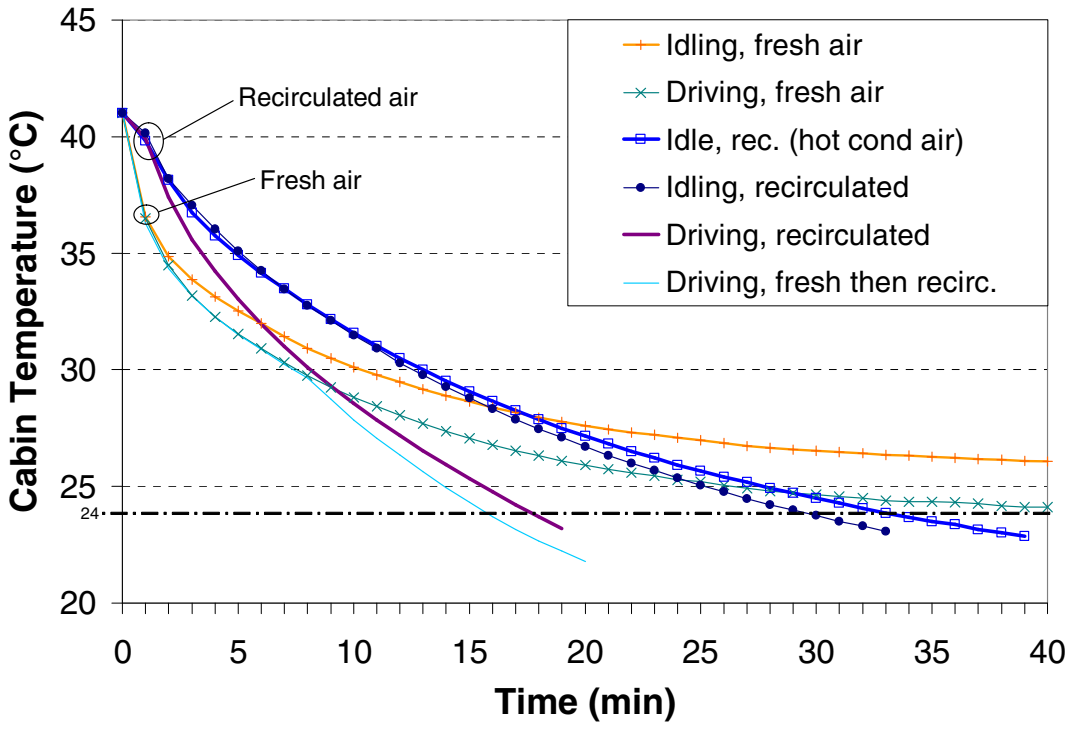

Figure 5.1 Pull-down at Ambient = 30°C & 50% RH for Tests with Hot-soak

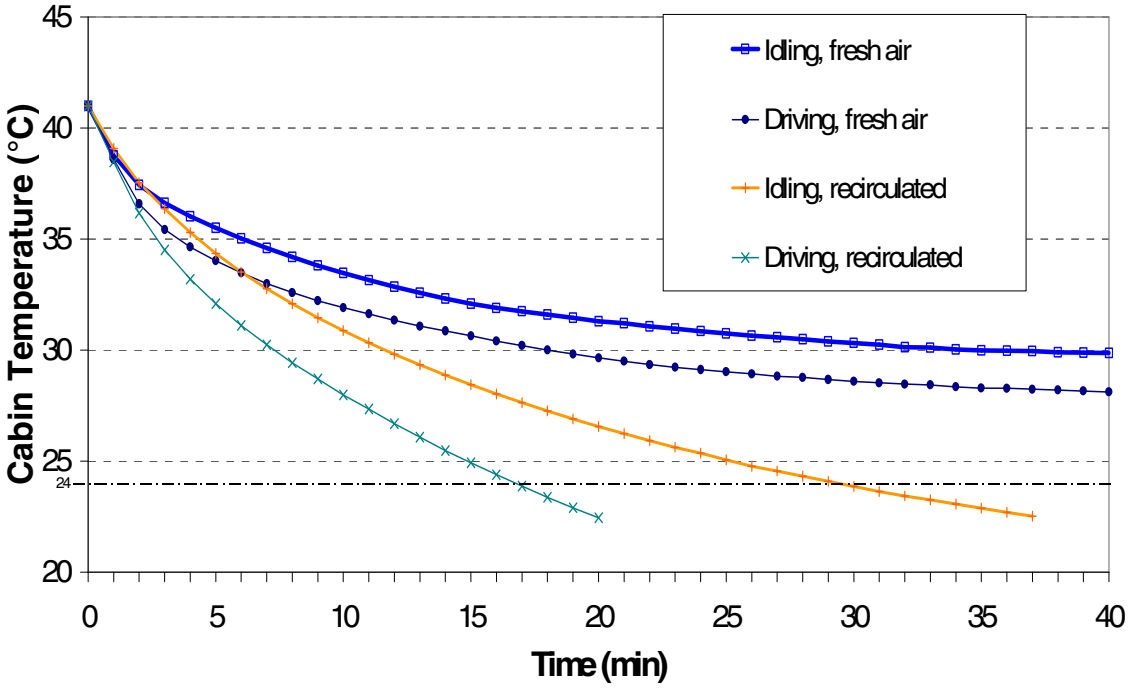

Figure 5.2 Pull-down at Ambient = 41°C & 32% RH for Tests without Hot-soak

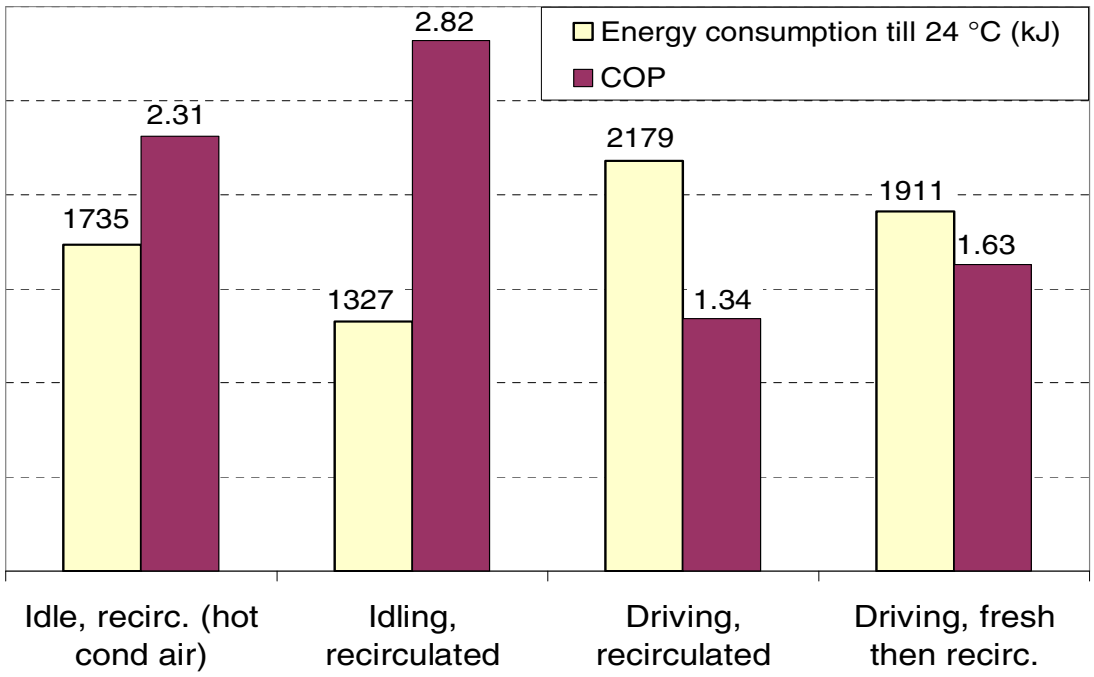

Figure 5.3 Energy Consumption and COP of Pull-down Tests with Hot-soak

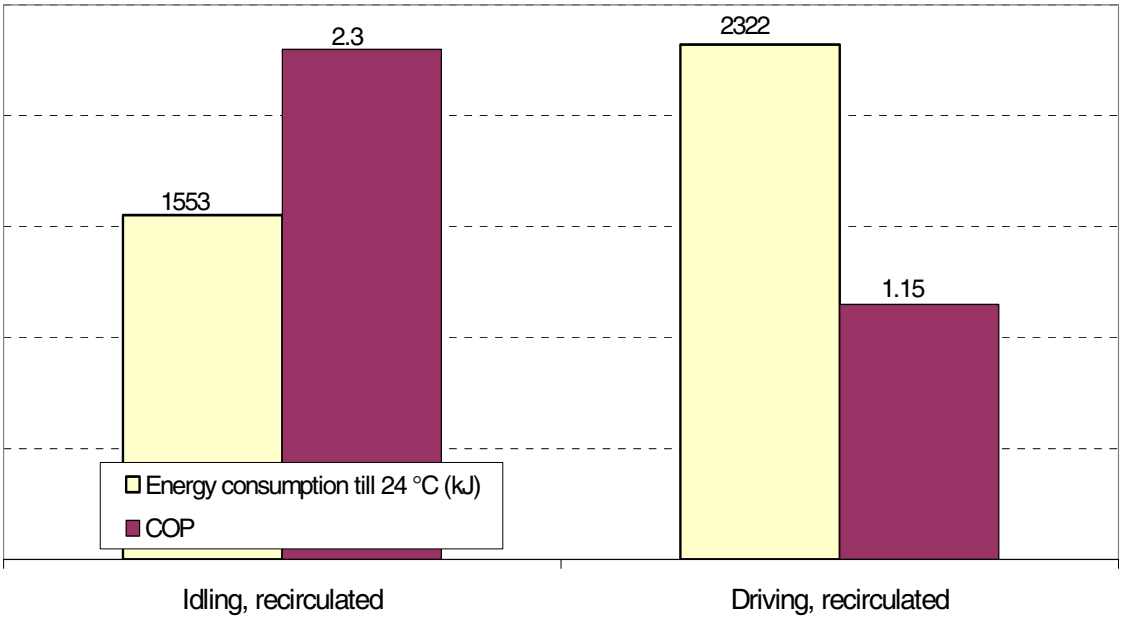

Figure 5.4 Energy Consumption and COP of Pull-down Tests without Hot-soak

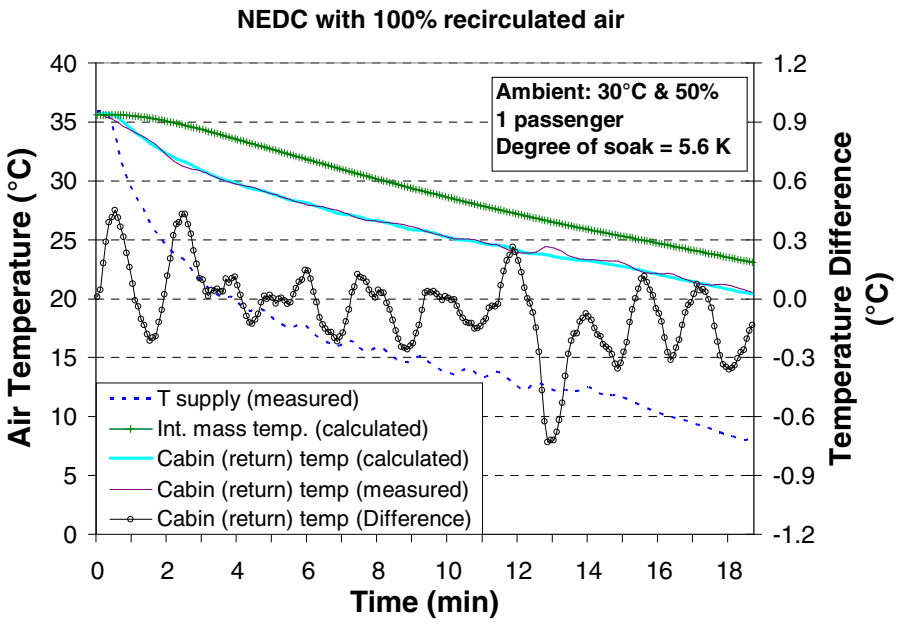

Figure 5.5 Cabin Temperatures During NEDC

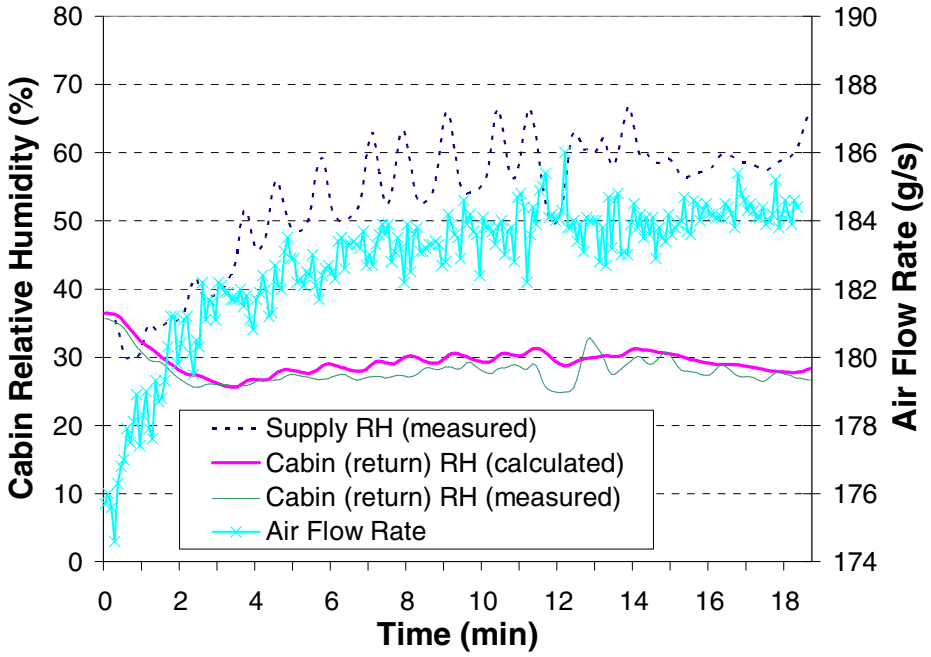

Figure 5.6 Cabin Relative Humidity During NEDC

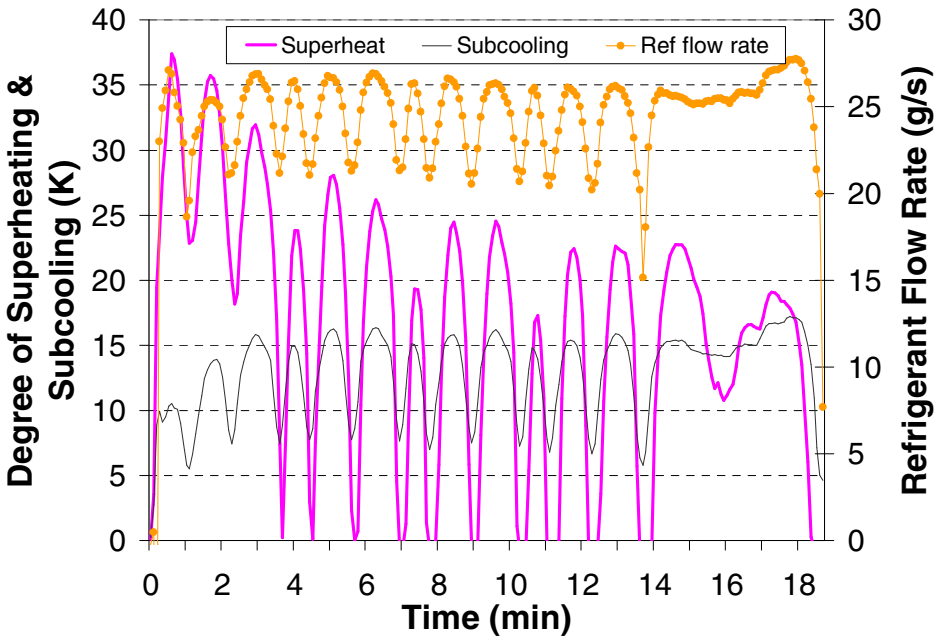

Figure 5.7 Degrees of Superheating and Subcooling During NEDC

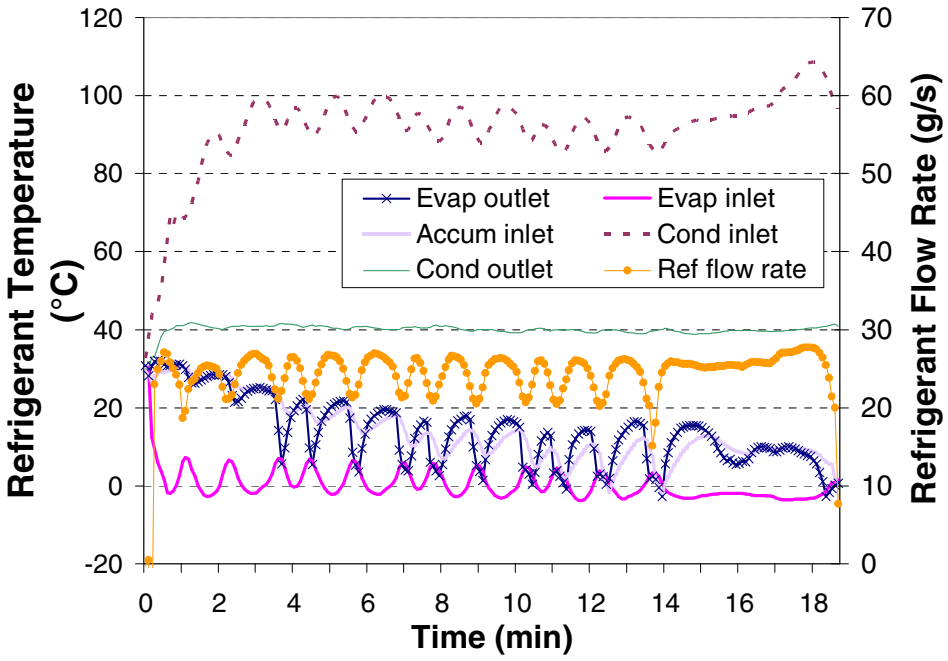

Figure 5.8 Refrigerant Temperatures During NEDC

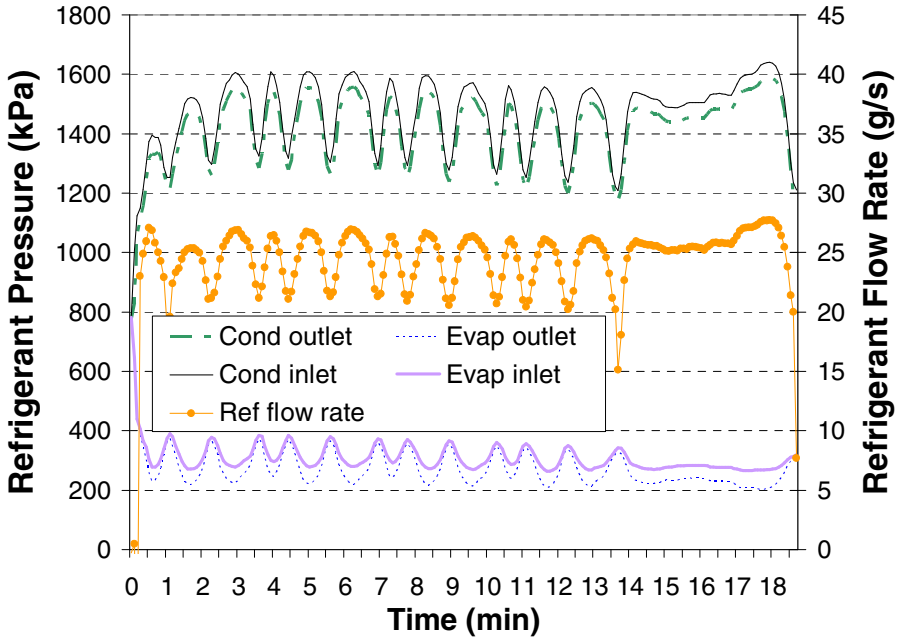

Figure 5.9 Refrigerant Pressures During NEDC

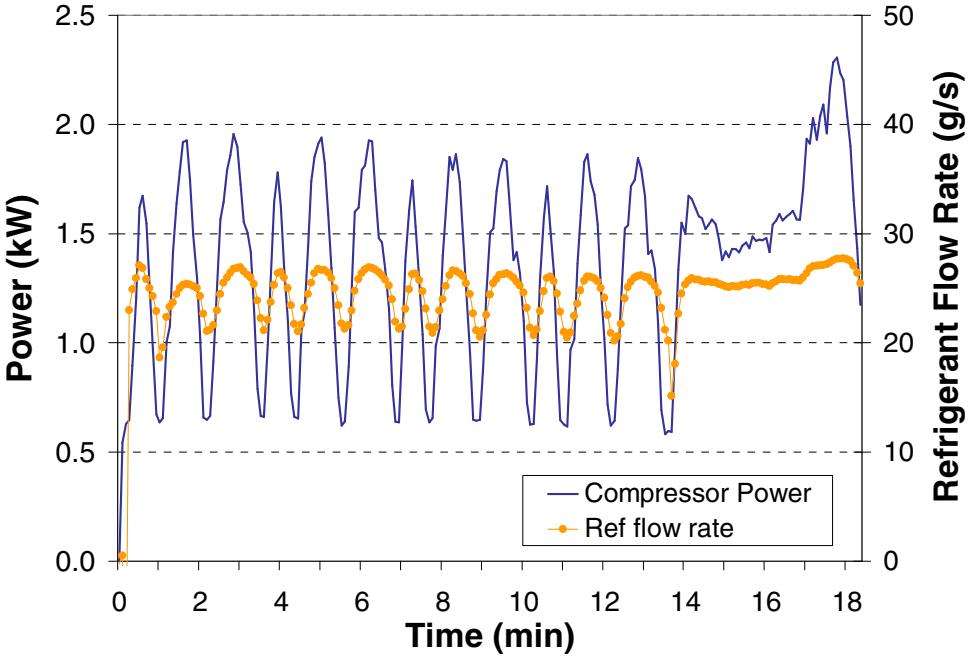

Figure 5.10 Compressor Power during NEDC

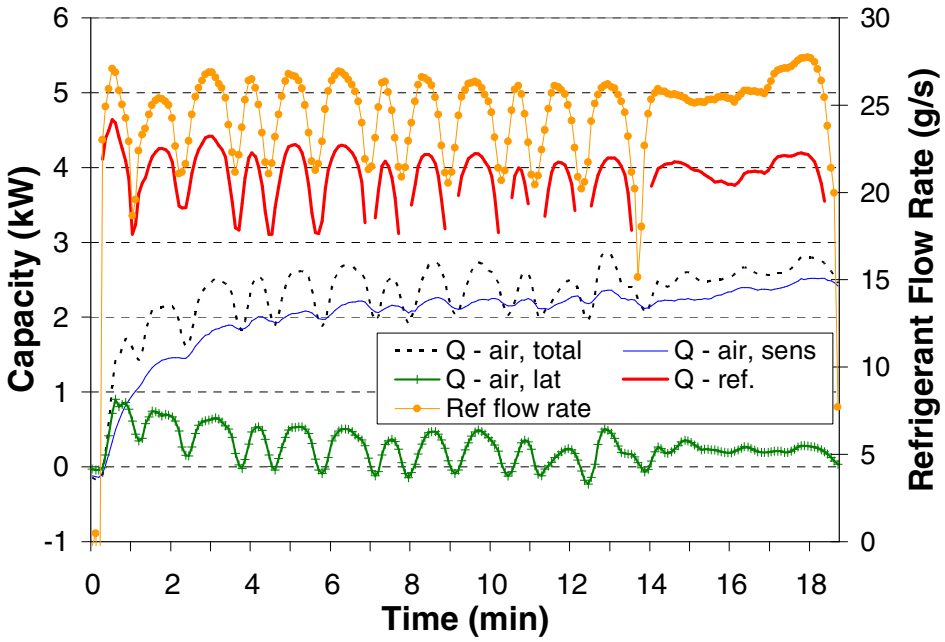

Figure 5.11 Capacity During NEDC

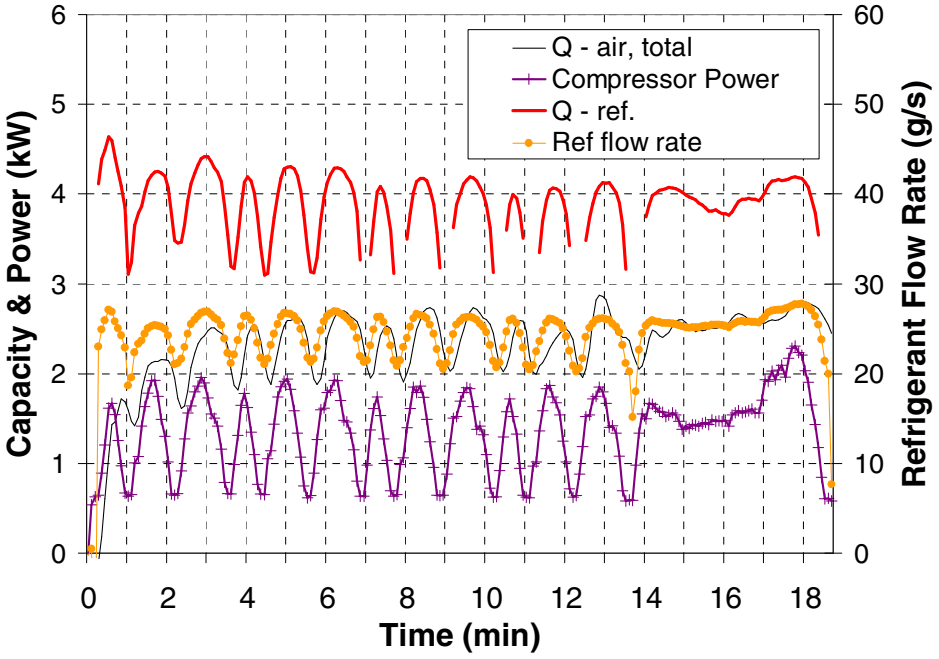

Figure 5.12 Refrigerant Capacity and Power During NEDC

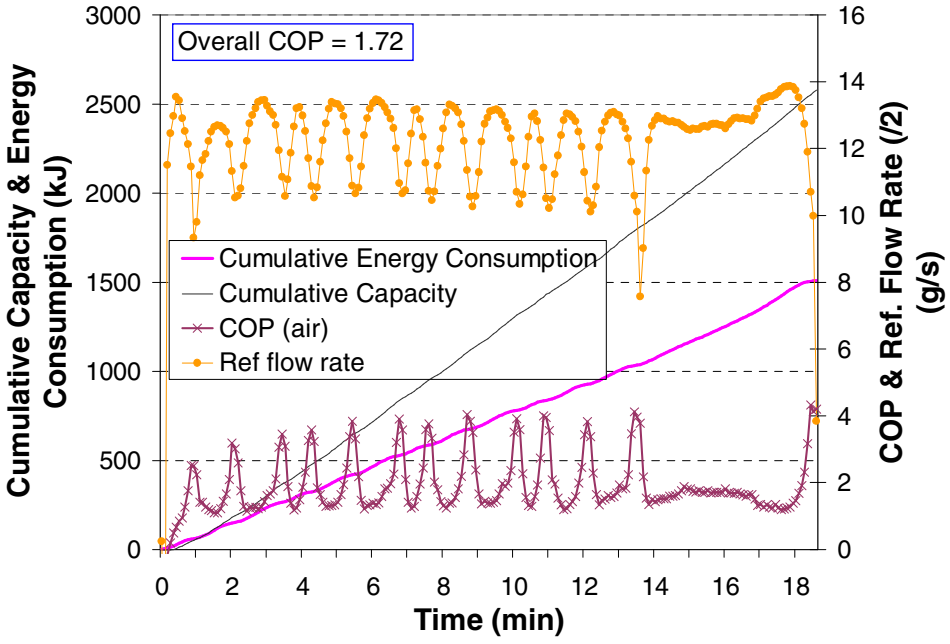

Figure 5.13 System Performance During NEDC

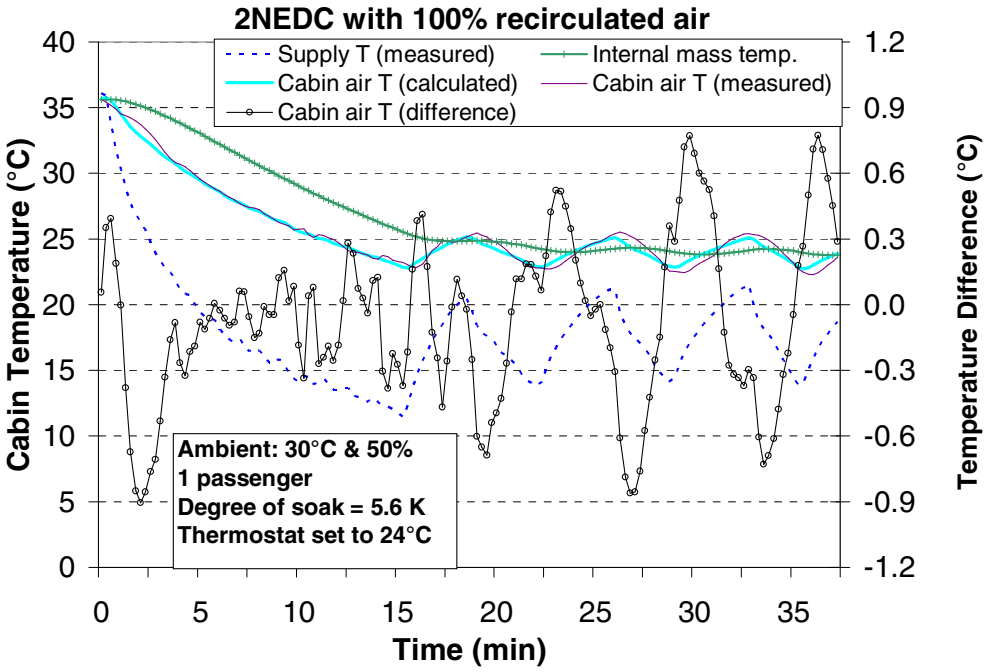

Figure 5.14 Cabin Temperatures During NEDC with Thermostat

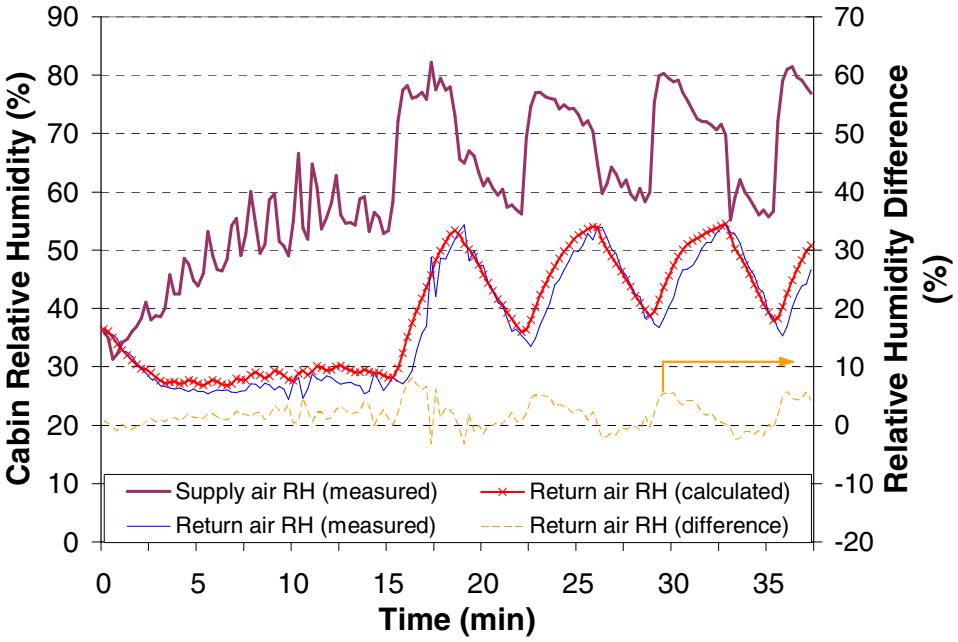

Figure 5.15 Cabin Humidity During NEDC with Thermostat

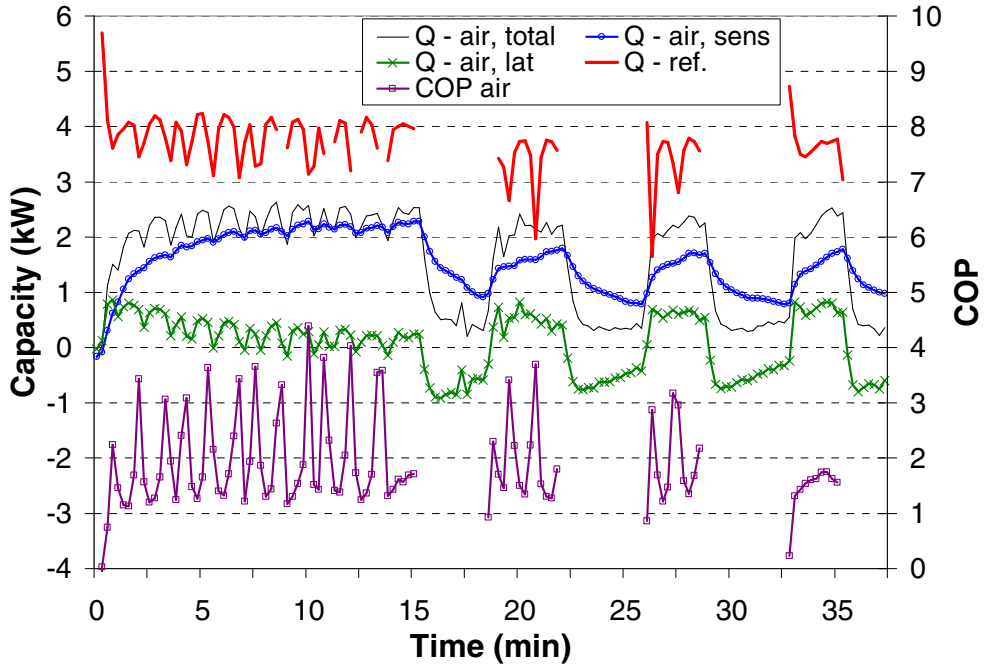

Figure 5.16 Capacity and COP During NEDC with Thermostat

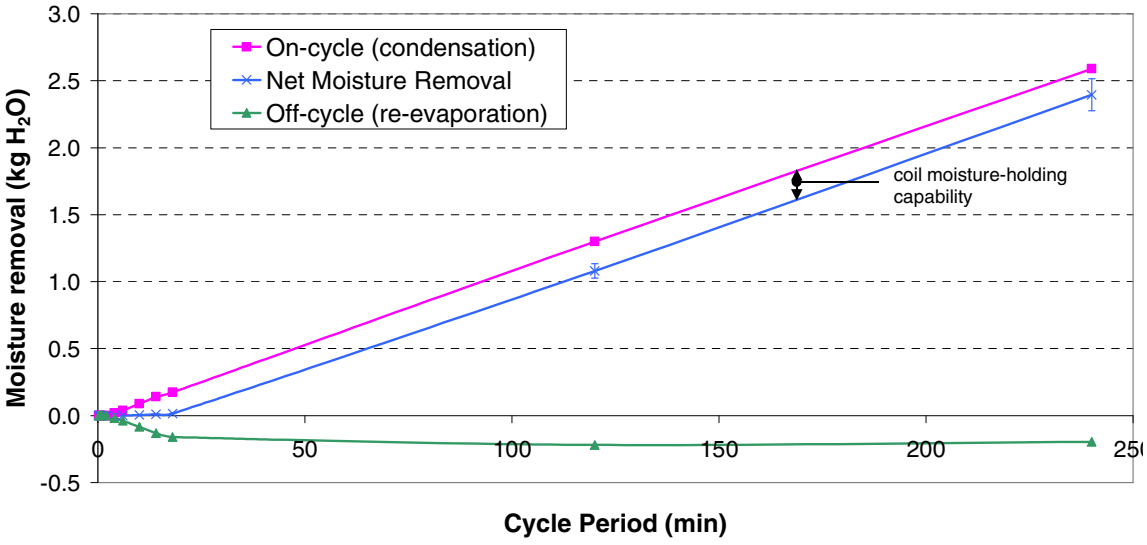

Figure 5.17 Moisture Removal During Cyclic Tests

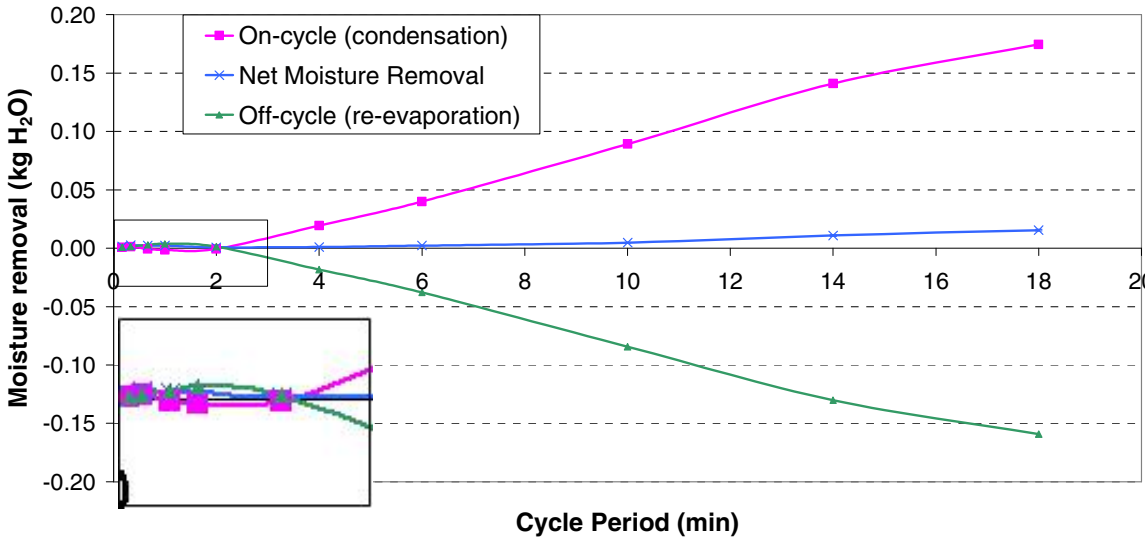

Figure 5.18 Moisture Removal During Cyclic Tests – Short Cycles

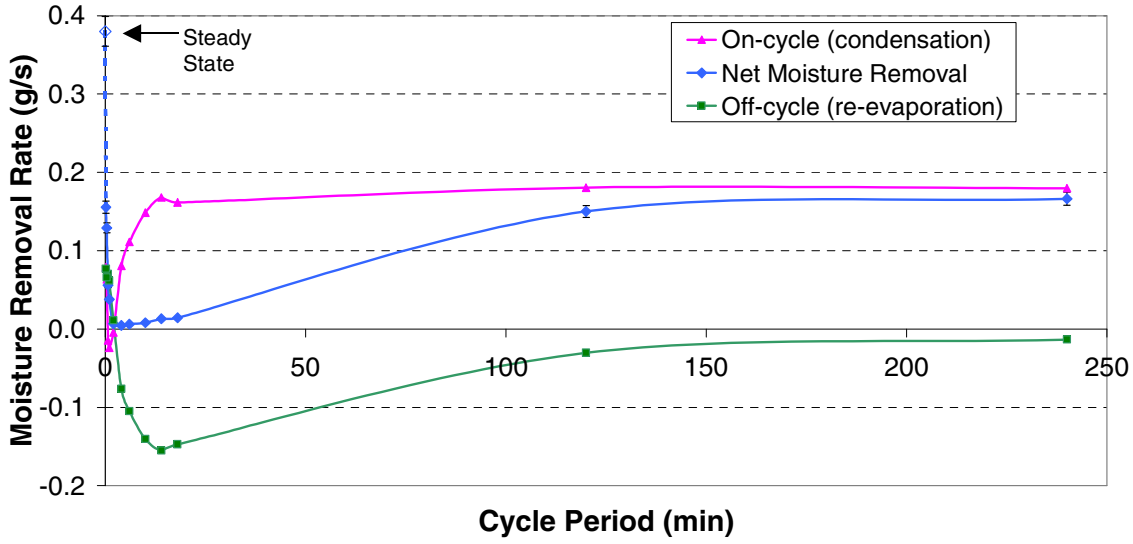

Figure 5.19 Moisture Removal Rate During Cyclic Tests

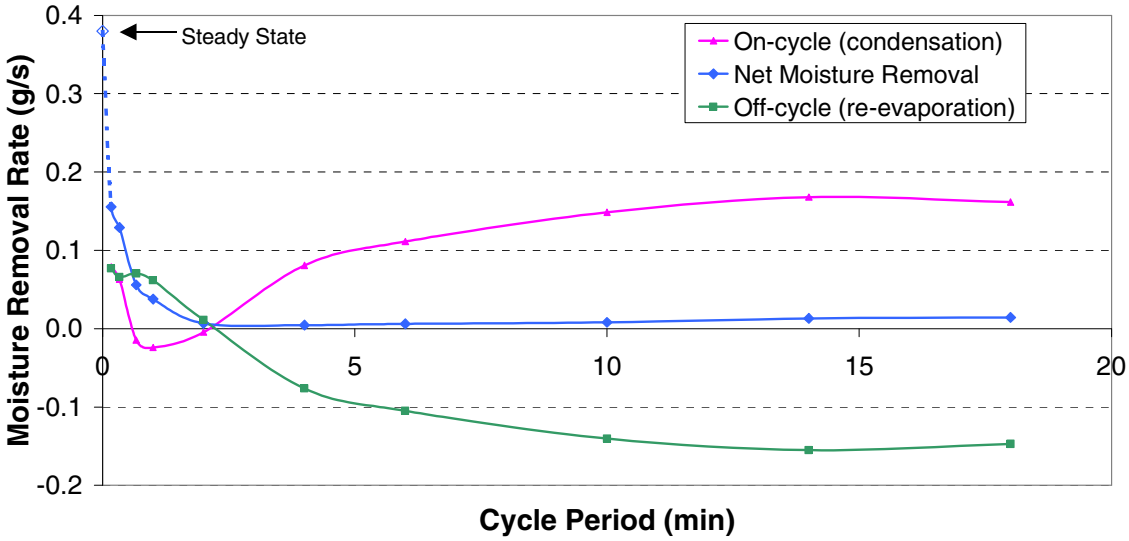

Figure 5.20 Moisture Removal Rate During Cyclic Tests – Short Cycles

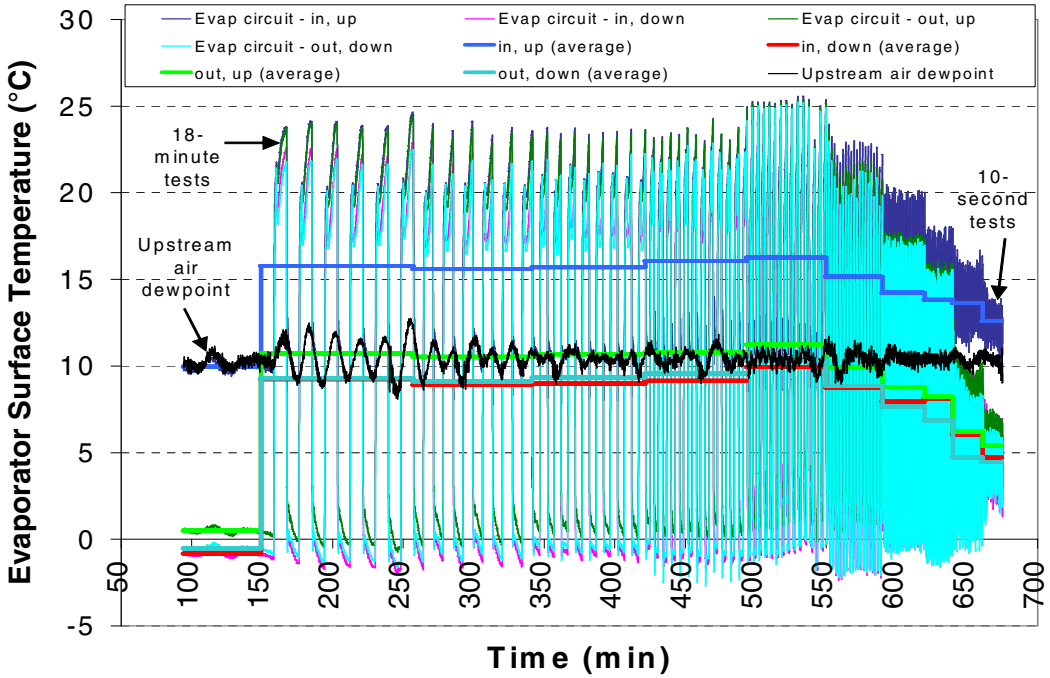

Figure 5.21 Coil Surface Temperature During Cyclic Tests

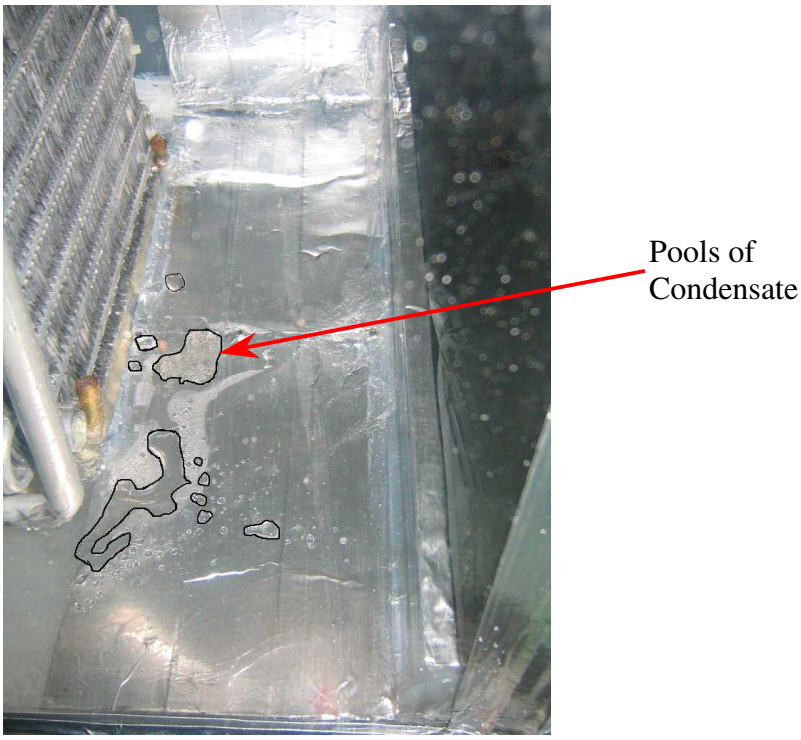

Figure 5.22 Drain Pan at the Beginning of an Off-cycle

Figure 5.23 Drain Pan 90 Minutes into an Off-cycle

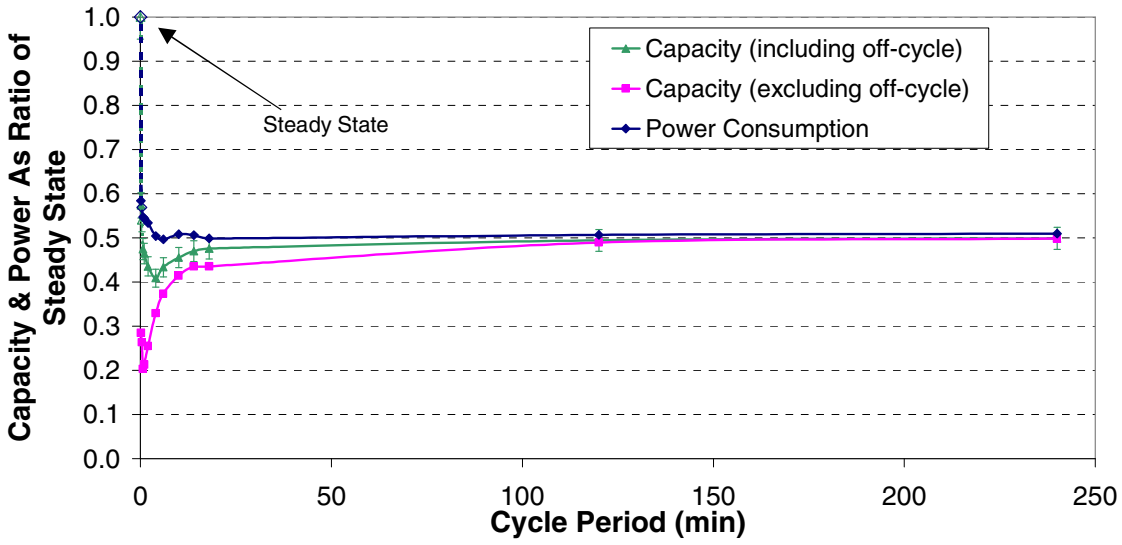

Figure 5.24 Capacity and Power as Ratio of Steady State Capacity and Power

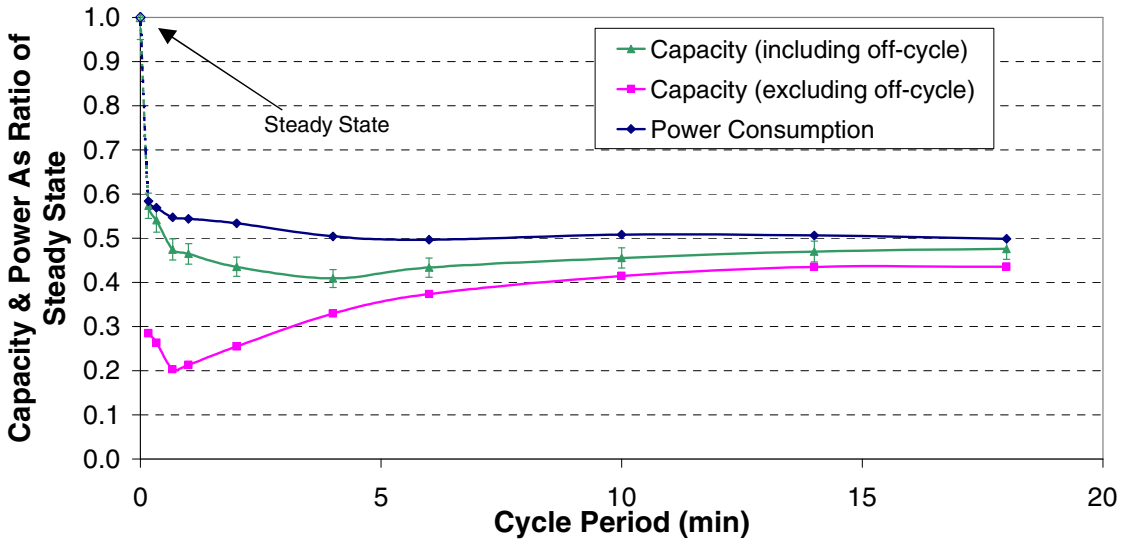

Figure 5.25 Capacity and Power as Ratio of Steady State Capacity and Power – Short Cycles

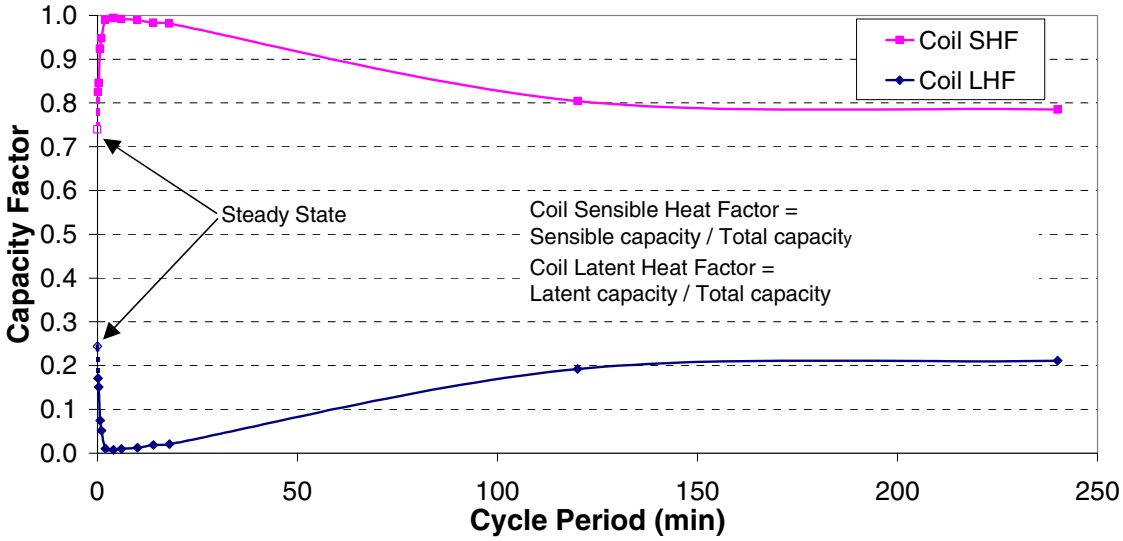

Figure 5.26 Coil Sensible and Latent Heat Factors

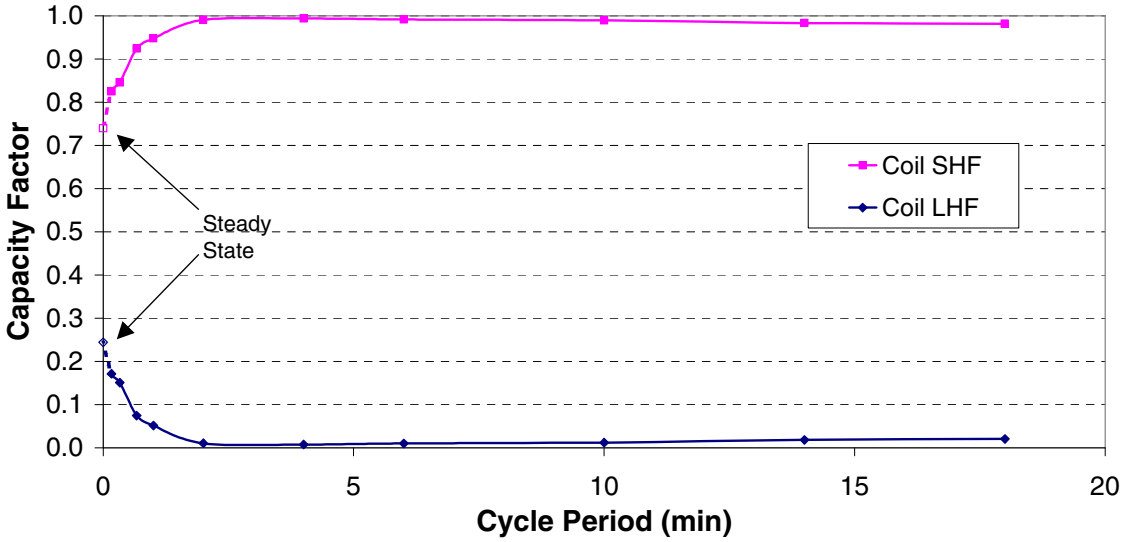

Figure 5.27 Coil Sensible and Latent Heat Factors – Short Cycles

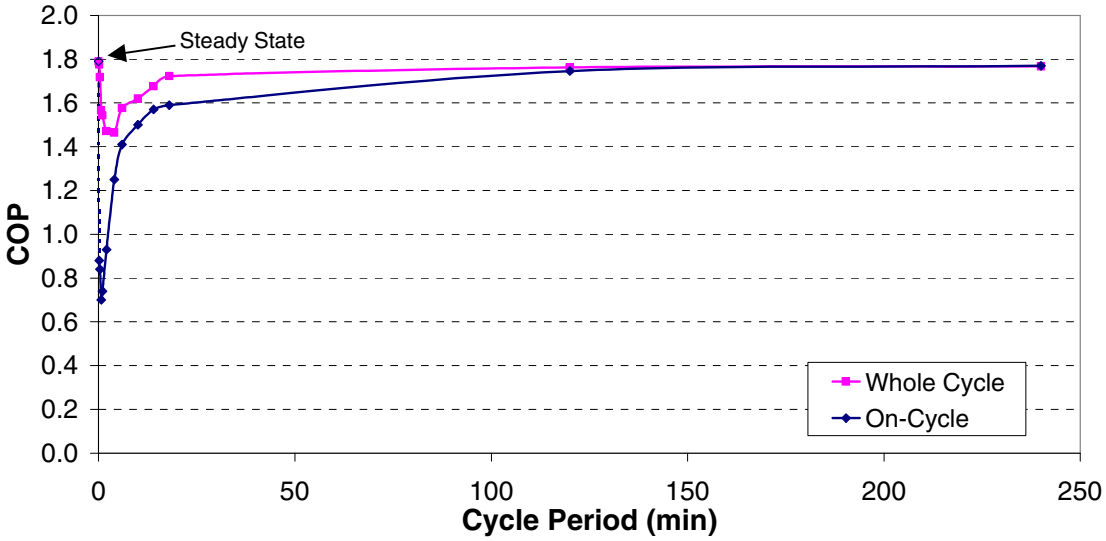

Figure 5.28 Coefficient of Performance as a Function of Duty Cycle

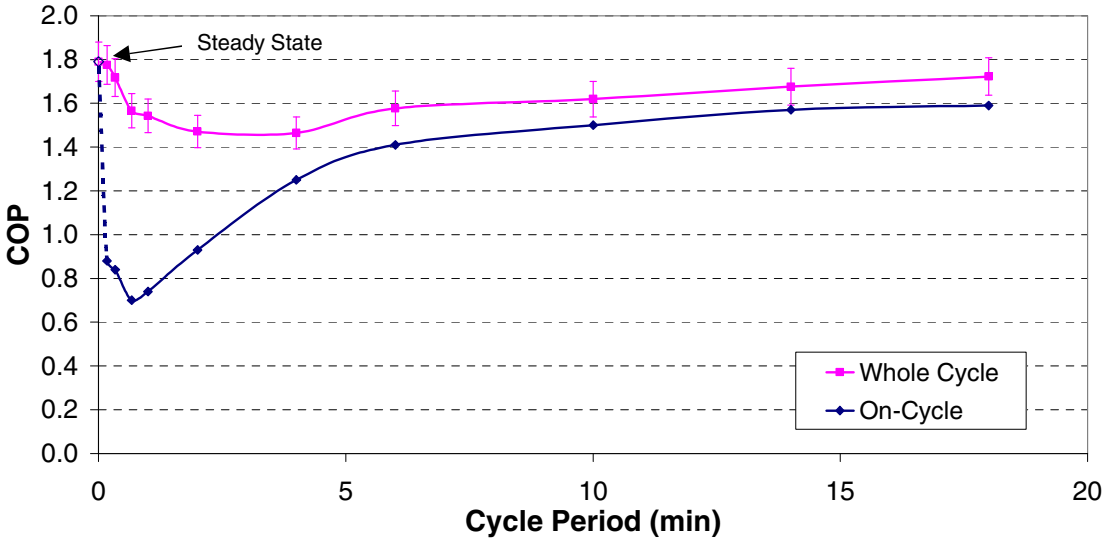

Figure 5.29 COP as a Function of Duty Cycle – Short Cycles

Chapter 6: Dynamic Modeling

6.1 Introduction

A combination of experimental tests and analytical tests is an effective way to reduce the cost of testing prototype air conditioning systems (Hager et al., 2003). To investigate the possibility of devising control schemes based on cycling, or a cyclic performance indicator, a numerical model is useful in decreasing the time and effort needed for experimental tests. In this chapter, the automotive air conditioning system will be numerically modeled by significantly updating an existing transient simulation tool that was originally designed to model household refrigerators. Focus will be directed towards the implementation of automotive system components and sensible and latent capacities. The results from the numerical simulation will be compared with the experimental results.

6.2 Literature Survey about Previous Models

Several whole-system numerical models can be found in the open literature. Table 6.1 lists four of the more popular ones: PUREZ, HPSIM, TRPUMP, and ACMODEL.
PUREZ (also known as MARK V) (Rice & Jackson, 1994 and Fischer & Rice, 1983) is a computer program that was developed to predict the steady state performance of conventional, electrically driven, air-to-air heat pumps in both heating and cooling modes. It assumes the heat exchanger is composed of several equivalent parallel circuits. This approach simplifies the modeling by eliminating the need for coil circuitry details, but it exposes all the circuits to the same entering air conditions and does not allow for variations in such air conditions to be considered. To model dehumidification on the evaporator coil, Rice and Jackson use enthalpy as the driving force for simultaneous heat and mass transfer. They then follow McQuiston (1975) and McQuiston and Parker (1994) in applying an overall wet surface effectiveness to the capacity equation in order to take the effect of the fins into consideration, therefore arriving at the form of Equation 6.1.

$$dQ = h\,\eta_{ft}\left(i_{\infty} - i_{w}\right)dA \qquad 6.1$$

where the effectiveness is defined as

$$\eta_{ft} = 1 - \frac{A_f}{A_{ft}}\left(1 - \frac{\tanh(FL)}{F\,L}\right), \text{ and } F = \frac{2h}{k\,\delta_f}\left(1 + \frac{h_{fg}\,D}{c}\right) \qquad 6.2$$

and D is the ratio between humidity ratio gradient and temperature gradient, which is considered constant. Several researchers (Wang, Hsieh & Lin, 1997 and Wu & Bong, 1994) have argued that the use of a constant D ratio is not appropriate because for a fixed entering air condition, it allows one possible value for the surface temperature, while this is not the practical case. The surface temperature is related to the saturated humidity and varies along the fin. Rice and Jackson simplify the model further by assuming that the energy content of the condensate is neglected.

The refrigerant-side calculations treat the single- and two-phase regions separately. The effectiveness-NTU method (Kays and London, 1964) is used. Dehumidification is assumed to occur only on the two-phase section.

The second model, HPSIM, (Domanski and Didion, 1983) is the first model in the open literature that is capable of simulating a heat pump with a constant flow area expansion device at imposed operating conditions without restrictions on refrigerant state at any system location. It is also the first model to be verified in the cooling mode as well as the heating mode. For the evaporator coil, the model treats each tube separately, i.e. each tube is isolated with an appropriate effective fin surface area and its performance is calculated independently, then the program proceeds in the proper tube sequence. This approach allows for complicated refrigerant circuitry (Domanski, 1991).

For dehumidification on the exterior surface of a finned tube, Domanski and Didion arrive at Equation 6.3 after applying the Colburn analogy and assuming the Lewis number is unity.

$$dQ = h_{ext}\left[1+\frac{h_{fg}}{C_p}\frac{\left(W_\infty - W_w\right)}{\left(T_\infty - T_w\right)}\right]\left[1-\frac{A_f}{A_{ft}}\left(1-\phi\right)\right]\left(T_\infty - T_w\right)dA \qquad 6.3$$

The resistance to heat and mass flow as implied in Equation 6.3 is used to calculate the overall heat transfer coefficient according to Equation 6.4 which assumes that the condensate film is at a uniform temperature and takes its resistance into consideration but neglects its effect on the fin efficiency. Equation 6.4 also considers the resistance of the fouling on the inner surface of the tube.

$$\frac{1}{U} = \left[\frac{A_{ft}}{h_i\, A_{p,i}} + \frac{A_{ft}}{h_{d,i}\, A_{p,i}} + \frac{A_{ft}\,\delta_p}{k_p\, A_{p,mean}} + \frac{1}{h_{ext}\left[1+\frac{h_{fg}}{C_p}\frac{\left(W_\infty - W_w\right)}{\left(T_\infty - T_w\right)}\right]\left[1-\frac{A_f}{A_{ft}}\left(1-\phi\right)\right]}\right] \qquad 6.4$$

TRPUMP is a component based dynamic model for describing the start-up operation of air-to-air heat pumps. Starting from the basic partial differential equations that govern the mass, momentum, and energy transfer for transient, one-dimensional fluid flow with heat transfer, Chi and Didion (1982) use the lumped parameters method to arrive at a set of 12 equations that calculate the response of the air, the refrigerant, and the wall of the heat exchangers.

ACMODEL (LeRoy et al., 1998) is similar to PUREZ in using the enthalpy potential method, but it breaks the heat exchanger into segments. Each segment has a uniform pipe temperature. This segment-by-segment approach allows the threshold between single- and two-phase conditions to be identified more closely (LeRoy et al., 1998). Also similar to PUREZ, ACMODEL consider the internal and external convection

processes only. However, ACMODEL employs only dry fin efficiency. On the refrigerant side, the effectiveness-NTU method (Kays and London, 1964) is used.

LeRoy, Groll, and Braun (1998) evaluated PUREZ, HPSIM, and ACMODEL in their ability to predict the dehumidification performance of four unitary systems (3 in case of ACMODEL) at three different conditions. The four systems that were used in the comparison had nominal capacities in the range between 2 to 5 ton of refrigeration and included packaged systems and split systems, fixed orifice and thermostatic expansion valves, and systems with reciprocating and scroll compressors.

LeRoy at al. (1998) used two measures of error to evaluate the accuracy of the models. The first measure of error is the mean (arithmetic) deviation, which was calculated using the absolute values of the individual errors as in Equation 6.5. The second measure of error is the standard deviation as calculated using Equation 6.6, where *n* is the number of data points in the set.

$$Mean\,Deviation = \frac{\sum_{i}^{n} 100\left[\left(\frac{Q_{calculated} - Q_{measured}}{Q_{measured}}\right)\right]_i}{n} \qquad 6.5$$

$$Std.Deviation = 100\sqrt{\frac{\sum_{i}^{n}\left[\left(\frac{Q_{calculated} - Q_{measured}}{Q_{measured}}\right)^2\right]_i}{n}} \qquad 6.6$$

LeRoy et al. (1998) concluded that PUREZ gives the closest agreement to the measured performance. One explanation for the fact that PUREZ does well particularly in predicting the latent capacity relative to the other models may be attributed to the fact that it accounts for wet fin efficiency. HPSIM takes into consideration the effect of the liquid film on the heat transfer coefficient to reduce the fin efficiency. The deviation of HPSIM in predicting the sensible cooling capacity is not quite as large as the deviation in predicting total cooling capacity, and the largest deviation is associated with the predictions of latent capacity. PUREZ and HPSIM

underpredict the latent component of the cooling capacity, whereas ACMODEL overpredict latent capacity and underpredict sensible capacity with the net effect of reasonably accurate total capacity predictions. The results are summarized in Table 6.2.

6.3 TRANSREF (TRANSient simulation of REFrigeration systems) Program

This section describes TRANSREF program before the beginning of the research work at hand.

TRANSREF (Anand 1999) is a transient numerical solver designed to simulate the thermal behavior of household refrigerators. TRANSREF is a component-based solver; i.e. each component of the system is modeled separately according to a specific standard. Each component can be divided into several control volumes, and the components communicate with each other through ports. Each component converges separately and the convergence of the system is satisfied when the convergence of each component is satisfied together with system energy and mass balances. The components that are available in TRANSREF are a generic compressor, heat exchangers, capillary tube with and without suction line heat exchanger, accumulator, damper, and refrigerator cabinet. TRANSREF can simulate loads such as single evaporator systems as well as two series and two parallel evaporator systems. It can also simulate side-by-side cabinets and top-and-bottom cabinets (Gercik, Aute, & Radermacher, 2005).

The evaporator in TRANSREF is divided into three control volumes; refrigerant, heat exchanger wall, and air. It is modeled according to the LMTD method. The following assumptions are made:

- Refrigerant flow is one-dimensional.
- The refrigerant side is divided into two regions; two-phase flow and superheated vapor.
- The change of air temperature in the superheated vapor region is negligible.

- A constant void fraction is employed in the two-phase region.
- Pressure drop in both the refrigerant side and the airside is neglected.
- The heat transfer coefficients between the refrigerant and the evaporator wall for the two regions are known, as well as between the wall and the air.
- The charge inside the evaporator is known.
- The heat exchanger wall is at a constant temperature.
- The latent capacity is neglected. Air is considered dry.

The solution method of choice in TRANSREF is the successive substitution method. Starting from the compressor, each component is solved independently and the resulting output properties are passed to the following component. The initial state of the system is to be provided to the program. After running all the components in the cycle and continuously updating the parameters, the convergence criterion is checked. If the convergence is satisfied a step in time is taken. The successive substitution method is observed to be self-convergent (Xiaoqiang and Clodic, 1996). The system is said to converge when none of the properties change with successive iteration by more than 0.01%. The properties that are checked for convergence are temperatures and/or qualities at the exit of each component and the mass flow rates at the exit of the compressor and the capillary tube. The time step utilized is adaptable in size depending on the rate of change of pressure. In addition to the initial states, inputs to the program include components' physical properties, the system charge and the charge distribution.

TRANSREF was validated by comparing its results with experimental results. Anand reported that the evaporator pressure was predicted within 6% of the actual pressure and the evaporator temperature within approximately 3 °C of the measured value. The condenser pressure was predicted within 4% of the actual condenser pressure and the simulated condenser temperature was found to be within 3 °C of the actual measured value. As for power, the predicted value is about 10% off from the actual value.

6.4 Dynamic Modeling of Automotive Systems

This section describes the modifications done to TRANSREF as part of the research work at hand.

6.4.1 Automotive Cabin

To make TRANSREF suitable for modeling automotive systems, the first step is to equip it with an automotive cabin component instead of the refrigerator cabinet. For this purpose, the cabin model derived in Chapter 2 is used again. The equations of the cabin model are rearranged to suit the computer programming language and the numerical format adopted for the components standard.

The automotive cabin component starts with listing the values of the physical and thermal properties of the cabin as well as the ambient conditions and passengers' settings. Then, the following equations, which are based on Equations 2.1 to 2.5 are used.

$$T_m = \frac{\left[m_{iv} \times C_{p,amb} \times T_{amb}\right] + \left[\left(m_e - m_{iv}\right) \times C_{pr} \times T_r\right]}{m_e \times C_{pm}} \qquad 6.7$$

$$Q_{sen} = m_e \times C_{pe} \times \left(T_m - T_s\right) \qquad 6.8$$

$$\frac{dT_r}{dt} = \frac{\left[h_c \times A_c \times \left(T_c - T_r\right)\right] - Q_{sen} + Q_{sol} + Q_{ps} + \left[U_o \times A_o \left(T_{amb} - T_r\right)\right] + \left[m_{iv} \times C_{p,amb} \times \left(T_{amb} - T_r\right)\right]}{M_r \times C_{pr}} \qquad 6.9$$

$$\frac{dT_c}{dt} = \frac{-h_c \times A_c \times \left(T_c - T_r\right)}{M_c \times C_c} \qquad 6.10$$

$$W_m = \frac{\left(m_e - m_{iv}\right) \times W_r + m_{iv} \times W_{amb}}{m_e} \qquad 6.11$$

$$\frac{dW_r}{dt} = \frac{m_{iv} \times h_{fg} \times (W_{amb} - W_r) - m_e \times h_{fg} \times (W_m - W_s) + Q_{pl}}{M_r \times h_{fg}} \quad 6.12$$

The terms of Equations 6.7 to 6.12 were previously discussed in Chapter 2; please refer to this chapter for detailed explanations. Equations 6.9 and 6.10 calculate the rate of change of cabin air temperature and internal mass temperature, respectively. Equation 6.12 calculates the rate of change of cabin air humidity ratio. The rates of change are used to calculate the values of the parameters using Equations 6.13 to 6.15.

$$T_r = T_r + \frac{dT_r}{dt} \times time\ step \quad 6.13$$

$$T_c = T_c + \frac{dT_c}{dt} \times time\ step \quad 6.14$$

$$W_r = W_r + \frac{dW_r}{dt} \times time\ step \quad 6.15$$

Finally, the values of the different parameters are ready to be passed to the evaporator component.

6.4.2 Automotive Evaporator and Latent Capacity

TRANSREF neglects the latent capacity. But for automotive systems, the latent capacity may constitute up to 25% of the total capacity as mentioned in Chapter 5. For this reason, provisions had to be made such that the latent capacity was taken into consideration.

The inputs to the evaporator component are:

- Internal volume.
- External surface area.
- Internal surface area.
- Evaporator heat capacity.

- Air-side heat transfer coefficient.
- Refrigerant-side heat transfer coefficient.
- Refrigerant charge.
- Initial wall temperature.
- Air flow rate.

The execution of the original TRANSREF evaporator component starts with detecting the portion of the heat exchanger that has two-phase refrigerant and the portion that has superheated vapor refrigerant. The LMTD method is used to calculate the refrigerant outlet temperature, therefore the refrigerant capacity in the superheated section. At this point, changes had to be made to calculate the evaporator total capacity.

The two-phase area of the heat exchanger is divided into smaller segments of equal areas. The incoming air temperature and enthalpy are assumed to be constant on each segment, and are taken to be equal to their respective inlet values for the first segment. Therefore by knowing the air temperature and the wall temperature and the coefficient of heat transfer from the air side the amount of sensible heat transfer between the wall and the air can be calculated. The sensible heat transfer in each segment is called q_{sen}. If the wall temperature is lower than the dew point temperature of the inlet air then the air enthalpy and the value of saturated air enthalpy at wall temperature and the coefficient of mass transfer are used to calculate the total heat transfer for the segment, q. To calculate the coefficient of mass transfer the Colburn analogy as given in Equation 6.16 is assumed to hold and by further assuming the Lewis number to be unity, then the coefficient of mass transfer, U_m, can be calculated using Equation 6.17.

$$\frac{U}{C_p U_m} = \left(\frac{Sc}{\Pr}\right)^{\frac{2}{3}} = Le^{\frac{2}{3}} \qquad 6.16$$

$$U_m = \frac{U}{C_p} \qquad 6.17$$

After calculating the total segment capacity, q, the sensible segment capacity is subtracted from it to calculate the latent segment capacity, q_{lat}. Afterwards, a heat balance is performed on the segment to calculate the air outlet temperature and enthalpy, which subsequently can be used as the values for the next segment. Also the air outlet humidity ratio can be calculated and therefore the amount of condensate over the segment is known. Finally, the capacities and amount of condensate of all the segments are integrated to establish the total sensible and latent capacities and total amount of condensate produced by the two-phase region. This technique assumes that the condensate occurs only in the two-phase region and neglects the energy content of the condensate layer which are the same assumptions adopted by Fischer and Rice in PUREZ. Figure 6.1 shows a flowchart that demonstrates the technique implemented.

By referring to Figure 6.1, first the two-phase area is divided into *n* number of segments. The sensible heat transfer for the first segment is calculated and the air temperature of the next segment is calculated as a result of the heat transfer. Then the total sensible heat transfer is updated and the whole process is repeated for all the segments. The final air outlet temperature is calculated next. Afterwards, the condensation condition is checked and, if true, the total heat transfer for the first segment is calculated using the enthalpy potential and the coefficient of mass transfer. Then the enthalpy of the next segment is calculated. The total capacity is updated next and the latent portion is calculated and the whole process is repeated for all the segments. Finally, the final air outlet enthalpy is calculated.

After calculating the air sensible and latent capacity, the original TRANSREF program goes on to calculate the two-phase capacity from the refrigerant side and the evaporator refrigerant pressure. At the end, the amounts of condensate from each iteration are summed up during the whole period of operation of the heat pump.

To choose the suitable number of segments, a sensitivity analysis was performed. A "component tester" was developed and used for this purpose. A component tester is a set of lines of code that wrap the component and allow it to run independently without the need to communicate with other components. In this process the evaporator wall temperature had to be set to a specific constant value, which is 288 K, and the initial air temperature was set to 298.15 K. The number of segments was varied from 1 to 10000 and the outlet air temperature was plotted against the number of segments. The process was then repeated at wall temperature of 278 K and 268 K. The results are shown in Figure 6.2 and, accordingly, 100 was chosen as an accurate and reasonable number of segments.

The air side heat transfer coefficient in TRANSREF is an input. Its value is calculated using Coil Designer (Jiang, 2003 and Schwentker 2005), which is a verified software package used to design air to refrigerant heat exchangers. The equation used by Coil Designer for this purpose was developed by Kim, Youn, and Webb, (1999).

6.4.3 Automotive Orifice

The only expansion device component in the original TRANSREF is a capillary tube. The manual expansion valve of the experimental automotive system had to be modeled as a new component. For this purpose the valve was approximated as a fixed area orifice using the flow equations given in the literature of the valve manufacturer (Swagelok, 2002).

The first step is to check if the flow through the orifice has reached the choking condition, which is done by calculating the critical pressure ratio using Equation 6.18 (ASHRAE, 2005, b). If the flow is not choked, Equation 6.19 is used and if the flow is choked Equation 6.20 is used.

$$P_{cr} = \left(\frac{2}{\gamma + 1} \right)^{\gamma / (\gamma - 1)} \qquad 6.18$$

If $P_{cr} < P_e / P_{cond} < 1$

$$Flow = 4.54 \times 10^{-6} \times P_{cond} \times \left[1 - \frac{2\left(P_{cond} - P_e\right)}{3 P_{cond}}\right] \times \sqrt{\frac{P_{cond} - P_e}{P_{cond} \times G_{cond} \times T_{cond,outlet}}} \qquad 6.19$$

If $P_e / P_{cond} < P_{cr}$

$$Flow = 0.942 \times 10^{-6} \times P_{cond} \times \sqrt{\frac{1}{G_e \times T_{cond,outlet}}} \qquad 6.20$$

If $P_e / P_{cond} > 1$

$$Flow = 4.54 \times 10^{-6} \times P_e \times \left[1 - \frac{2\left(P_e - P_{cond}\right)}{3 P_e}\right] \times \sqrt{\frac{P_e - P_{cond}}{P_e \times G_e \times T_e}} \qquad 6.21$$

where,

G_{cond} = Specific gravity of refrigerant upstream of the orifice

G_e = Specific gravity of refrigerant downstream of the orifice

Equation 6.21 (Swagelok, 2002) is used in the case wherein the evaporator pressure is higher than the condenser pressure. This situation arises after the shutdown of the compressor due to refrigerant migration. Equation 6.21 is the same as Equation 6.19 after swapping the upstream and the downstream pressures.

The constants in Equation 6.19 and Equation 6.20 are a result of a calibration process to fit the outputs of the equations to the experimental results.

6.4.4 Other Automotive Components

Other than the automotive cabin, evaporator, and orifice, the rest of the components of the cycle, viz. condenser, accumulator, and compressor, were not created new, but were just adjusted to the specifications of the automotive system components.

The parameters requiring adjustment in the condenser are the internal volume, external surface area, internal surface area, coil heat capacity, air-side heat transfer coefficient, refrigerant-side heat transfer coefficient, refrigerant charge, and air flow rate. The values of the heat transfer coefficients are again calculated using Coil Designer (Jiang, 2003 and Schwentker 2005) via the Kim, Youn, and Webb (1999) equation.

The TRANSREF compressor component was used after removing the equations dealing with cooling of the motor by suction refrigerant; this is to suit the open-type compressor of the automotive system. The inputs to the compressor component are the displacement volume, surface area, heat transfer coefficient of the external surface, heat capacity, polytropic constant, isentropic efficiency, mechanical efficiency, and rotational speed. The clearance volume is assumed to be 4% of the displacement volume. For the compressor used in experiments, the known values are the displacement volume, surface area, heat capacity (approximately) and rotational speed. The rest of the values were left as they originally were in TRANSREF.

The TRANSREF accumulator was also used. It specifies that the compressor suction is saturated vapor, but it does not store refrigerant and it does not have a surface area or mass. The rest of the refrigerator components, such as the sweat loop and the damper, were not used.

6.5 Modeling Results and comparison with Experimental Results

Experimental test number 6 in Table 5.1 was chosen to be modeled with TRANSREF. It has a driving condition with recirculated air and no hot-soak. Tables 6.3 thru 6.6 list the values of the model inputs of the evaporator, condenser, compressor, and orifice, respectively. The values of the coefficient of overall heat transfer had to be changed within 16% from the values produced by Coil Designer such that the numerical results match the experimental results better.

Figure 6.3 shows the experimental and the numerical values of the refrigerant evaporation and condensation temperatures against time. It is clear from the figure that the simulated evaporation and condensation temperatures follow the correct trend but with a deviation in values. This is attributed to the uncertainty in calculating the internal volume of the heat exchangers. Figure 6.4 shows the evaporation and condensation pressures, which are the saturation pressures corresponding to the temperatures in Figure 6.3.

Figures 6.5, 6.6, and 6.7 show the numerical and experimental refrigerant mass flow rate, cabin air temperature, and power consumption against time. The maximum deviations in these values are 6%, 1.5 K, and 5%, respectively. Figure 6.8 shows the numerical and experimental cooling capacity against time. It is clear from the figure that the numerical capacity builds up faster than the experimental capacity. The two curves converge after about 10 minutes. The deviation between the experimental capacity and the numerical capacity happen although the refrigerant mass flow rate has the correct value. This is because of the degree of subcooling that was calculated by TRANSREF to be 21K at the beginning of the test while it was only between 15 K and 17 K in the experiment. Figure 6.9 shows the numerical and experimental latent capacity against time. The numerical curve follows the correct trend but with a big deviation from the experimental values. This might be attributed to the assumption of limiting the condensation to the two-phase section of the evaporator. Also the decrease in evaporation temperature increases the sensible capacity, which causes the latent capacity to decrease since it is the difference between the total and the sensible capacities.

6.6 Conclusions

The model is a simplified one and many details have to be taken into consideration but it manages to deliver acceptable results for the cabin air temperature and mass flow rate and power consumption. The refrigerant temperatures and capacities need to be enhanced.

Table 6.1 Four of The More Popular Vapor Compression Models

	PUREZ (MARK V)	HPSIM	TRPUMP	ACMODEL
Developer	Rice & Jackosn	Domanski & Didion	Chi & Didion	Rossi, {modified by LeRoy}
From	Oak Ridge National Lab.	National Bureau of Standards	National Bureau of Standards	Purdue University
Year	1994	1983	1982	1995, {1997}
Type	Steady-state	Steady-state	Transient	Steady-state

Table 6.2 Comparison Between The Accuracy of Three Modeling Programs

	PUREZ (MARK V)		HPSIM		ACMODEL	
	Mean Deviation	Standard Deviation	Mean Deviation	Standard Deviation	Mean Deviation	Standard Deviation
Total Capacity	**4.9%**	**7.7%**	6.6%	7.8%	5.3%	8.8%
Latent Capacity	**6.1%**	**7.6%**	13.1%	16.5%	18.3%	19.0%
Sensible Capacity	5.5%	7.7%	**5.3%**	**6.9%**	9.5%	10.2%
Sensible Heat Ratio	**2.2%**	**2.8%**	3.6%	4.4%	5.6%	6.6%

Bold typeface means lowest deviation

Table 6.3 TRANSREF Inputs of Evaporator Component

Parameter name	Value	Unit	Verification
Internal volume	0.0006	m^3	Component specification
External area	3	m^2	Component specification
Internal area	4.6	m^2	Component specification
Heat capacity	1749	J/K	Calculated
Air-side heat transfer	80	W/m^2K	Estimated by Coil Designer to be 67, then changed to get better results

coefficient			
Refrigerant-side heat transfer	850	W/m^2K	Estimated by Coil Designer to be 761, then changed to get better results
Initial charge	0.2	Kg	Empirical
Air flow rate	0.13	m^3/s	Experimental test condition
Initial wall temperature	41	°C	Experimental test condition
Void fraction constant	0.8	--	Originally in TRANSREF

Table 6.4 TRANSREF Inputs of Condenser Component

Parameter name	**Value**	**Unit**	**Verification**
Internal volume	0.0006	m^3	Component specification
External area	8.41	m^2	Component specification
Internal area	0.46	m^2	Component specification
Heat capacity	1952	J/K	Calculated
Air-side heat transfer	95	W/m^2K	Estimated by Coil Designer to be 90, then changed to get better results
Refrigerant-side heat transfer	1200	W/m^2K	Estimated by Coil Designer to be 1060, then changed to get better results
Initial charge	0.24	Kg	Empirical
Air flow rate	0.645	m^3/s	Experimental test condition
Initial wall temperature	41	°C	Experimental test condition
Void fraction constant	0.7	--	Originally in TransREF

Table 6.5 TRANSREF Inputs of Compressor Component

Parameter name	**Value**	**Unit**	**Verification**
Displacement volume	0.000155	m^3	Component specification
Speed	2500	RPM	Experimental test condition
Clearance volume	4%		Empirical
Surface area	0.0608	m^2	Measurement

Heat capacity	2025	J/K	Calculated
Polytropic index	1.09	--	Originally in TransREF
Isentropic efficiency	0.6	--	Empirical
Mechanical efficiency	0.95	--	Empirical
Surface heat transfer coefficient	10	W/m^2K	Originally in TRANSREF

Table 6.6 TRANSREF Inputs of Orifice Component

Parameter name	**Value**	**Unit**	**Verification**
Diameter	0.00025	m	Component specification

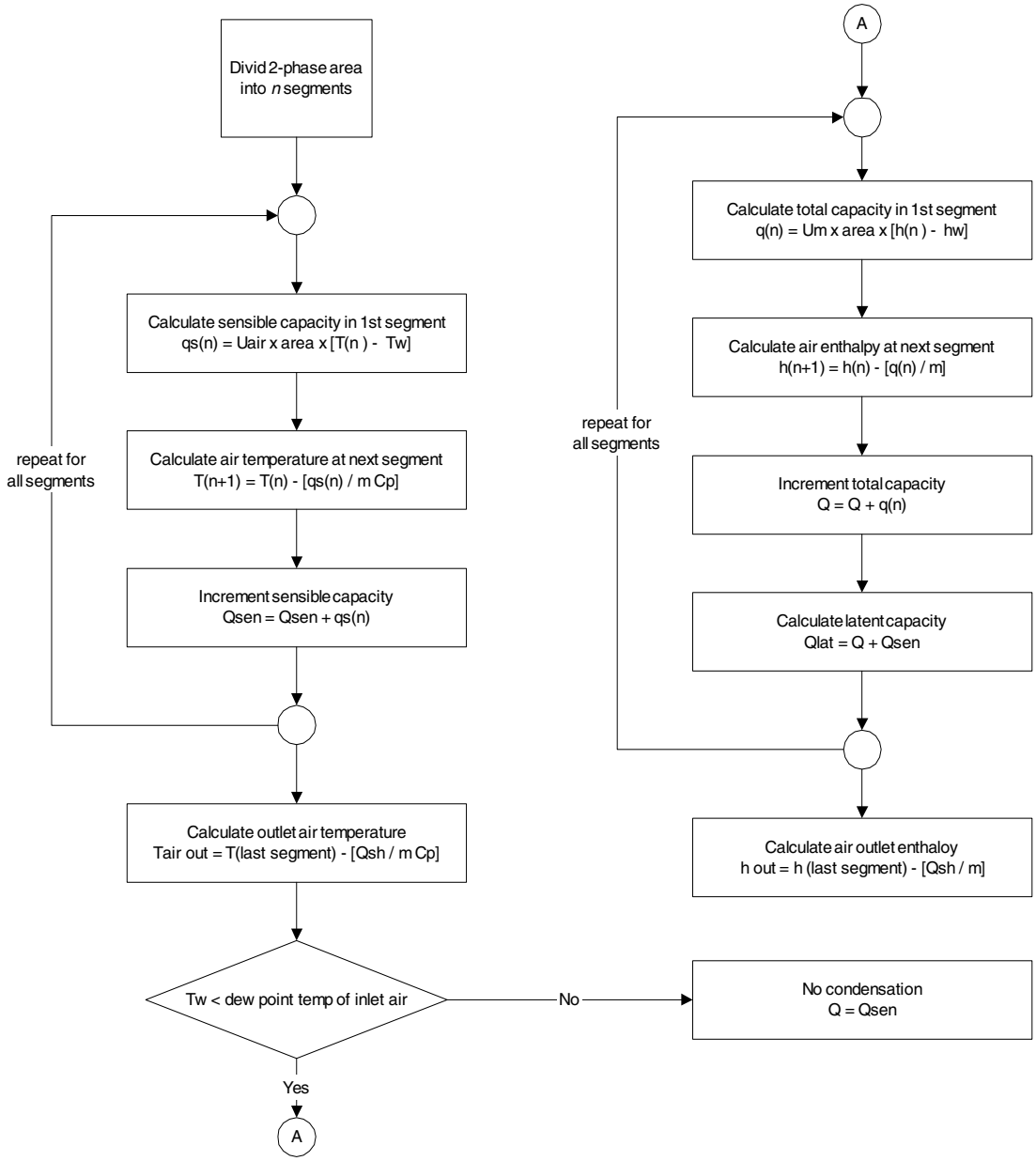

Figure 6.1 Flowchart of Capacity Calculation in Evaporator Component

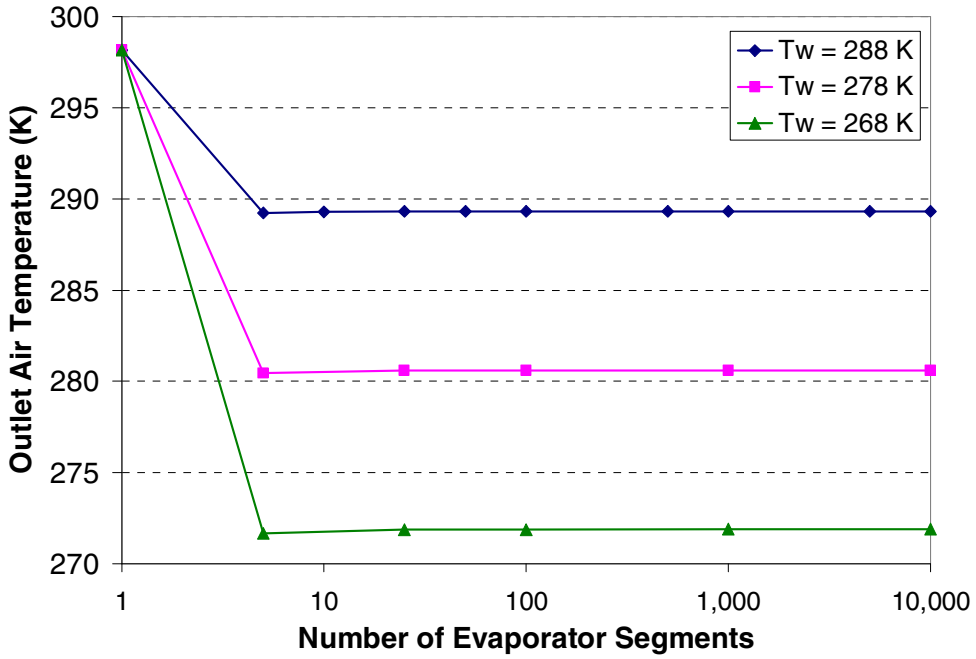

Figure 6.2 Sensitivity Analysis for Number of Evaporator Segments

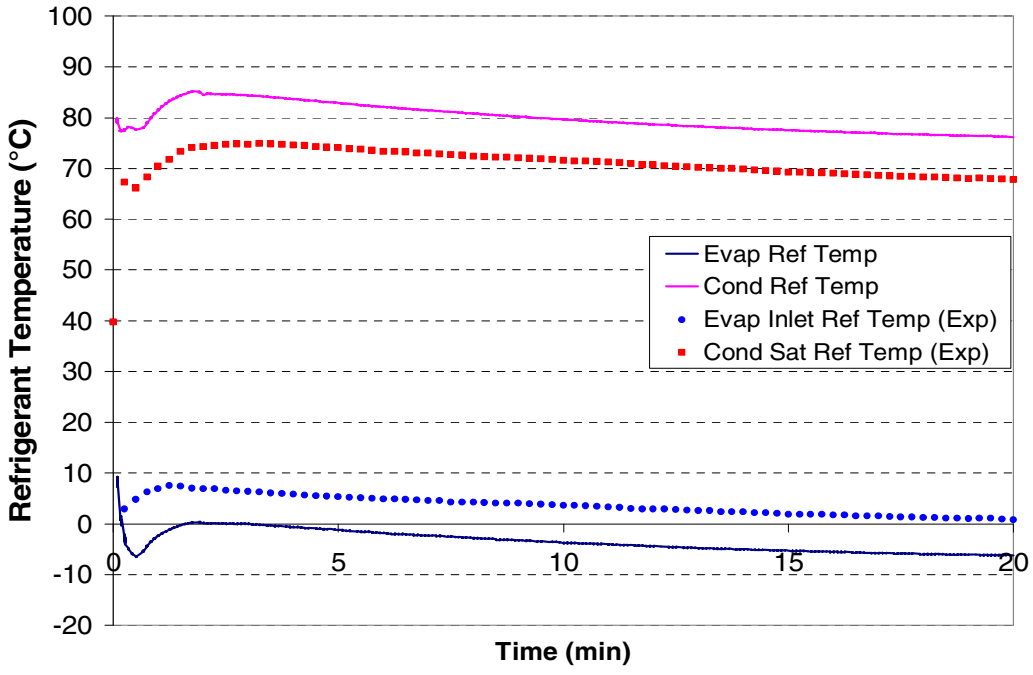

Figure 6.3 Numerical vs. Experimental Refrigerant Temperatures

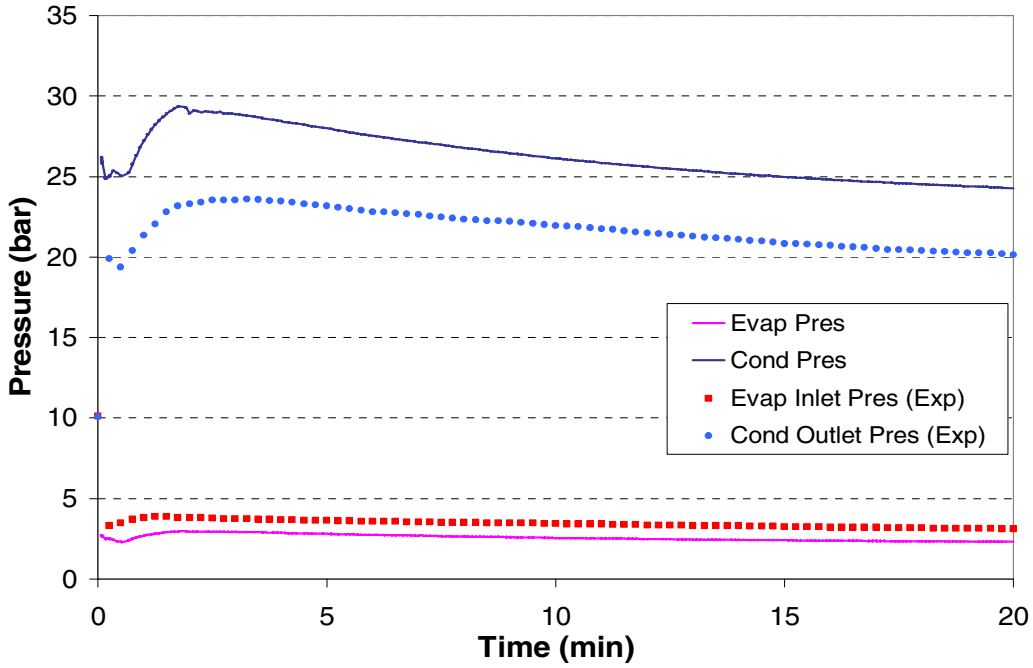

Figure 6.4 Numerical vs. Experimental Refrigerant Pressures

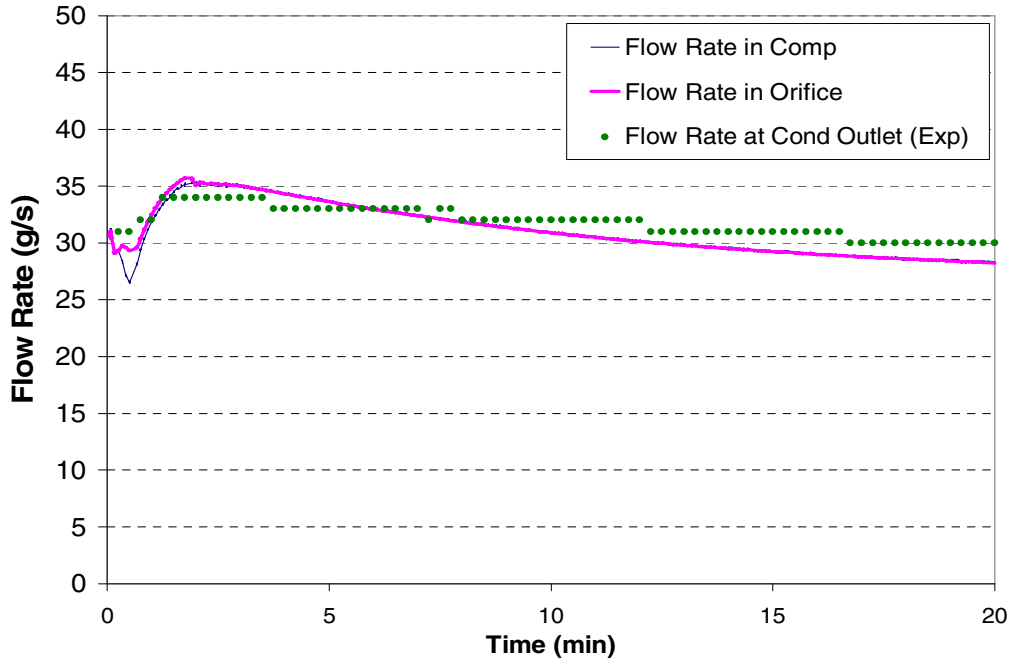

Figure 6.5 Numerical vs. Experimental Refrigerant Flow Rate

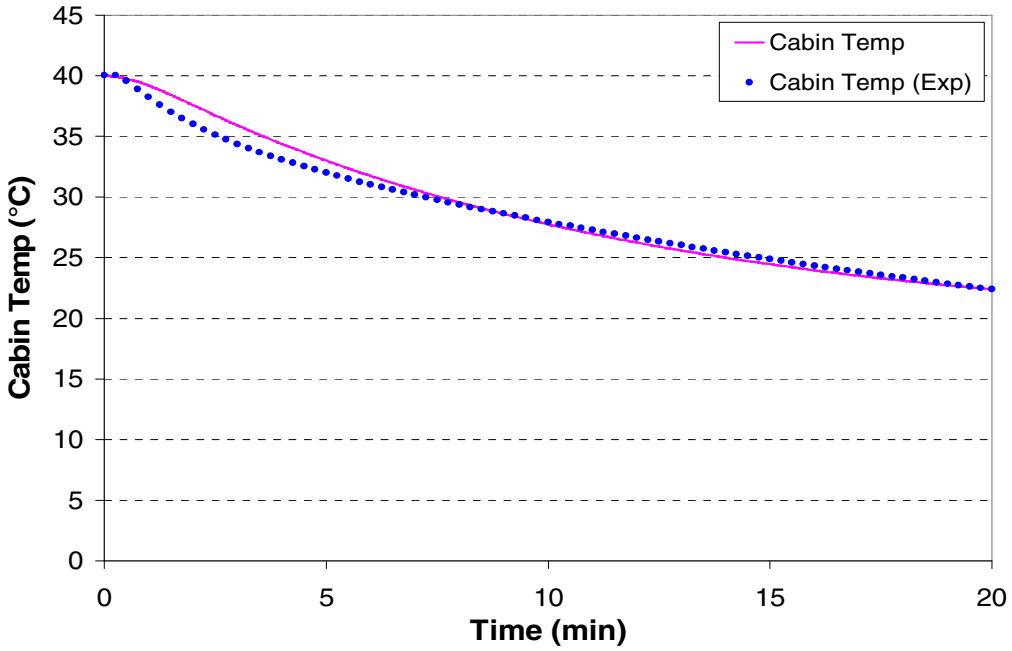

Figure 6.6 Numerical vs. Experimental Cabin Air Temperature

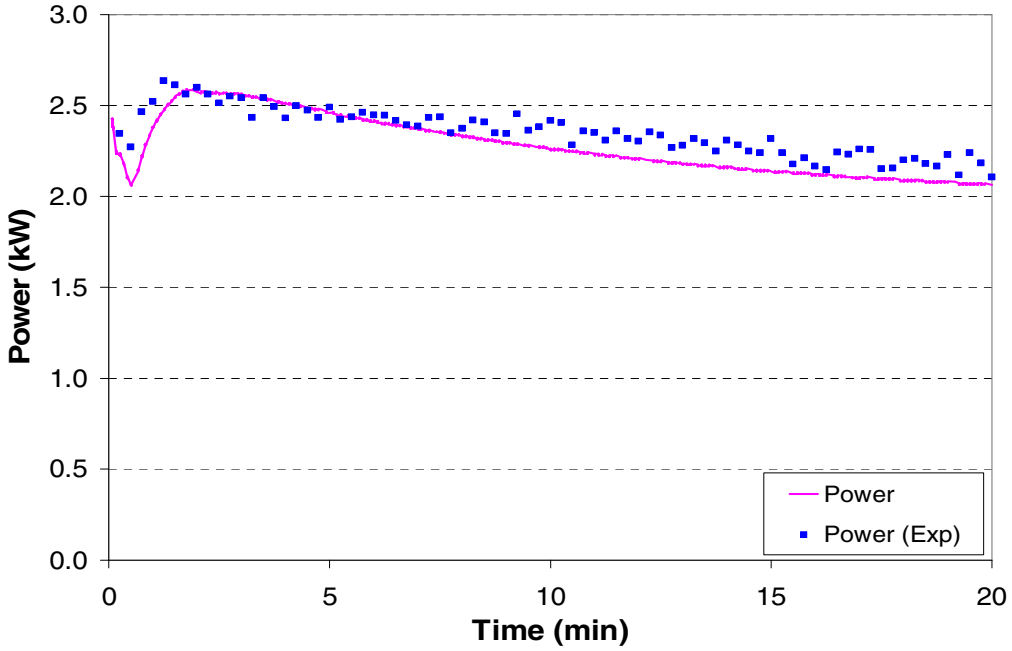

Figure 6.7 Numerical vs. Experimental Power Consumption

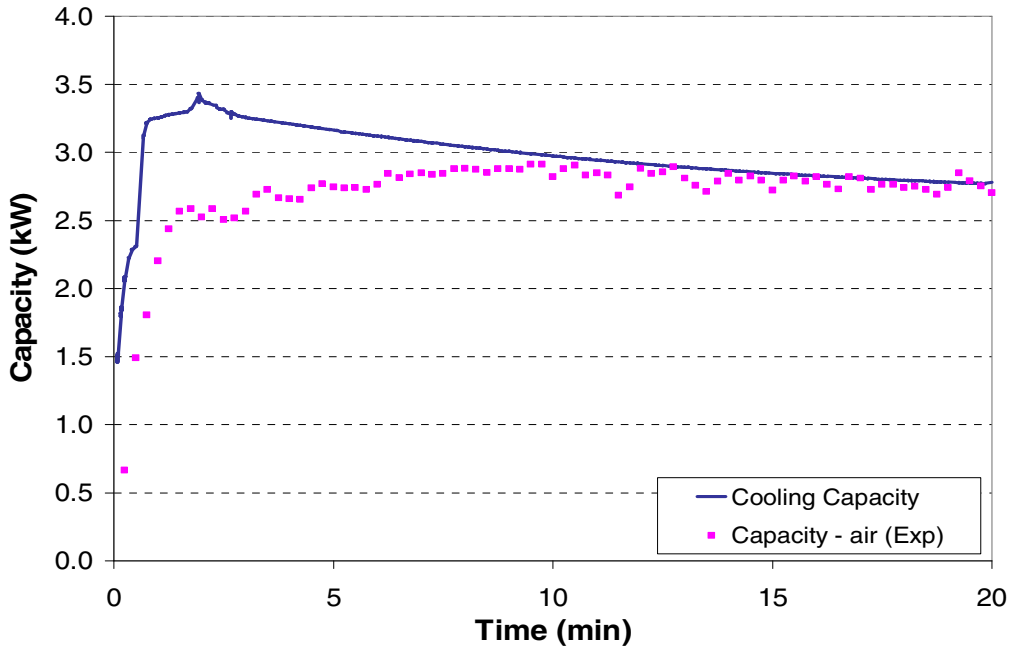

Figure 6.8 Numerical vs. Experimental Cooling Capacity

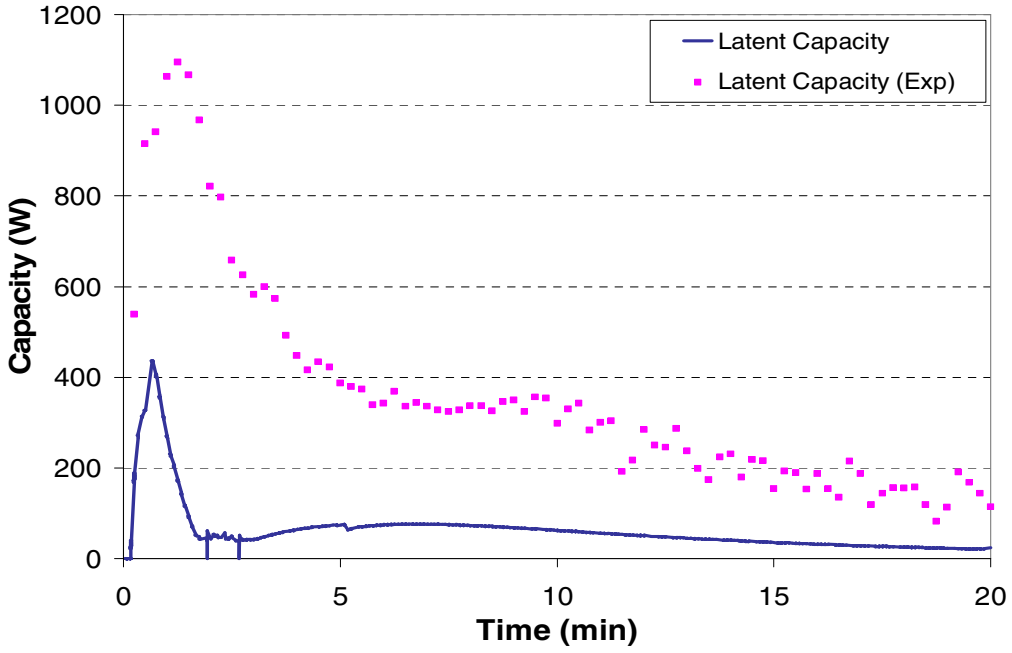

Figure 6.9 Numerical vs. Experimental Latent Capacity

Chapter 7: New Contributions, Future Work and Epilogue

7.1 New Contributions

The following are the new contributions of the research work:

- Realization of a new, smart test facility for dynamic testing.
- Integration of the cabin model with the test facility controls.
- In case of a hot-soaked cabin, starting the pull-down from fresh air then switching to recirculated air when cabin temperature is equal to fresh air temperature saves time (11%) and energy (12%).
- Coil latent heat factor can drop to practically zero at certain duty cycle.
- Off-cycle capacity can represent up to 58% of total capacity at certain duty cycle.
- Transient losses are negligible at very short (< 1 min.) and very long (>20 min.) duty cycles.
- TRANSREF verification initiated.

7.2 Future Work

The following are suggestions for future work as a continuation of this research:

- Testing applications other than automotive air conditioning, such as residential or refrigerated containers.
- Testing other refrigerants.
- Conducting reliability tests for compressors during short cycling.
- Investigation of the recovery time as a cyclic performance indicator.
- Developing control schemes to enhance energy efficiency and comfort.
- Test cycling at other than 50% on-portion time.
- Additional verification and tuning of model.
- Modeling of cycling.

7.3 End Notes

During the few years that are the course of this research work, a few things became clear that the author wishes to mention for the purpose of transfer of experience and making future research work more worthwhile.

- There are currently no test standards for rating the capacity and efficiency of mobile air conditioning systems and heat pumps. The test standards used for residential systems cannot be used for automotive systems simply because the later requires more specifications such as compressor speed and air flow rates. Devising such standards will be most helpful for reusing and comparing results from different researchers.
- In the major portion of the research work about MACs available in the open literature, researchers do not give the complete list of conditions at which they ran their tests. If only one condition is missing, e.g. initial cabin air temperature, or evaporator air flow rate, the results become useless for the purpose of validation.

7.4 Long-term Vision

By presenting a test facility that makes it relatively more affordable to run dynamic tests in the controlled environment of a laboratory, and by focusing the analysis on latent capacity and moisture removal, it is hoped that this dissertation would open the door for setting new test standards for rating the dynamic performance of heat pumps taking into consideration the system – space interactions and the air humidity conditions.

References

Althouse, A. D., Turnquist, C. H., and Bracciano, A. F., 2000, "Modern Refireration and Air Conditioning." Goodheart-Willcox Co., Inc., 2nd Edition.

Anand, G., 1999, "Transient and steady state model of a household refrigerator." M.S. Thesis, University of Maryland, College Park, USA

ANSI/ASHRAE 116-1995, 1995, "Methods of testing for rating seasonal efficiency of unitary air conditioners and heat pumps." American Society of Heating, Refrigeration and Air-Conditioning Engineers, Inc., Georgia, USA.

ARMINES, 2002, "MACSim: Software for dynamic simulation of mobile air-conditioning systems." Centre d'Energétique, Ecole des Mines de Paris, France, www.cenerg.ensmp.fr/english/logiciel/indexmacsim.html.

Aroussi, A. and Aghil, S., 2001, "The effects of air vents locations on the internal climate control of vehicles." SAE paper number 2001-01-0287.

ASHRAE, 2005 a, "Fluid flow.", Chapter 2 in ASHRAE Handbook of Fundamentals, American Society of Heating, Refrigeration and Air-Conditioning Engineers, Inc., Georgia, USA.

ASHRAE, 2005 b, "Residential cooling and heating load calculations." Chapter 28 in ASHRAE Handbook of Fundamentals, American Society of Heating, Refrigeration and Air-Conditioning Engineers, Inc., Georgia, USA.

Ataer, O. E., 2004, "An approximate method for transient behavior of finned-tube cross-flow heat exchanger." International Journal of Refrigeration, Vol. 27, pp. 529-539.

Bahatti, M. S., 1999, "Enhancement of R134a Automotive Air Conditioning System." Society of Automotive Engineers, Paper no. 1999-01-0870.

Behr GmbH, 2004, www.behrgroup.com.

Bejan, A., and Kraus, A. D., 2003, "Heat Transfer Handbook." John Wiley & Sons.

Belth, M. I., Grzymala, T. E., and Tree D. R., 1988, "Transient mass flow rate of a residential air-to-air heat pump." International Journal of Refrigeration, Vol. 11, pp. 298-304.

Chi, J. and Didion, D., 1982, "A simulation model of the transient performance of a heat pump." International Journal of Refrigeration, Vol. 5, No. 3, pp. 176-184.

Choquart, F. Clodic, D, El Khoury, K, Roy, D, and Petitjean, P, 2003, "Assembly model for predictive thermal comfort in vehicle." Proceedings of Vehicle Thermal Management Systems, paper number C599/005/2003.

Coulter, W., and Bullard, C., 1997, "An experimental analysis of cycling losses in domestic refrigerator-freezers." ASHRAE Trans., Vol. 103, Part 1, pp. 587-596.

Didion, D., and Kelly, G., 1979, "New testing and rating procedures for seasonal performance of heat pumps." ASHRAE Journal, September 1979, pp. 40-44.

Ding, Y. and Zito, R., 2001, "Cabin heat transfer and air conditioning capacity." SAE paper number 2001-01-0284.

Domanski, P., 1991, "Simulation of an evaporator with nonuniform one-dimensional air distribution." ASHRAE Trans., Vol. 97, Part 1, pp. 793-802.

Domanski, P., and Didion, D., 1983, "Computer modeling of the vapor compression cycle with constant flow area expansion device." National Bureau of Standards, Washingto D.C.

Ehrbar, M. et al., 2003, "On part-load-behavior of on/off-controlled heat pumps." International Congress of Refrigeration, Paper number ICR0116.

El Bakkali, A. and Olivier, G., 2003, "Design of components libraries for the transient simulation of an automotive refrigeration loop." Proceedings of SAE Vehicle Thermal Management Systems, Paper number C599/024/2003.

Environmental Protection Agency, 2005, http://www.epa.gov/otaq/sftp.html.

Fisher, S. K., and Rice, C. K., 1983, "The Oak Ridge heat pump models: I – A steady-state computer design model for air-to-air heat pumps." ORNL/CON-80/R1.

Gercik, E., Aute, V., and Radermacher, R., 2005, "Transient simulation tool for refrigeration systems." Proceedings of IIR Conference, Paper number TP079.

Ghani, S. A., and Aroussi, A., Rice, E., 2001. "A closed loop full-scale automotive climatic wind tunnel for vehicle environment simulation." Advanced Vehicle Technologies, Vol. 106, pp. 165-174.

Ghani, S. A., and Aroussi, A., Rice, E., 2001. "Simulation of road vehicle natural environment in a climatic wind tunnel." Simulation Practice and Theory, Vol. 8, pp. 359-375.

Goldschmidt, V. W., Hart, G. H., and Reiner, R. C., 1980, "A note on the transient performance and degradation coefficient of a field tested heat pump - cooling and heating mode." ASHRAE Trans., Vol. 86, Part 2, pp. 368-375.

Hager, J., Stroh, C., and Reitbauer, R., 2003, "Optimization strategies for the transient behavior of the thermal systems of commercial vehicles." Proceedings of SAE Vehicle Thermal Management Systems, Paper number C599/019/2003.

Han, T. Huang, L, Kelly, S, Huizenga, C, and Hui, Z, 2001, "Virtual thermal comfort engineering." SAE paper number 2001-01-0588.

Hendricks, T., 2003, "Multi-variable optimization of electrically driven vehicle air-conditioning systems using transient performance analysis." Proceedings of SAE Vehicle Thermal Management Systems, Paper number C599/061/2003.

Hill, W. et al., 2004, “Effect off windows down on vehicle fuel economy as compared to A/C load.” Proceedings of SAE Alternate Refrigerant Systems Symposium, Scottsdale, Arizona.

Hrnjak, P., 2002, “Some lessons learned from SAE alternate refrigerant cooperative research program.” Proceedings of SAE Alternate Refrigerant Systems Symposium, Scottsdale, Arizona.

Hrnjak, P., and Hill, B., 2003, “Overview of the SAE alternate refrigerant cooperative research program.” VDA Alternate Refrigerant Winter Meeting, Saalfelden, Austria.

Huang, C. D., 1998, “A dynamic computer simulation model for automobile passenger compartment climate control and evaluation.” Ph.D. Thesis, Michigan Technological University, USA.

Huang, L. and Han, T., 2002, “Validation of 3-D passenger compartment hot soak and cool-down analysis for virtual thermal comfort engineering.” SAE paper number 2002-01-1304.

Hwang, R., 2004, “Solving Global Warming.” SAE Mobile Air Conditioning Summit, Washington D.C.

Hwang, Y. J., and Kim, h. Y., 1998, “Experimental and theoretical studies on the transient characteristics during speed up of inverter heat pump.” Proceedings of the Seventh International Refrigeration and Air Conditioning Conference at Purdue, pp. 189-194.

Idris, M. and Cowell, T., 2003, “The management of ice built-up in an automotive heat pump.” Proceedings of SAE Vehicle Thermal Management Systems, Paper number C599/066/2003.

Inui, K., and Tomatsu, Y., 2004, “Concerns and solutions for CO2 A/C systems for compact vehicles.” SAE Mobile Air Conditioning Summit, Washington D.C.

Janssen, M. J. P., De Wit, J. A., and Kuijpers, L. J. M., 1992, "Cyclic losses in domestic appliances: an experimental and theoretical analysis." International Journal of Refrigeration, Vol. 15, No. 3.

Jiang, H., 2003, "Development of a simulation and optimization tool for heat exchanger design." Ph.D. Thesis, University of Maryland, College Park, USA

Judge, J. and Radermacher, R., 1995, "The transient and steady state performance of R-22 and R407C." Proceedings of ASME, AES 34, pp. 1-9.

Kampf, H. et al., 2003, "Control technologies to optimize operating performance of R744 climate control systems." Proceedings of SAE Vehicle Thermal Management Systems, Paper number C599/052/2003.

Kataoka, T., 2001, "Prediction of occupant's thermal sensation under the transient environment in a vehicle compartment." SAE paper number 2001-01-0586.

Katipamula, S., and O'Neal, D. L., 1991, "Performance degradation during on-off cycling of single-speed heat pumps operating in the cooling mode: experimental results." ASHRAE Trans., Vol. 97, Part 2, pp. 331-339.

Kays, W. M. and London A. L., 1964, "Compact Heat Exchangers." McGraw-Hill Book Company, 2nd Edition.

Khamsi, Y. and Petitjean, C., 2000, "Validation results of automotive passenger compartment and its air conditioning system modeling." SAE paper number 2000-01-0982.

Kim and Bullard, 2001, "Dynamic characteristics of a R410a split air-conditioning system." International Journal of Refrigeration, Vol. 24, pp. 652-659.

Kim, N.H., Youn, B., and Webb, R.L., 1999, "Air-Side Heat Transfer and Friction Correlations for Plain Fin-and-Tube Heat Exchangers With Staggered Tube Arrangements." Transactions of the ASME, Journal of Heat Transfer, Vol. 121, pp. 662-667.

Kohler, J. Kuhn, B, Sonnekalb, M, and Beer, H, 1996, "Numerical calculation of the distribution of temperature and heat flux in buses under the influence of the vehicle air-conditioning system." ASHRAE Transactions, pp. 432-446.

Kojima, K. Itoh, S, Ohtaki, H, and Watanuki, K, 1999, "An estimate of temperature in a passenger compartment by numerical simulation using the linear graph theory." SAE paper number 1999-01-1188.

LeRoy, J. T., Groll, E. A., and Braun, J. E., 1998, "Computer model predictions of dehumidification performance of unitary air conditioners and heat pumps under extreme operating conditions." ASHRAE Trans., Vol. 104, pp. 773-788.

Lovins A. B., et al., 2004 "Winning the Oil Endgame." Rocky Mountain Institute Publishing.

Magna – Steyr, 2001, "KULI 5.0." by Magna Powertrain and Engineering Center Steyr GmbH & Co KG., www.magnapowertrain.com.

Magnetto, D. et al., 2003, "The 'cab-lounge concept' integrated systems for long-distance truck cabin thermal manegement." Proceedings of SAE Vehicle Thermal Management Systems, Paper number C599/071/2003.

Martini, S. et al., 2003, "High-efficiency air conditioning-improving comfort and reducing impact on fuel consumption." Proceedings of SAE Vehicle Thermal Management Systems, Paper number C599/077/2003.

McQuiston, F. C. and Parker, J. D., 1994, "Heating, Ventilating, and Air Conditioning Analysis and Design." John Wiley & Sons, Inc., 4th Edition.

McQuiston, F. C., 1975, "Fin efficiency with combined heat and mass transfer." ASHRAE Trans. Vol. 81, Part 1.

Meyer, J. J., Southwood, J., and Chan, M., 2003, "Energy efficient thermal vehicle for reduced climate system load." Proceedings of SAE Vehicle Thermal Management Systems, Paper number C599/094/2003.

Meyer, J., 2002, “HMC sonata: thermal energy efficient vehicle.” SAE Automotive Alternate Refrigerant Systems Symposium.

Mithraratne, P. and Wijeysundera, N. E., 2002, “An experimental and numerical study of hunting in thermostatic-expansion-valves-controlled evaporators.” International Journal of Refrigeration, Vol. 25, pp. 992-998.

Moffat, R. J., 1962, “Gas Temperature Measurement,” in Temperature, Its Measurement and Control in Science and Industry, Rheinhold, New York, P. 553.

Mulroy, 1986, “The effect of sort cycling and fan delay on the efficiency of a modified residential heat pump.” ASHRAE Trans., Vol. 1992, Part 1.

Mulroy, W., and Didion, D., 1983, “A laboratory investigation of refrigerant migration in a split unit air conditioner”, National Bureau of Standards, Report # NBSIR 83-2756.

Murphy, W. E., and Goldschmidt, V. w., 1979, “The degradation coefficient of a field-tested self-contained 3-ton air conditioner.” ASHRAE Trans., Vol. 85, Part 2, pp. 396-405.

Murphy, W. E., and Goldschmidt, V. W., 1985, “Cyclic Characteristics of a typical residential air conditioner - modeling of start-up transients.” ASHRAE Trans., Vol. 91, Part 2A, pp. 427-444.

National Highway Traffic Safety Administration, 1999, “Federal motor vehicle safety standards and regulations.” U.S. Department of Transportation, Washington D.C.

National Instruments, 2005, “LabVIEW.” http://www.ni.com

Omega, 2003, “Handbook and encyclopedia of temperature.” Omega Engineering, Onc.,Stamford, CT. Also on http://www.omega.com/literature.

O'Neal, D. L., and Katipamula, S., 1993, "Development of nondimensional cycling model for estimating the seasonal performance of air conditioners." Transactions of the ASME, Journal of Solar Energy Engineering, Vol. 115, pp. 176-181.

Perez, J and Rogers, P. 2003, "Crew/passneger compartment thermal load analysis using a holistic vehicle thermal model." Proceedings of SAE Vehicle Thermal Management Systems, Paper number C599/021/2003.

Preisner, M., "Carbon Dioxide Vapor Compression Cycle Improvements with Focus on Scroll Expanders." Ph.D. Thesis, University of Maryland, College Park, USA.

Ratts, E.B. and Brown, J. S., 2000, "An experimental analysis of cycling in an automotive air conditioning system." Applied Thermal Engineering, Vol. 20, pp. 1039-1058.

Rice, C. K., and Jackson, W. L., 1994, "PUREZ, The MARK V heat pump design model for chlorine-free, pure and near-azeotropic refrigerant alternatives." Preliminary documentation package.

Roy, D. Petitjean P, Clodic, D, and El Khoury, K, 2003, "Influence of thermal preconditioning technologies on A/C system power and passengers' thermal comfort." Proceedings of Vehicle Thermal Management Systems, paper number C599/004/2003.

Rubas, P. J., Bullard, C. W., 1995, Factors contributing to refrigerator cycling losses, International Journal of Refrigeration, Vol. 18, No. 3: pp. 168-176.

Rugh, J. P. Farrington, R. B., and Boettcher, J. A., 2001, "The impact of metal-free solar reflective film on vehicle climate control." SAE paper number 2001-01-1721.

Schlenz, D. and Koch, F., 2002, "Supplimentary heater concepts to improve warm-up in vehicles with DI engines." VDA Alternate Refrigerant Winter Meeting, Saalfelden, Austria.

Schwartz, W., 2002, “R134a emissions from passenger car air conditioning systems.” VDA Alternate Refrigerant Winter Meeting, Saalfelden, Austria.

Schwentker, R. A., 2005, “Advances to a computer model used in the simulation and optimization of heat exchangers. ” M.S. Thesis, University of Maryland, College Park, USA

Sumantran, V., et al., 1999, “An Assessment of Alternative Refrigerants for Automotive Applications based on Environmental Impact” Proceedings of SAE Alternate Refrigerant Systems Symposium, Scottsdale, Arizona.

Swagelok, 2002, “Valve Sizing Technical Bulletin.” Swagelok Company, Solon, OH.

Tanaka, Ikeuchi & Yamanaka, 1982, “Experimental study on the dynamic characteristics of a heat pump.” ASHRAE Trans. Vol. 88, Part 2, pp 323-331.

Tassou, S. A., Marquand, C. J., and Wilson, D. R., 1983, “Comparison of the performance of capacity controlled and conventional on/off controlled heat pumps.” Applied Energy, Vol. 14, pp. 241-256.

Thelon, W. and Zoz, S., 2003, “An approach for modeling an automotive vapor cycle refrigeration system and passenger cabin.” Proceedings of Vehicle Thermal Management Systems, paper number C599/046/2003.

Thermal Analysis Partners, 2004, “XProps.” http://www.thermalanalysispartners.com/XProps.htm

Vargas, J. V. C., and Parise, J. A. R., 1995, “Simulation in transient regime of a heat pump with closed-loop and on-off control.” International Journal of Refrigeration, Vol. 18, No. 4, pp. 235-243.

Wang, C., Hsieh, Y., and Lin, Y., 1997, “Performance of plate finned tube heat exchangers under dehumidifying conditions.” Journal of Heat Transfer, Vol. 119.

Wang, J. and Wu, Y., 1990, “Start-up and shut-down operation in a reciprocating compressor refrigeration system with capillary tubes.” International Journal of Refrigeration, Vol. 13, pp. 187-190

Wertenbach, J., 2003, Energy Analysis of Refrigerant Cycles, Automotive Alternate Refrigerant Systems Symposium.

Wu, G., and Bong, T. Y., 1994, “Overall efficiency of a straight fin with combined heat and mass transfer.” ASHRAE Transactions, Vol. 100, Part 1, pp. 376 – 374.

Xiaoqiang, X., and Clodic, D., 1996, “Dynamic simulation model of a vapor compression domestic refrigerator running with R134a.” Proceedings of the 1996 International Refrigeration Conference at Purdue, pp. 489-494.